

Response to the first reviewer _____	2
Response to the second reviewer _____	10
Marked-up Manuscript _____	16

# Evaluating a land surface model at a water-limited site: implications for land surface contributions to droughts and heatwaves

Response to Reviewer 1

We thank the reviewer for the positive comments and constructive suggestions. We have addressed the various concerns below. Our responses to reviewer comments are highlighted in blue below each reviewer comment.

In this study the authors validate the CABLE land surface model against measurements representing multiple relevant state variables and fluxes from a site in Australia. Using different model configurations they test the relevance of a range of processes known to affect modelling performance and find that most of them are also important at the considered site. They conclude that land surface modelling and model development should focus on several variables and correspondingly multiple processes at the same time to ensure meaningful model performance is obtained, and for the right reasons.

Recommendation: I think the paper requires moderate revisions.

The topic of this study is timely, and relevant for the community and even beyond in the context of climate change projections. While there are many studies investigating particular known challenges in land surface modelling, I find it very insightful to see a joint consideration of these challenges, and of their interactions. But I also see some shortcomings in this paper which should be addressed before the paper is suitable for publication in HESS:

(1) The order of the changes applied to the model configuration is not motivated. I think it should at least be discussed why and how this order was chosen, as I believe that the different changes applied to the model interact with each other, thereby leading to over- or underestimation of the effect of individual changes.

We chose to first resolve the soil evaporation bias because although this affects overall evapotranspiration partitioning, the impact of changes in soil evaporation should be constrained to the top-soil layers and would be of greatest importance following rain. We next tackled the initialisation of the water table as this fundamentally affects the root-zone moisture state. We then explored assumptions related to soil layer resolution/parameters, on the basis that the previous experiments would have (largely) resolved biases affecting overall soil moisture availability. Next, we explored optimising soil parameters on the basis that we had resolved substantive biases in the simulated hydrology. Finally, we explored assumptions related to the soil moisture stress function. We felt it was important to do this last as this water stress factor integrates, and arises from, the state of the soil moisture profile. As a result, exploring this water stress factor first and then fixing other biases (*e.g.* drainage) would affect the overall soil moisture and would overstate the relative importance of the water stress factor. We note this is what is commonly done in studies that resolve a single process *e.g.* the water stress factor.

We agree with the reviewer that the order of experiments may affect interpretation; however, we contend that there is no “perfect” experimental order and would argue there is merit to our chosen order. One could select an alternative order, but without any obvious reasoning, and the possible permutations are vast. We can assure the reviewer that we discussed the merits of these choices at length.

We have added to our justification of the experimental order on line 240-250:

*“We choose to first resolve a soil evaporation bias as it affects ET partitioning; however, its importance is limited to the top soil layers and particularly to the period following rain. We then modified the initial water table depth as this fundamentally affects the root-zone soil moisture state. Next, we explored assumptions related to soil column discretisation and parameters, and further optimised key hydraulic parameters to improve overall soil moisture biases. We choose to explore parameter assumptions at this point in the experimental set up as the previous experiments aimed to resolve existing biases that affected the overall soil moisture availability. Finally, we explored alternative soil moisture stress functions as the last step because this factor integrates, and arises from, the soil moisture state. The experimental order allowed us to probe model biases in a systematic way but it is important to note that there is no perfect experimental order and alternative permutations would lead to subtly different interpretation of results. In fact, this is what commonly happens in model evaluation that explore a single factor (e.g. the soil moisture stress factor).”*

(2) The observations with which the model simulations are compared are themselves subject to uncertainty. While I acknowledge that the authors are aware of this, and mention this here and there in section 4, I would like to see a more extensive discussion of this, particularly in the results section where model performance differences are assessed without discussing the significance of these changes in the light of observation uncertainties.

Thanks for the suggestion. We have now added a discussion of observation uncertainties in three locations:

[line 520-523]: *“Notably, soil evaporation was not directly measured at the site, but instead derived from the change in observed soil moisture over the top 5 cm, while ignoring days following rain (when the soil evaporative flux would likely be largest) (Gimeno et al., 2018a). As such, it contains soil moisture changes due to transpiration from a seasonal grass understorey but ignores evaporation below the top 5 cm, complicating model evaluation.”*

[line 578-584]: *“On the other hand, the neutron probe measurements of soil moisture used for calibration also involve uncertainties (Gimeno et al. 2018a). The soil moisture estimates were derived by fitting two distinctive linear relationships between soil volumetric water content and raw neutron probe counts (see Figure S6) for clay (below 3m) and non-clay soil (above 3m). As a result, the observation error would be greatest in layers where the soil type differs from the assumed soil type at that depth. However, the fitted relationships were robust, since clay soils largely dominated the deeper profile (below 3 m depth) and sand soils mostly dominated shallow profile (above 3m depth).”*

[line 115-118]: *“Etr estimates are derived from tree sapflow velocities (3-4 trees per experimental ring) using the heat pulse compensation technique (Gimeno et al., 2018a). Sapflow velocity is translated to Etr by multiplying the sapwood area estimated from basal area inside each ring and a correlation between sapwood and basal areas based on 35 trees adjacent to the experimental rings.”* And [line 120-121]: *“To represent variability in Etr and Es across rings, we show the mean and the uncertainty within ring estimates in all figures.”*

(3) It would be nice to have some discussion on the representativeness of the obtained conclusions across spatial and temporal scales (actually I could not even find the temporal scale at which the model simulations were done). Are these model improvements expected to hold at larger spatial scales relevant

for climate (change) modelling? And more generally, to which extent can we possibly learn from such small scale analyses to improve large scale modelling?

Model performance in water limited conditions has been widely identified as a key source of weakness in model evaluations. Perhaps due to data limitations, past studies have focused on individual processes in isolation. By contrast, we have aimed to achieve a more holistic model evaluation of a range of processes, enabled by the exceptionally comprehensive observations. While we do not anticipate our findings to directly constrain any single model's global simulations, we hope that elements of our findings guide future model improvements at temporal scales including daily extremes, seasonal and annual scales.

The observational data covers a relatively short time period (2013-2019) but some of the biases identified here have been shown to re-occur annually in many LSMs (particularly at seasonally dry sites; Ukkola et al., 2016). Fixing these biases is therefore likely to be valuable in longer term simulations. More broadly, understanding gained from this study better informs how process assumptions feedback and affect coupled simulations of droughts and heatwaves. More specifically, we intend to extend these evaluations in future work (see future directions section) to resolve existing biases, working from the end point of these sensitivity experiments. While our study concentrates on the CABLE model, the process representation noted here are broadly shared across a number of other leading LSMs.

We now highlight the relevance and lessons learnt for other LSMs in multiple sections of the discussion:

[line 514-515]: *“LSMs commonly overestimate soil evaporation especially under a sparse canopy or over bare land (De Kauwe et al., 2017; Swenson and Lawrence, 2014), suggesting this is a key model weakness.”*

[line 538-540]: *“When we initialised from a drier starting position (Watr), the simulated soil moisture profile matched the observed better, with implications for other models using similar groundwater schemes (e.g. CLM4.5, Noah-MP, JULES and LEAFHYDRO).”*

[line 552-554]: *“LSMs typically define a fixed number of soil layers globally, anywhere up to 20 layers. Most LSMs assume constant parameters across the entire soil profile, either using an experimental look-up table based on soil classification or estimating parameters from empirical pedotransfer functions.”*

[line 588-590]: *“Studies commonly highlight the functions used to limit photosynthesis and stomatal conductance with water stress as a key weakness among models. The lack of theory in this space (Medlyn et al., 2016) has led to models employing a range of functions encompassing different shapes and sensitivities that are not constrained by data.”*

[line 598-599]: *“the linear  $\theta$ -based function used in Ctl (common among models, e.g. SDGVM, Orchidee-CN and JULES)”*

We also mentioned the possibility to utilize the depth-varying soil parameters on a global scale with the novel dataset:

[line 562-564]: *“High-resolution global soil datasets (e.g. SoilGrids, Hengl et al., 2017) covering*

*multiple soil layers up to 2m depth offer opportunities to improve LSM simulations of soil moisture by incorporating depth-varying soil parameters.”*

Additionally, we now explicitly state that CABLE was run at 30-min resolution as the reviewer correctly pointed out that this was not made clear in the original manuscript:

[line 105-107]: *“Following Yang et al. (2020), the meteorological data were gap-filled (0.8% of values, from 1 January 2013 to 31 December 2019) using linear interpolation, aggregated to 30-minute averages and subsequently used to force CABLE at the 30-min resolution.”*

(4) Similarly, I was missing some discussion on the potential applicability of the derived conclusions to other models and regions. How can modellers using different models and focusing on other sites/regions benefit from the results obtained in this study?

We wrote our discussion *deliberately* to be general in its findings such that the lessons learned extend beyond the CABLE model. We ordered our sub-headings accordingly to offer insight into: soil evaporation, aquifer initialization, pedotransfer functions, optimisation and water stress functions.

As for the point about regions, it is a little speculative to comment on. Clearly our analysis is site specific, but the processes we identify and discuss (see list above) are more general. Furthermore, the biases and processes explored here have been shown to lead to systematic biases in LSMs across multiple sites in previous studies (Ukkola et al., 2016; Trugman et al., 2018). We anticipate our findings would be applicable in many water-limited conditions, but equally, more mesic systems too.

To make these points clearer we now add two sentences (line 495-496, *“Whilst our analysis is site specific, the issues indicated here have been reported to lead to systematic biases in LSMs across multiple sites (Ukkola et al., 2016a; Trugman et al., 2018)”*, and line 503-505, *“Since our study attempts to articulate the common issues in the simulated dry conditions in LSMs, we anticipate our findings would be applicable in many water-limited conditions, but equally, more mesic systems too”*) in the general discussion and a few sentences in these sub-headings to explain to the reader that our discussion is intended to be generally applicable to models and our thoughts on regional transferability. We have also added examples where other LSMs share similar parameterisations to CABLE (see previous comment).

Specifically, we illustrated and rephrased our suggestions to other LSMs in every sub-section of discussion:

[line 526-533]: *“However, a number of studies using alternative process-based schemes have been shown to improve individual model simulations (Haverd and Cuntz, 2010; Lehmann et al., 2018; Or and Lehmann, 2019). For example, Swenson and Lawrence (2014) introduced a dry surface layer-based soil evaporation resistance into CLM to depict water diffusion from dry soil, reducing biases in evapotranspiration and total water storage relative to FLUXNET-MTE and GRACE datasets. Based on a pore-scale model (Haghighi and Or, 2015), Decker et al. (2017) added the resistances of capillary-viscous and boundary layer to CABLE soil evaporation scheme and lowered the positive Es bias in springtime and improved seasonality of evapotranspiration. Hence, a focussed intercomparison of competing approaches against data originating from different ecosystems would be a valuable area of future work.”*

[line 540-550]: “*First, our results imply that LSMs that incorporate groundwater schemes need to be careful about aquifer initialisation because this strongly affects soil moisture dynamics. Second, there is no obvious solution to this initialisation and spin-up problem because drainage into the aquifer is a slow process, and it may take hundreds of years to reach a realistic equilibrium state. For global simulations, this suggests the need to a priori initialise the starting aquifer state and to assess against satellite-based products like GRACE (Döll et al., 2014; Niu et al., 2007) or implement off-line spin-up using meteorological forcing consistent with the subsequent simulations. However, while spin-up with observations is attractive, when the resulting states are incorporated into a coupled global model, inconsistencies are inevitable. Third, CABLE currently assumes an identical spin-up approach for the aquifer as the soil moisture, iterating until state changes between sequences of years are smaller than some threshold. LSMs that employ similar iteration approaches (Gilbert et al., 2017) are likely to encounter similar problems as CABLE because the rate of drainage into the aquifer is very slow, leading to negligible changes between iterations and thus satisfying the criteria for equilibrium.*”

[line 561-567]: “*The development in pedotransfer functions via machine learning or multi-model ensemble provides new avenues to reduce errors from parameters (Zhang and Schaap, 2017; Dai et al., 2019). High-resolution global soil datasets (e.g. SoilGrids, Hengl et al., 2017) covering multiple soil layers up to 2m depth offer opportunities to improve LSM simulations of soil moisture by incorporating depth-varying soil parameters. It is noteworthy that these global datasets of soil hydraulic parameters (Montzka et al, 2017; Zhang et al., 2019) have existed for several years but have not been widely used. Furthermore, at the EucFACE site, the observed soil texture information enabled the separation of parameter uncertainties from biases in process representations and model structural errors, a valuable step in better constraining LSM simulations.*”

[line 611-617]: “*Alternatives to the  $\beta$  functions have emerged to fill the theoretical gap, including plant hydraulic (Christoffersen et al., 2016; Xu et al., 2016) and stomatal optimality approaches (Sperry et al., 2017) but are yet to be widely adopted in LSMs (but see Eller et al., 2020; De Kauwe et al., 2020; Kennedy et al., 2019; Sabot et al., 2020). Replacing the empirical soil water stress factor by these plant physiology schemes reduces model arbitrariness associated with the representation of soil water stress and reduces the simulated biases in transpiration either over water deficit regions or areas with obvious dry seasons (Bonan et al., 2014; De Kauwe et al., 2020; Sabot et al., 2020). We can envision a wider application of these processes-based models will offer a chance to improve water stress representation in more LSMs.*”

Specific comments:

lines 23-24: not clear at this point what ‘median level of water stress’ is

We have clarified the text to now read, “*reduced the soil water stress on plants by 36 % during drought and 23 % at other times*”, which we think is enough detail in the abstract (line 23-24).

line 25: ‘Alternative’ could be replaced by ‘The range of tested’ for improved clarity

Agreed – we have made this change (line 26).

lines 42-43: you could cite here Orth and Destouni 2018



Thanks, and we have added the reference (line 44).

line 79: 'soil moisture extending root zone', please improve phrasing

Agreed – this is clumsy English. We have modified the text to “*to utilise observations of soil moisture extending through the root zone with concurrent measurements of water fluxes at high temporal frequency*” (line 79-80).

line 95: what is meant with 'Sm' here?

It is common practice for some species to also include an abbreviation after the genus and species name, this denoted the person or persons who first formally described/discovered the species. In this case Sm. refers to Smith.

line 105: You talk about gap filling here. How many gaps were filled this way?

Only 0.8% of the meteorological forcing was gap filled and we have added this detail in the paper (line 106).

lines 120-123: Could you give some details on how the neutron probe measurement works and is done at 12 different depths?

We have provided additional detail (line 127-129, “*The neutron probe counts are converted to  $\theta$  via the site specific linear correlation between the raw reading of neutron probe and the lab measured soil  $\theta$  sampled at the same depth as probes (Gimeno et al. 2018a)*”), but more critically added the reference to the details of how this was done.

line 286: why 31 layers?

This was done to match the resolution of observed soil texture which were mostly sampled at 15 cm intervals (leading to 31 layers in total over the total soil depth). We now make this clear in the text (line 301-302, “*the number of vertical soil layers was increased from 6 to 31 (to match the resolution of observed soil texture which was sampled at 15-cm intervals)*”).

line 309: 'Due to muted variability', can you please give more details here?

We have reworded the sentence for clarity (line 323-325, “ *$\theta_{sat}$  was not adjusted below 30 cm as the observed maximum  $\theta_{sat}$  is unlikely to represent saturated conditions due to lower soil moisture variability at depth.*”).

line 339: Why not stating the applied exponent 0.425 here?

Agreed, and we have added the value into the text (line 354).

line 354: Why would accounting for defoliation by decreased LAI be insufficient?

Insect attack can also damage the phloem hence the full impact may not be captured by a reduction in LAI. We have modified the text to clarify this (line 369-370, “*CABLE only accounts for canopy*”).

*defoliation via a decline in LAI but not other damage e.g. to the phloem”).*

line 379: it is not mentioned in the respective section 2.4.3 that the aquifer is 'initialised' drier

*We have added additional text to clarify this in Section 2.4.3 (line 289-290, “which reduced the initial saturation of aquifer from 100% to 52%”).*

lines 407-411: Figure 6 should be mentioned earlier in this paragraph

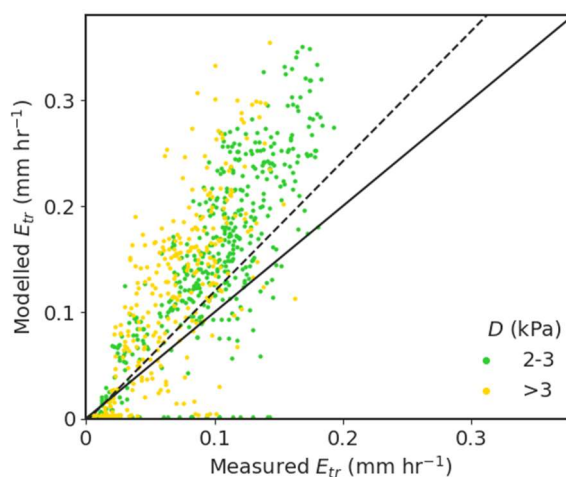
*Agreed and corrected (line 424).*

line 439: 98% is relative to the maximum I guess?

*We have modified the text to make our statement clear (line 455-456, “a difference of 98 % relative to the averaged median of all the simulations for  $\beta$  simulated during drought”).*

line 467-469: Shouldn't this be the other way round?

*We have clarified our text to make our meaning clear as: “during heatwaves **when  $D$  is higher the model would overestimate  $E_{tr}$** ” in line 484-485, and the figure below demonstrates this.*



line 598: typo in 'transpiration'

*Thanks, and corrected (line 637).*

line 615: you could cite here Orth et al. 2017

*Agreed, and we have added the reference at line 655.*

Figures 2-7: Please point the reader to the different time axes used in this plot, and/or use a regular time step spacing in plots c,d,e while showing data gaps e.g. in gray. This can improve readability and comparability across plots I think.

*We have modified the figure legend to make this much clearer and explicit. We now state “Note the different time axis for (c-e) relative to (a-b) due to different sampling intervals for soil moisture and fluxes.”*



Figure 10: The different timing of the peaks which you repeatedly refer to in the text could be illustrated by vertical thin lines with respective colors highlighting these peaks.

Thanks for the suggestion. We tried to plot these vertical lines but they are too crowded and hard to be read. However, we have added vertical reference lines at a 6-hour interval to assist reading Figure 10.

#### References:

Trugman, A. T., Medvigy, D., Mankin, J. S. and Anderegg, W. R. L.: Soil moisture stress as a major driver of carbon cycle uncertainty, *Geophys. Res. Lett.*, 45(13), 6495–6503, doi:10.1029/2018GL078131, 2018.

Ukkola, A. M., De Kauwe, M. G., Pitman, A. J., Best, M. J., Haverd, V., M., D., G., A. and Haughton, N.: Land surface models systematically overestimate the intensity, duration and magnitude of seasonal-scale evaporative droughts. In review., *Environ. Res. Lett.*, 11, 104012, 2016.

# Evaluating a land surface model at a water-limited site: implications for land surface contributions to droughts and heatwaves

Response to Reviewer 2

We thank the reviewer for the positive comments and constructive suggestions. We have addressed the various concerns below. Our responses to reviewer comments are highlighted in blue below each reviewer comment.

Mu et al., evaluate the performance of the Community Atmosphere-Biosphere Land Exchange (CABLE) land surface model for a water-limited measurement site in southeastern Australia. The stand-alone model performance is assessed by comparing the simulation results to soil moisture and evapotranspiration measurements. By changing specific model configurations, the general model bias is tried to be reduced. In this context, one focus of the study is on heatwaves and droughts. Results show that a meaningful improvement of the model performance can only be achieved if both quantities, soil moisture and evapotranspiration, are considered for model validation.

Recommendation: The study is within the scope of HESS and addresses a relevant and interesting topic for the modelling community. The manuscript is well structured and comprehensibly written. Nevertheless, there are some issues which should be addressed before publication.

Comments:

1) The study highlights the large uncertainties related to the simulation of evapotranspiration and soil moisture. Thus, averaged land use specific parameters used in LSMs can deviate considerably from the actual hydrological characteristics at measurement sites. Large differences between simulation results and observations are the consequence. In order to improve the model performance, therefore, model configurations have to be adapted. This issue is clearly and comprehensibly demonstrated in the manuscript. But due to such site-specific changes the adapted model can only be applied at the location for which it is tuned and the model results are not transferable to other situations (or would the authors say that the results are transferable? If yes, please discuss it). Therefore, it is difficult to state lessons learned from this study beyond its specific application on southeastern Australia.

We agree that our study is site-specific and that some of the insights gained are only applicable at this scale. Nevertheless, we attempted to frame our discussion (as the reviewer notes below) in a general sense, such that findings would be of interest to other model groups. Similarly, whilst it is speculative to state how widespread the biases we identified are, it has been demonstrated that CABLE displays similar biases in other water-limited ecosystems as well as mesic sites (Haverd et al., 2016, Decker et al., 2017; Ukkola et al., 2016b). Furthermore, similar biases have also been identified in evaluations of other state-of-the-art LSMs over multiple sites (De Kauwe et al., 2017; Powell et al., 2013; Ukkola et al., 2016a).

We have added more details to our original discussion on the common problems in LSMs and how the CABLE processes explored here offer lessons for other LSMS:

[line 514-515]: *“LSMs commonly overestimate soil evaporation especially under a sparse canopy or*

*over bare land (De Kauwe et al., 2017; Swenson and Lawrence, 2014), suggesting this is a key model weakness.”*

[line 538-540]: *“When we initialised from a drier starting position (Watr), the simulated soil moisture profile matched the observed better; with implications for other models using similar groundwater schemes (e.g. CLM4.5, Noah-MP, JULES and LEAFHYDRO).”*

[line 552-554]: *“LSMs typically define a fixed number of soil layers globally, anywhere up to 20 layers. Most LSMs assume constant parameters across the entire soil profile, either using an experimental look-up table based on soil classification or estimating parameters from empirical pedotransfer functions.”*

[line 588-590]: *“Studies commonly highlight the functions used to limit photosynthesis and stomatal conductance with water stress as a key weakness among models. The lack of theory in this space (Medlyn et al., 2016) has led to models employing a range of functions encompassing different shapes and sensitivities that are not constrained by data.”*

[line 598-599]: *“the linear  $\theta$ -based function used in Ctl (common among models, e.g. SDGVM, Orchidee-CN and JULES)”*

We also explain more clearly how our study has relevance beyond SE Australia:

[line 495-496]: *“Whilst our analysis is site specific, the issues indicated here have been reported to lead to systematic biases in LSMs across multiple sites (Ukkola et al., 2016a; Trugman et al., 2018)”*

[line 503-505]: *“Since our study attempts to articulate the common issues in the simulated dry conditions in LSMs, we anticipate our findings would be applicable in many water-limited conditions, but equally, more mesic systems too.”*

At a few places in the discussion section the authors try to derive general conclusions, which could be beneficial also for modelling groups in other regions and with other models (e.g. implications for incorporated groundwater schemes, suitability of satellite-derived soil moisture estimates for model calibration), but this discussion should be more detailed. For instance, are there any processes to which special attention should be paid in LSM developments, or can you derive minimum requirements (e.g. spatial resolution) for external model data (e.g. soil texture), etc., or are such statements not possible for the chosen model setup? I recommend to address this in a separate sub-section in the discussion.

Thanks for the suggestion. We have opted to add detail to the existing sections to avoid repetition and now provide implications for other LSMs at the end of each sub-section and added more details to substantiate our recommendations:

[line 526-533]: *“However, a number of studies using alternative process-based schemes have been shown to improve individual model simulations (Haverd and Cuntz, 2010; Lehmann et al., 2018; Or and Lehmann, 2019). For example, Swenson and Lawrence (2014) introduced a dry surface layer-based soil evaporation resistance into CLM to depict water diffusion from dry soil, reducing biases in evapotranspiration and total water storage relative to FLUXNET-MTE and GRACE datasets. Based*

*on a pore-scale model (Haghighi and Or, 2015), Decker et al. (2017) added the resistances of capillary-viscous and boundary layer to CABLE soil evaporation scheme and lowered the positive Es bias in springtime and improved seasonality of evapotranspiration. Hence, a focussed intercomparison of competing approaches against data originating from different ecosystems would be a valuable area of future work.”*

[line 540-550]: *“First, our results imply that LSMs that incorporate groundwater schemes need to be careful about aquifer initialisation because this strongly affects soil moisture dynamics. Second, there is no obvious solution to this initialisation and spin-up problem because drainage into the aquifer is a slow process, and it may take hundreds of years to reach a realistic equilibrium state. For global simulations, this suggests the need to a priori initialise the starting aquifer state and to assess against satellite-based products like GRACE (Döll et al., 2014; Niu et al., 2007) or implement off-line spin-up using meteorological forcing consistent with the subsequent simulations. However, while spin-up with observations is attractive, when the resulting states are incorporated into a coupled global model, inconsistencies are inevitable. Third, CABLE currently assumes an identical spin-up approach for the aquifer as the soil moisture, iterating until state changes between sequences of years are smaller than some threshold. LSMs that employ similar iteration approaches (Gilbert et al., 2017) are likely to encounter similar problems as CABLE because the rate of drainage into the aquifer is very slow, leading to negligible changes between iterations and thus satisfying the criteria for equilibrium.”*

[line 561-567]: *“The development in pedotransfer functions via machine learning or multi-model ensemble provides new avenues to reduce errors from parameters (Zhang and Schaap, 2017; Dai et al., 2019). High-resolution global soil datasets (e.g. SoilGrids, Hengl et al., 2017) covering multiple soil layers up to 2m depth offer opportunities to improve LSM simulations of soil moisture by incorporating depth-varying soil parameters. It is noteworthy that these global datasets of soil hydraulic parameters (Montzka et al, 2017; Zhang et al., 2019) have existed for several years but have not been widely used. Furthermore, at the EucFACE site, the observed soil texture information enabled the separation of parameter uncertainties from biases in process representations and model structural errors, a valuable step in better constraining LSM simulations.”*

[line 611-617]: *“Alternatives to the  $\beta$  functions have emerged to fill the theoretical gap, including plant hydraulic (Christoffersen et al., 2016; Xu et al., 2016) and stomatal optimality approaches (Sperry et al., 2017) but are yet to be widely adopted in LSMs (but see Eller et al., 2020; De Kauwe et al., 2020; Kennedy et al., 2019; Sabot et al., 2020). Replacing the empirical soil water stress factor by these plant physiology schemes reduces model arbitrariness associated with the representation of soil water stress and reduces the simulated biases in transpiration either over water deficit regions or areas with obvious dry seasons (Bonan et al., 2014; De Kauwe et al., 2020; Sabot et al., 2020). We can envision a wider application of these processes-based models will offer a chance to improve water stress representation in more LSMs.”*

2) please discuss the uncertainties in the observations in more detail. I suppose that especially for the “indirect” or “derived” observations of Etr und Es, uncertainties are quite large and thus affect the assessment of the model performance.

We have added further details about the uncertainties of soil evaporation and volumetric water content and now also discuss transpiration measurements:

[line 520-523]: *“Notably, soil evaporation was not directly measured at the site, but instead derived from the change in observed soil moisture over the top 5 cm, while ignoring days following rain (when the soil evaporative flux would likely be largest) (Gimeno et al., 2018a). As such, it contains soil moisture changes due to transpiration from a seasonal grass understorey but ignores evaporation below the top 5 cm, complicating model evaluation.”*

[line 578-584]: *“On the other hand, the neutron probe measurements of soil moisture used for calibration also involve uncertainties (Gimeno et al. 2018a). The soil moisture estimates were derived by fitting two distinctive linear relationships between soil volumetric water content and raw neutron probe counts (see Figure S6) for clay (below 3m) and non-clay soil (above 3m). As a result, the observation error would be greatest in layers where the soil type differs from the assumed soil type at that depth. However, the fitted relationships were robust, since clay soils largely dominated the deeper profile (below 3 m depth) and sand soils mostly dominated shallow profile (above 3m depth).”*

[line 115-118]: *“Etr estimates are derived from tree sapflow velocities (3-4 trees per experimental ring) using the heat pulse compensation technique (Gimeno et al., 2018a). Sapflow velocity is translated to Etr by multiplying the sapwood area estimated from basal area inside each ring and a correlation between sapwood and basal areas based on 35 trees adjacent to the experimental rings.”*

[line 120-121]: *“To represent variability in Etr and Es across rings, we show the mean and the uncertainty within ring estimates in all figures.”*

3) the control run exhibits an overestimated Es in conjunction with a soil moisture wet bias. Because of that, I was quite surprised about the first step to improve the model performance by increasing the resistance for soil evaporation Sres. Of course, such an increase in Sres results in a reduced Es, but must, at the same time, inevitably cause an intensified wet bias. Therefore, it would have been more intuitive to first increase the vertical drainage (as it is later done in the Watr experiment) to reduce the available water amount for evaporation in the upper soil. Is there any reason for the chosen sequence of experiments? I suppose that especially for the chosen “layering” approach, the order of the experiments is essential.

We agree with the reviewer that the order of experiments may influence our understanding of these parameterisations. However, our sequence was decided under the following considerations. We have stated our justification of the experiment order in Ln 240-250 (also see our response to Reviewer 1): *“We choose to first resolve a soil evaporation bias as it affects ET partitioning; however, its importance is limited to the top soil layers and particularly to the period following rain. We then modified the initial water table depth as this fundamentally affects the root-zone soil moisture state. Next, we explored assumptions related to soil column discretisation and parameters, and further optimised key hydraulic parameters to improve overall soil moisture biases. We choose to explore parameter assumptions at this point in the experimental set up as the previous experiments aimed to resolve*

*existing biases that affected the overall soil moisture availability. Finally, we explored alternative soil moisture stress functions as the last step because this factor integrates, and arises from, the soil moisture state. The experimental order allowed us to probe model biases in a systematic way but it is important to note that there is no perfect experimental order and alternative permutations would lead to subtly different interpretation of results. In fact, this is what commonly happens in model evaluation that explore a single factor (e.g. the soil moisture stress factor).”*

We agree with the reviewer that the order of experiments is important and may affect interpretation; however, we contend that there is no “perfect” experimental order and would argue there is merit to our chosen order. One could select an alternative order, but without any obvious reasoning, and the possible permutations are vast. We can assure the reviewer that we discussed the merits of these choices at length. We do note that we examine the impact of increasing the vertical drainage first, but it did not lead to differences that affected our conclusions.

4) In this study, the influence of non-hydrological factors on evapotranspiration (e.g. temperature, aerodynamic characteristics of the surface) is neglected. For instance, how good are the surface temperatures (soil and vegetation surface) simulated in CABLE? Are there any surface or soil temperature measurements which can be used for validation?

Thanks for the suggestion. We agree that non-hydrological factors are also significant for evapotranspiration but several of these factors were constrained in our experiments using observations. We have added details into the future direction text (see below).

We note that we did not evaluate our modelled canopy temperature against site measurements. We think that such a comparison would only be relevant had we used a vertically layered canopy model (e.g. <https://bg.copernicus.org/articles/17/265/2020/>), set up to accurately depict ring-to-ring tree variability, which would affect canopy-scale light interception/shading (and so evapotranspiration). Direct comparison of data to a big-leaf (two-leaf) model would have been unlikely to have added further constraints due to the importance of the position within the canopy of the measurements. Besides, we use half-hourly meteorology observations (e.g. radiation, air temperature and humidity) to force the model which ensures the simulated soil surface and canopy temperatures cannot diverge far from the observed state.

We have added:

[line 657-661]: *“While the focus of our study has been primarily on the parameterisations of hydrology and sub-surface processes, we did aim to minimise the uncertainties from the non-hydrological factors by using site characteristics, such as the aerodynamic conductance (determined by setting the canopy height) and photosynthesis parameters (e.g. maximum carboxylation rate and maximum rate of electron transport). However, due to the significance of these non-hydrological factors on evapotranspiration (e.g. Breil et al., 2020), further evaluation should be considered in future studies.”*

References:

Decker, M., Or, D., Pitman, A. and Ukkola, A.: New turbulent resistance parameterization for soil evaporation based on a pore-scale model: Impact on surface fluxes in CABLE, *J. Adv. Model. Earth Syst.*, 9(1), 220–238, doi:10.1002/2016MS000832, 2017.

Haverd, V., Cuntz, M., Nieradzki, L. P. and Harman, I. N.: Improved representations of coupled soil–



canopy processes in the CABLE land surface model (Subversion revision 3432), *Geosci. Model Dev.*, 9(9), 3111–3122, doi:10.5194/gmd-9-3111-2016, 2016.

De Kauwe, M. G., Medlyn, B. E., Walker, A. P., Zaehle, S., Asao, S., Guenet, B., Harper, A. B., Hickler, T., Jain, A. K., Luo, Y., Lu, X., Luus, K., Parton, W. J., Shu, S., Wang, Y. P., Werner, C., Xia, J., Pendall, E., Morgan, J. A., Ryan, E. M., Carrillo, Y., Dijkstra, F. A., Zelikova, T. J. and Norby, R. J.: Challenging terrestrial biosphere models with data from the long-term multifactor Prairie Heating and CO<sub>2</sub> Enrichment experiment, *Glob. Chang. Biol.*, 23(9), 3623–3645, doi:10.1111/gcb.13643, 2017.

Powell, T. L., Galbraith, D. R., Christoffersen, B. O., Harper, A., Imbuzeiro, H. M. A., Rowland, L., Almeida, S., Brando, P. M., da Costa, A. C. L., Costa, M. H., Levine, N. M., Malhi, Y., Saleska, S. R., Sotta, E., Williams, M., Meir, P. and Moorcroft, P. R.: Confronting model predictions of carbon fluxes with measurements of Amazon forests subjected to experimental drought, *New Phytol.*, 200(2), 350–365, doi:10.1111/nph.12390, 2013.

Ukkola, A. M., De Kauwe, M. G., Pitman, A. J., Best, M. J., Abramowitz, G., Haverd, V., Decker, M. and Haughton, N.: Land surface models systematically overestimate the intensity, duration and magnitude of seasonal-scale evaporative droughts, *Environ. Res. Lett.*, 11(10), 104012, doi:10.1088/1748-9326/11/10/104012, 2016a.

Ukkola, A. M., Pitman, A. J., Decker, M., De Kauwe, M. G., Abramowitz, G., Kala, J. and Wang, Y. P.: Modelling evapotranspiration during precipitation deficits: identifying critical processes in a land surface model, *Hydrol. Earth Syst. Sci.*, 20(6), 2403–2419, doi:10.5194/hess-20-2403-2016, 2016b.

# Evaluating a land surface model at a water-limited site: implications for land surface contributions to droughts and heatwaves

Mengyuan Mu<sup>1</sup>, Martin G. De Kauwe<sup>1</sup>, Anna M. Ukkola<sup>2</sup>, Andy J. Pitman<sup>1</sup>, Teresa E. Gimeno<sup>3,4</sup>, Belinda E. Medlyn<sup>5</sup>, Dani Or<sup>6</sup>, Jinyan Yang<sup>5</sup> and David S. Ellsworth<sup>5</sup>

<sup>1</sup>ARC Centre of Excellence for Climate Extremes and Climate Change Research Centre, University of New South Wales, Sydney 2052, Australia

<sup>2</sup>ARC Centre of Excellence for Climate Extremes and Research School of Earth Sciences, Australian National University, Canberra 0200, Australia

<sup>3</sup>Basque Centre for Climate Change, Leioa 48940, Spain

<sup>4</sup>IKERBASQUE, Basque Foundation for Science, 48008, Bilbao, Spain

<sup>5</sup>Hawkesbury Institute for the Environment, Western Sydney University, Sydney 2751, Australia

<sup>6</sup>Department of Environmental Sciences, ETH Zurich, Zurich 8092, Switzerland

Correspondence to: Mengyuan Mu (mu.mengyuan815@gmail.com)

**Abstract.** Land surface models underpin coupled climate model projections of droughts and heatwaves. However, the lack of simultaneous observations of individual components of evapotranspiration, concurrent with root-zone soil moisture, has limited previous model evaluations. Here, we use a comprehensive set of observations from a water-limited site in southeastern Australia including both evapotranspiration and soil moisture to [4.5 ma](#) depth [of 4.5 m](#) to evaluate the Community Atmosphere-Biosphere Land Exchange (CABLE) land surface model. We ~~demonstrated~~[demonstrate](#) that alternative process representations within CABLE had the capacity to improve simulated evapotranspiration, but not necessarily soil moisture dynamics - highlighting problems of model evaluations against water fluxes alone. Our best simulation was achieved by resolving a soil evaporation bias; a more realistic initialisation of the groundwater aquifer state; higher vertical soil resolution informed by observed soil properties; and further calibrating soil hydraulic conductivity. Despite these improvements, the role of the empirical soil moisture stress function in [influencing the](#) simulated water fluxes remained important: using a site calibrated function reduced the [median level of soil](#) water stress [on plants](#) by 36 % during drought and 23 % at other times. These changes in CABLE not only improve the seasonal cycle of evapotranspiration, but also affect the latent and sensible heat fluxes during droughts and heatwaves. ~~Alternative~~[The range of](#) parameterisations [tested](#) led to differences of  $\sim 150 \text{ W m}^{-2}$  in the simulated latent heat flux during a heatwave, implying a strong impact of parameterisations on the capacity for evaporative cooling and feedbacks to the boundary layer (when coupled). Overall, our results highlight the opportunity to advance the capability of land surface models to capture water cycle processes, particularly during meteorological extremes, when sufficient observations of both evapotranspiration fluxes and soil moisture profiles are available.

## 1 Introduction

Droughts and heatwaves can have severe and long-lasting impacts on terrestrial ecosystems (Allen et al., 2015; Reichstein et al., 2013) and humans (Matthews et al., 2017; Pal and Eltahir, 2016). Global climate models are commonly used to project how anthropogenic climate change will affect the magnitude, frequency and intensity of droughts and heatwaves. Heatwaves are projected to increase in the future in response to climate change (Dosio et al., 2018; Zhao and Dai, 2017). The future of droughts is less clear: projections of an increase in future droughts are common in the literature (Ault, 2020), yet regional precipitation projections remain uncertain (Collins et al., 2013) and land surface processes relevant to drought are poorly represented in climate models (Ukkola et al., 2018a).

While there is no universal definition, drought can be classified into meteorological, agricultural, hydrological and socioeconomic drought. From a climate model perspective, drought is an anomalous lack of water at the land-atmosphere

42 interface sustained over time. It begins with a reduction in precipitation (“meteorological” drought) and if this persists it can  
43 evolve into “agricultural” drought via low soil moisture or into “hydrological” drought through low streamflow or  
44 groundwater- (Orth and Destouni, 2018). A critical feedback exists between low soil moisture availability and heatwaves  
45 (Seneviratne et al., 2010; Teuling et al., 2010; Vogel et al., 2017). As soil moisture becomes depleted, the surface energy  
46 partitioning becomes increasingly dominated by sensible heat fluxes ( $Q_H$ ) relative to latent heat fluxes ( $Q_E$ ). This can lead to a  
47 positive feedback whereby the high sensible heat fluxes warm the boundary layer, which, combined with the reduced  
48 evaporation, leads to increased atmospheric demand for moisture exacerbating land desiccation (Miralles et al., 2019). A  
49 combination of drought and heatwaves lead to wide ranging impacts on the functioning of terrestrial ecosystems (Reichstein  
50 et al., 2013; Schumacher et al., 2019). For example, during the European heatwave and drought in 2003, terrestrial carbon  
51 losses of up to 0.5 Pg C were reported, corresponding to roughly four years of European terrestrial net carbon uptake (Ciais et  
52 al., 2005).

53  
54 Given projections of worsening heatwaves and potentially more droughts under future climate change, the importance of land  
55 surface models (LSMs) to capture land responses and feedbacks to the atmosphere during climate extremes is becoming  
56 increasingly recognised (Mazdiyasi and AghaKouchak, 2015; Schumacher et al., 2019; Yang et al., 2019). Despite many  
57 improvements to LSMs over the past decades, LSMs have remained poor at simulating water fluxes during water-stressed  
58 periods (Egea et al., 2011; De Kauwe et al., 2017; Powell et al., 2013; Trugman et al., 2018; Ukkola et al., 2016a), which likely  
59 contributes to biases in land-atmosphere feedbacks during heatwaves (Sippel et al., 2017). LSMs commonly underestimate  
60 interannual variations in terrestrial water storage (Humphrey et al., 2018), underestimate  $Q_E$  during droughts (Powell et al.,  
61 2013; Ukkola et al., 2016a) and lack “persistence” by responding too strongly to short-term precipitation variation (Tallaksen  
62 and Stahl, 2014). Poor representation of hydrological processes has been identified as a key reason for model biases. There is  
63 uncertainty around soil moisture dynamics, how soil texture information is translated to soil hydraulic properties through  
64 pedotransfer functions and how water fluxes are partitioned to different components of evapotranspiration and runoff (Clark  
65 et al., 2015; Lian et al., 2018; Van Looy et al., 2017). Various approaches have been adopted to improve LSM hydrology, such  
66 as the introduction of groundwater dynamics (Niu et al., 2007), alternative pedotransfer functions (Best et al., 2011) and  
67 subgrid-scale processes for runoff generation (Decker, 2015). By contrast, the functions used in LSMs to represent the effect  
68 of declining water availability on vegetation function are poorly constrained by data (Medlyn et al., 2016), and not consistently  
69 applied. Specifically, some models down-regulate the maximum rate of Rubisco carboxylation, whilst others reduce stomatal  
70 parameters (De Kauwe et al., 2013). Models also do not account for differences in species-level sensitivity to drought (De  
71 Kauwe et al., 2015; Klein, 2014; Zhou et al., 2014). This model gap has driven a significant investment in new theoretical  
72 approaches (Dewar et al., 2018; Sperry et al., 2017; Wolf et al., 2016).

73  
74 Despite model developments, it has remained difficult to disentangle the reasons behind poor model performance due to a lack  
75 of suitable observations. Root-zone soil moisture estimates are rare and whilst satellite estimates are available, they only cover  
76 the top few centimetres or are only available at coarse spatial resolution. Meanwhile,  $Q_E$  is routinely measured at the site-scale,  
77 but gridded large-scale estimates remain highly uncertain (Pan et al., 2020). As such, many past model evaluations have  
78 focused on observed  $Q_H$  and  $Q_E$  from eddy-covariance observations (Best et al., 2015) or near-surface soil moisture and  
79 evaporation from water balance sites (e.g. Schlosser et al., 2000). ~~What~~However, it is rare ~~is evaluation for evaluations~~ of  
80 LSMs, designed for use in climate models, ~~utilising to utilise~~ observations of soil moisture extending ~~through the~~ root zone  
81 with concurrent measurements of water fluxes at high temporal frequency. In this paper, we use a novel dataset from the water-  
82 limited *Eucalyptus* Free-Air CO<sub>2</sub> Enrichment (EucFACE) experiment site in southeastern Australia to evaluate the Community  
83 Atmosphere-Biosphere Land Exchange (CABLE) LSM. At this site, frequent measurements of each component of the water  
84 balance were made coincident with soil moisture observations to a depth of 4.5 m. The highly variable rainfall at this site leads

85 to extended dry-downs, and the heatwaves in summer commonly exceed 35°C. We use this high-quality dataset to assess  
86 multiple model assumptions commonly used across LSMs within a single model framework, evaluating both simulated fluxes  
87 and state variables at seasonal to annual scales and across weather (heatwaves) and climate (drought) phenomena.

## 88 2. Methods and data

### 89 2.1 Site information

90 The EucFACE experiment is located on an ancient alluvial floodplain, 3.6 km from the Hawkesbury River in Western Sydney,  
91 Australia (33°36'59"S, 150°44'17"E) (Gimeno et al., 2018a; Figure 1). The site has a temperate-subtropical transitional climate  
92 with a mean annual temperature of 17.8 °C and the mean annual precipitation of 719.1 mm evenly distributed over the year.  
93 EucFACE is a water-limited site experiencing frequent droughts and low water availability. The site is in an open woodland  
94 with a canopy height of 18–23 m and a plant area index (including leaf and woody components) that varied between 1.3 and  
95 2.2 m<sup>2</sup> m<sup>-2</sup> (mean = 1.7 m<sup>2</sup> m<sup>-2</sup>) over the study period. The overstorey is dominated by a single species *Eucalyptus tereticornis*  
96 Sm. with scattered individuals of *Eucalyptus amplifolia* Naudin. The upper soil layer is a loamy sand with a sand fraction  
97 >75%; at 30–80 cm depth, there is a higher clay content layer (15%–35% clay), and below the clay layer sand clay loam soil  
98 extends to the depth of 300 cm. Between 300–350 cm and 450 cm depth, the soil is > 40% clay (Gimeno et al., 2016). The  
99 observed water table is at ~ 12 m. The site is characterized as nutrient poor, especially lacking in available phosphorus (Crous  
100 et al., 2015; Ellsworth et al., 2017). In this paper we evaluate CABLE against the averaged data from Rings 2, 3 and 6, which  
101 are exposed to the ambient atmospheric CO<sub>2</sub> concentration.

### 102 2.2 Observation data

103 In our study, CABLE is driven by *in situ* meteorological data and observed leaf area index (LAI) from 2013 to 2019. The  
104 photosynthetically active radiation (PAR; LI-190, LI-COR, Inc., Lincoln, NE, USA), air temperature, and relative humidity  
105 (HUMICAP ® HMP 155, Vaisala, Vantaa, Finland) were measured every second and one-minute averages were recorded on  
106 data loggers (CR3000, Campbell Scientific Australia, Townsville, Australia). ~~Meteorological data were gap-filled by linear  
107 interpolation and aggregated to 30-minute averages following Yang et al. (2020).~~ Following Yang et al. (2020), the  
108 meteorological data were gap-filled (0.8% of values, from 1 January 2013 to 31 December 2019) using linear interpolation,  
109 aggregated to 30-minute averages and subsequently used to force CABLE at the 30-min resolution. LAI was calculated from  
110 the measurements of above- and below-canopy PAR at each ring following Duursma et al. (2016). Since the site LAI represents  
111 the plant area index (including both woody part and leaves), to reflect the actual leaves condition we follow Yang et al. (2020)  
112 and reduce the LAI by a constant branch and stem cover (0.8 m<sup>2</sup> m<sup>-2</sup>) estimated by the lowest LAI when the canopy shed  
113 almost all leaves during November 2013. The CO<sub>2</sub> concentration was measured every 5 minutes at each ring and then gap-  
114 filled and aggregated to 30-minute averages.

115  
116 To evaluate CABLE, we used measurements of transpiration ( $E_{tr}$ ), soil evaporation ( $E_s$ ) and volumetric water content ( $\theta$ ) at  
117 different soil depths (see below).  ~~$E_{tr}$  and  $E_s$  come from a dataset published in Gimeno et al. (2018a).~~  $E_{tr}$  estimates are derived  
118 from tree sapflow using the heat pulse compensation technique (Gimeno et al., 2018a).  $E_{tr}$  estimates are derived from tree  
119 sapflow velocities (3-4 trees per experimental ring) using the heat pulse compensation technique (Gimeno et al., 2018a).  
120 Sapflow velocity is translated to  $E_{tr}$  by multiplying the sapwood area estimated from basal area inside each ring and a  
121 correlation between sapwood and basal areas based on 35 trees adjacent to the experimental rings.  $E_s$  is computed from the  
122 soil moisture change in the top 5 cm depth monitored at two locations in each of the three ambient rings. The  $E_s$  data also  
123 includes transpiration from the dynamic (flushes and wilts) understorey vegetation (Collins et al., 2018; Pathare et al., 2017).

124 For  $E_s$ , Gimeno et al. (2018a) excluded rainy days and days preceded by a day with  $> 2 \text{ mm d}^{-1}$  of precipitation. [To represent](#)  
125 [variability in  \$E\_{tr}\$  and  \$E\_s\$  across rings, we show the mean and the uncertainty within ring estimates in all figures.](#)

126  
127 We used two sets of observations for  $\theta$  to evaluate CABLE's simulated soil hydrology. The first dataset is from neutron probe  
128 measurements monitored at two locations in each ring every 10 to 21 days (lower frequency in 2017), covering the period  
129 January 2013 to July 2019. These data are collected at 12 different depths: 25 cm intervals from 25 to 150 cm depth, and 50  
130 cm intervals from 150 to 450 cm depth. [The neutron probe counts are converted to  \$\theta\$  via the site specific linear correlation](#)  
131 [between the raw reading of neutron probe and the lab measured soil  \$\theta\$  sampled at the same depth as probes \(Gimeno et al.](#)  
132 [2018a\).](#) The second dataset is daily derived measurements from frequency-domain reflectometers (CS650, Campbell Scientific  
133 Australia, Garbutt, Qld.) at each ring, monitoring to a depth of 25 cm and covering the period January 2013 to December 2019.

## 134 2.3 Model description

135 CABLE is a LSM that can be used in stand-alone mode with prescribed meteorological forcing (Haverd et al., 2013; Ukkola  
136 et al., 2016b; Yang et al., 2020), or coupled to the Australian Community Climate and Earth System Simulator (ACCESS (Bi  
137 et al., 2013; Law et al., 2017)) or the Weather and Research Forecasting (WRF) model (Decker et al., 2017; Hirsch et al.,  
138 2019b) to provide energy, water and momentum fluxes to the lower atmosphere. The standard version of CABLE has been  
139 widely evaluated (De Kauwe et al., 2015; Li et al., 2012; Lorenz et al., 2014; Ukkola et al., 2016b; Wang et al., 2011; Williams  
140 et al., 2009) and the model's overall performance in simulating energy, water and energy fluxes is in line with other LSMs  
141 (Best et al., 2015). A detailed description of model components can be found in Kowalczyk et al. (2006) and Wang et al.  
142 (2011). The version of CABLE used here includes multiple process updates (Decker, 2015; Decker et al., 2017; Kala et al.,  
143 2015).

### 144 2.3.1 Hydrology scheme

145 We use the hydrology scheme from Decker (2015) that includes an improved representation of sub-surface hydrology similar  
146 to that implemented in the Community Land Model (Lawrence and Chase, 2007; Oleson et al., 2008). Saturation- and  
147 infiltration-excess runoff generation mechanisms are represented, and a dynamic groundwater component with aquifer water  
148 storage is included. CABLE uses six soil layers covering a depth to 4.6 m and allows for vertical heterogeneity in soil  
149 parameters. The scheme solves the vertical redistribution of soil water following the modified Richards equation (Decker and  
150 Zeng, 2009):

$$152 \frac{\partial \theta}{\partial t} = - \frac{\partial}{\partial z} K \frac{\partial}{\partial z} (\Psi - \Psi_E) - F_{soil} \quad (1)$$

153  
154 where  $\theta$  is the volumetric water content of the soil ( $\text{mm}^3 \text{ mm}^{-3}$ ),  $K$  ( $\text{mm s}^{-1}$ ) is the hydraulic conductivity,  $\Psi$  (mm) is the soil  
155 matric potential,  $\Psi_E$  (mm) is the equilibrium soil matric potential,  $z$  (mm) is soil depth and  $F_{soil}$  ( $\text{mm mm}^{-1} \text{ s}^{-1}$ ) is the sum of  
156 subsurface runoff and  $E_{tr}$  (Decker, 2015). A [2522.8](#) m deep unconfined aquifer is simulated below the 6-layer soil column by  
157 incorporating a simple water balance model:

$$159 \frac{dW_{aq}}{dt} = q_{re} - q_{aq,sub} \quad (2)$$

160  
161 where  $W_{aq}$  (mm) is the mass of water in the aquifer,  $q_{aq,sub}$  ( $\text{mm s}^{-1}$ ) the subsurface runoff removed from aquifer and  $q_{re}$  ( $\text{mm}$   
162  $\text{s}^{-1}$ ) the water flux between the aquifer and the bottom soil layer, computed by the modified Darcy's law as  
163

$$q_{re} = K_{aq} \frac{(\Psi_{aq} - \Psi_n) - (\Psi_{E, aq} - \Psi_{E, n})}{z_{wtd} - z_n} \quad (3)$$

where  $K_{aq}$  ( $\text{mm s}^{-1}$ ) is the hydraulic conductivity within the aquifer,  $\Psi_{aq}$  and  $\Psi_{E, aq}$  (mm) are the soil matric potential and the equilibrium soil matric potential for the aquifer, and  $\Psi_n$  and  $\Psi_{E, n}$  (mm) are the soil matric potential and the equilibrium soil matric potential for the bottom soil layer.  $z_{wtd}$  and  $z_n$  (mm) are the depth of the water table and the lowest soil layer, respectively. The groundwater aquifer is assumed to sit above an impermeable layer of rock, giving a bottom boundary condition of

$$q_{out} = 0 \quad (4)$$

Subsurface runoff ( $q_{sub}$ ,  $\text{mm s}^{-1}$ ) is calculated from

$$q_{sub} = \sin \frac{\bar{d}_z}{d_l} \hat{q}_{sub} e^{-\frac{z_{wtd}}{f_p}} \quad (5)$$

where  $\frac{\bar{d}_z}{d_l}$  is the mean subgrid-scale slope,  $\hat{q}_{sub}$  ( $\text{mm s}^{-1}$ ) is the maximum rate of subsurface drainage assumed to be achieved when the whole soil column is saturated and  $f_p$  is a tunable parameter.  $q_{sub}$  is generated within the aquifer and for each saturated soil layer below the third soil layer.

### 2.3.2 Soil evaporation ( $E_s$ )

The computation of  $E_s$  ( $\text{kg m}^{-2} \text{s}^{-1}$ ) considers the subgrid-scale soil moisture heterogeneity within a grid square (Decker, 2015), and is given as

$$E_s = F_{sat} E_s^* + (1 - F_{sat}) \beta_s E_s^* \quad (6)$$

where  $F_{sat}$  is the saturated fraction of a grid cell,  $E_s^*$  ( $\text{kg m}^{-2} \text{s}^{-1}$ ) is the potential evaporation without soil moisture stress, and  $\beta_s$  is an empirical soil moisture stress factor (see below) that limits evaporation as water becomes limiting in the top soil layer (Sakaguchi and Zeng, 2009).  $E_s^*$  is given by

$$E_s^* = \frac{\rho_a (q_{sat}(T_{srf}) - q_a)}{r_g} \quad (7)$$

where  $\rho_a$  ( $\text{kg m}^{-3}$ ) is the air density,  $q_{sat}(T_{srf})$  ( $\text{kg kg}^{-1}$ ) is the saturated specific humidity at the surface temperature,  $q_a$  ( $\text{kg kg}^{-1}$ ) is the specific humidity of the air and  $r_g$  ( $\text{s m}^{-1}$ ) is the aerodynamic resistance term.

$\beta_s$  is computed as:

$$\beta_s = 0.25 \left( 1 - \cos \left( \pi \frac{\theta_{unsat}}{\theta_{fc}} \right) \right)^2 \quad (8)$$

where  $\theta_{unsat}$  ( $\text{mm}^3 \text{mm}^{-3}$ ) is the volumetric water content in the unsaturated portion of the top soil layer (top 2 cm), and  $\theta_{fc}$  ( $\text{mm}^3 \text{mm}^{-3}$ ) is the field capacity in the top soil layer.



195 **2.3.3 Transpiration ( $E_{tr}$ )**

196 CABLE's canopy is represented using a two-leaf model, which computes photosynthesis, stomatal conductance,  $E_{tr}$  ( $\text{kg m}^{-2}$   
 197  $\text{s}^{-1}$ ) and leaf temperature separately for sunlit and shaded leaves.  $E_{tr}$  (for each sunlit/shaded leaf) is calculated following the  
 198 Penman-Monteith equation:

199  
 200 
$$E_{tr} = \frac{\Delta R_{n*} + C_p M_a D_l (g_h + g_r)}{\lambda \left( \Delta + \gamma \left( \frac{g_h + g_r}{g_w} \right) \right)} \quad (9)$$

201 where  $\lambda$  ( $\text{J kg}^{-1}$ ) is the latent heat of vapourisation,  $D_l$  (Pa) is the vapour pressure deficit at the leaf surface,  $C_p$  ( $\text{J kg}^{-1} \text{K}^{-1}$ ) is  
 202 the air heat capacity,  $M_a$  ( $\text{kg mol}^{-1}$ ) is the molar mass of air,  $\Delta$  ( $\text{Pa K}^{-1}$ ) is the slope of the curve relating saturation vapour  
 203 pressure to air temperature and  $\gamma$  ( $\text{Pa K}^{-1}$ ) is the psychrometric constant.  $g_h$ ,  $g_r$ , and  $g_w$  ( $\text{mol m}^{-2} \text{s}^{-1}$ ) are the conductances for  
 204 heat, radiation and water, respectively.  $R_{n*}$  ( $\text{W m}^{-2}$ ) is the non-isothermal net radiation calculated as:

205  
 206 
$$R_{n*} = R_n - C_p M_a (T_a - T_l) g_r \quad (10)$$

207  
 208 where  $R_n$  ( $\text{W m}^{-2}$ ) is the net radiation under isothermal conditions and  $T_a$  and  $T_l$  is the air and leaf temperature (K),  
 209 respectively.

210  
 211  $g_w$  is calculated as:

212  
 213 
$$g_w^{-1} = g_a^{-1} + g_b^{-1} + g_s^{-1} \quad (11)$$

214  
 215 where  $g_a$  ( $\text{mol m}^{-2} \text{s}^{-1}$ ) is canopy aerodynamic conductance, and  $g_b$  ( $\text{mol m}^{-2} \text{s}^{-1}$ ) is leaf boundary layer conductance for free  
 216 and forced convection (Kowalczyk et al., 2006).  $g_s$  ( $\text{mol m}^{-2} \text{s}^{-1}$ ) is the leaf stomatal conductance following Medlyn et al.(2011):

217  
 218 
$$g_s = g_0 + 1.6 \left( 1 + \frac{g_1 \beta}{\sqrt{D_l}} \right) \frac{A}{C_s} \quad (12)$$

219  
 220 where  $A$  ( $\mu\text{mol m}^{-2} \text{s}^{-1}$ ) is the photosynthetic rate,  $C_s$  ( $\mu\text{mol mol}^{-1}$ ) is the  $\text{CO}_2$  concentration at the leaf surface,  $\beta$  (unitless) is  
 221 the soil moisture stress factor on plants,  $g_0$  ( $\text{mol m}^{-2} \text{s}^{-1}$ ) and  $g_1$  ( $\text{kPa}^{0.5}$ ) are fitted parameters representing the residual stomatal  
 222 conductance when  $A = 0$  and the sensitivity of conductance to the assimilation rate, respectively.  $g_1$  reflects the plant's water  
 223 use strategy and was derived for each plant functional type in CABLE (De Kauwe et al., 2015) based on a global synthesis of  
 224 stomatal behaviour (Lin et al., 2015).  $\beta$  is calculated as:

225  
 226 
$$\beta = \sum_{i=1}^n f_{root,i} \frac{\theta_i - \theta_{w,i}}{\theta_{f_c,i} - \theta_{w,i}} \quad (13)$$

227  
 228 where  $\theta_i$ ,  $\theta_{f_c,i}$  and  $\theta_{w,i}$  ( $\text{mm}^3 \text{mm}^{-3}$ ) are the soil moisture content, the field capacity and wilting point for soil layer  $i$ , and  $f_{root,i}$   
 229 is the root mass fraction of soil layer  $i$ .

230  
 231 CABLE does not have the capacity to simulate interacting water fluxes between the understorey and overstorey vegetation.  
 232 Instead, it uses a “tiling” approach (fractionally weights separate simulations). As a result, comparisons between CABLE's  $E_s$   
 233 and data-derived  $E_s$  during wetter periods would be expected to be an underestimate as we only consider the fluxes from the

234 overstorey trees. To quantify the effect of the understorey transpiration on the water balance, we also ran an extra simulation  
235 for the grass understorey at this site with the same setting as *Watr* (see below) but using CABLE default grass physiology  
236 parameters and a fixed LAI ( $1 \text{ m}^2 \text{ m}^{-2}$  – site average). The estimated multi-year mean transpiration of  $0.94 \text{ mm d}^{-1}$  can be  
237 regarded as an upper estimate since the simulation does not consider grass dynamics, overstorey rainfall interception, or water  
238 and energy competition between tree and grass. Not accounting for understorey transpiration will lead to an overestimate of  
239 moisture availability in the soil profile.

## 241 2.4 Experiment design

242 We conducted a series of model experiments based on weaknesses identified in previous LSM evaluation studies. In our  
243 experiments, we deliberately adopted a “layering” approach: sequentially resolving a key systematic model bias and then  
244 layering additional experiments to examine how much additional benefit each experiment added to model performance. [We  
245 choose to first resolve a soil evaporation bias as it affects ET partitioning; however, its importance is limited to the top soil  
246 layers and particularly during the period following rain. We then modified the initial water table depth as this fundamentally  
247 affects the root-zone soil moisture state. Next, we explored assumptions related to soil column discretisation and parameters,  
248 and further optimised key hydraulic parameters to improve overall soil moisture biases. We choose to explore parameter  
249 assumptions at this point in the experimental set up as the previous experiments aimed to resolve existing biases that affected  
250 the overall soil moisture availability. Finally, we explored alternative soil moisture stress functions as the last step because this  
251 factor integrates, and arises from, the soil moisture state. The experimental order allowed us to probe model biases in a  
252 systematic way but it is important to note that there is no perfect experimental order and alternative permutations would lead  
253 to subtly different interpretation of results. In fact, this is what commonly happens in model evaluation that explore a single  
254 factor \(e.g. the soil moisture stress factor\). Each experiment is described in detail below and a summary of all experiments is  
255 provided in Table 1.](#)

256  
257 In all experiments, LAI and physiology parameters were prescribed based on site observations (Table S1). We tested the  
258 difference of using the CABLE default evergreen broadleaf physiology parameters (Figure S1) compared to using the site  
259 physiology (Figure 2) and found that using site parameters increases  $E_r$  (due to higher  $g_l$  and increased sensitivity of carbon  
260 fixation to temperature), in turn reducing  $E_s$  and  $\theta$ .

261  
262 All experiments were spun-up using an iterative process, recycling all years of the meteorological forcing until the change  
263 between two iterations was  $< 0.001 \text{ m}^3 \text{ m}^{-3}$  for soil moisture,  $< 0.01^\circ\text{C}$  for soil temperature and  $< 0.0001 \text{ m}^3 \text{ m}^{-3}$  for aquifer  
264 moisture.

### 265 2.4.1 Control experiment (*Ctl*)

266 The control simulation (*Ctl*) uses the default version of CABLE with 6 soil layers (but with site [specific](#) physiology and LAI).  
267 The soil hydraulic parameters are derived via the pedotransfer functions based on Cosby et al. (1984) using the global soil  
268 texture map from the Harmonized World Soil Database (Fischer et al., 2008). Soil parameters are the same throughout the 6-  
269 layer soil column.

### 270 2.4.2 Increasing the resistance for soil evaporation (*Sres*)

271 Previous studies suggest LSMs vary widely in their simulation of  $E_s$ . For example, De Kauwe et al. (2017) found that in an  
272 ensemble of 10 models, six models simulated  $\sim 2$ -3.5 times more  $E_s$  than the other four models. LSMs also partition  
273 evapotranspiration between  $E_r$  and  $E_s$  with a high degree of uncertainty (Lian et al., 2018). At many sites, high springtime

274 evapotranspiration can be linked to excessive  $E_s$  rather than  $E_{tr}$  (Decker et al., 2017; Ukkola et al., 2016b) and can lead to  
275 biases in soil moisture availability later in the growing season.

276  
277 We note that models have attempted to resolve this  $E_s$  bias through different mechanisms, for example, via a litter layer (Haverd  
278 and Cuntz, 2010; Sakaguchi and Zeng, 2009) or by limiting  $E_s$  via adding the resistances to vapour diffusion through the soil  
279 pores and the surface viscous sublayer (Decker et al., 2017; Haghghi and Or, 2015; Swenson and Lawrence, 2014). Here, we  
280 adopt a simple litter layer (Decker et al., 2017) which adds an additional surface resistance to vapour and heat fluxes but does  
281 not limit rainfall infiltration. After adding the additional resistance,  $E_s^*$  is calculated as

$$282 \quad E_s^* = \frac{\rho_a(q_{sat}(T_{srf}) - q_a)}{r_g + r_{lit}} \quad (14)$$

284  
285 where  $r_{lit}$  is the resistance ( $s\ m^{-1}$ ) for diffusion via the litter layer of depth  $z_l$  (m) (default value is 10cm) given by:

$$286 \quad r_{lit} = \frac{z_l}{d} \quad (15)$$

288  
289 where  $d$  is the diffusivity of water vapour in air ( $m^2\ s^{-1}$ ).

#### 290 **2.4.3. Water table initialisation experiment (*Watr*)**

291 The parameters governing the groundwater aquifer saturation and water table depth are both highly uncertain and difficult to  
292 constrain from observations. We investigated the importance of a correct water table depth to the simulation soil moisture and  
293 water fluxes. To better match the observed water table depth at EucFACE, we changed the aquifer  $\theta_{sat}$  from the model default  
294 value ( $0.235\ m^3\ m^{-3}$ ) to  $\theta_{sat}$  set based on the observed soil texture at 4.5m depth ( $0.448\ m^3\ m^{-3}$ ), [which reduced the initial](#)  
295 [saturation of aquifer from 100% to 52%](#). This has the effect of lowering the water table to  $\sim 12$  m, in line with observations  
296 (Gimeno et al. 2018a).

#### 297 **2.4.4 High resolution soil experiment (*Hi-Res*)**

298 Most LSMs assume that soil parameters are depth invariant through the soil profile. The number of layers typically ranges  
299 from a minimum of 2, through to 6 in CABLE and up to 20 in Community Land Model (Lawrence et al., 2019). Here, we test  
300 the impact of increasing the number of discrete soil layers, informed by observations of the varying vertical soil texture at the  
301 EucFACE site. Recent soil maps (e.g. SoilGrids (Hengl et al., 2017)) have begun to capture vertical variations in soil texture,  
302 so it is important to test the impact in LSMs.

303  
304 We performed two sub-experiments in *Hi-Res*:

- 305  
306 1) the number of vertical soil layers was increased from 6 to 31 (~~for later maximising to match~~ the [utilization resolution](#) of  
307 [observed](#) soil texture ~~observations which was sampled at 15-cm intervals~~) (*Hi-Res-1*);
- 308  
309 2) soil parameters were allowed to vary vertically based on observed soil texture (*Hi-Res-2*).

310  
311 To implement vertically varying soil parameters, the observed fractions of sand, clay and silt, soil bulk density and organic  
312 carbon fraction were taken from measurements at each ambient CO<sub>2</sub> ring and interpolated into 31 layers using the  $\sim 15$  cm  
313 resolution of the observations. Soil hydraulic parameters are computed using the same pedotransfer functions as used in *Ctl*

314 but allowed to vary with depth based on the vertical heterogeneity in soil properties. Since CABLE assumes the aquifer's  
315 suction at saturation and Clapp and Hornberger parameter are identical to the bottom soil layer, adding depth-varying soil  
316 parameters in *Hi-Res-2* also changes these two parameters for the aquifer.

#### 317 **2.4.5 Soil parameter optimisation experiment (*Opt*)**

318 As it is impractical to measure soil hydraulic parameters at the global scale, pedotransfer functions are used to convert widely  
319 measured soil properties into global soil hydraulic parameter datasets (Dai et al., 2013; Kishné et al., 2017). However, most of  
320 the widely-used pedotransfer functions are empirical equations derived from the limited experimental samples measured for  
321 the specific locations (Cosby et al., 1984; van Genuchten, 1980). The adaptability of these pedotransfer functions are always  
322 confined by their underrepresentation of some soil properties, such as soil aggregate stability or macroporosity (Puhlmann and  
323 von Wilpert, 2012) and can lead to a divergence in model parameters (Van Looy et al., 2017; Zhang and Schaap, 2019). As a  
324 result, parameter calibrations are common to obtain more accurate representations.

325  
326 First, we used the site observations to adjust the plant wilting point ( $\theta_w$ ) and volumetric water content at saturation ( $\theta_{sat}$ ). With  
327 each layer as  $\theta_w$  is changed, the corresponding residual water content ( $\theta_{res}$ ) was also updated to ensure it was smaller than  $\theta_w$ .  
328  $\theta_{sat}$  was set to the observed maximum from the daily data measured by frequency-domain reflectometers for the top 30 cm.  
329 ~~Due to muted variability in deeper soil layers,  $\theta_{sat}$  below 30 cm was not adjusted.~~  $\theta_{sat}$  was not adjusted below 30 cm as the  
330 ~~observed maximum  $\theta_{sat}$  is unlikely to represent saturated conditions due to lower soil moisture variability at depth.~~  $\theta_w$  and  $\theta_{res}$   
331 were adjusted for each 15 cm layer in the soil column using the observed minimum (OBS<sub>min</sub>) in each layer. When OBS<sub>min</sub> was  
332 below the default  $\theta_{res}$ ,  $\theta_{res}$  was set to OBS<sub>min</sub> and  $\theta_w$  to OBS<sub>min</sub> + 0.0001 m<sup>3</sup> m<sup>-3</sup>. When  $\theta_{res} < \text{OBS}_{\min} < \theta_w$ ,  $\theta_w$  was set to OBS<sub>min</sub>.  
333 Otherwise  $\theta_{res}$  and  $\theta_w$  were not adjusted.

334  
335 Second, we optimised  $K_{sat}$  to test whether allowing the soil column to drain faster or slower reduced model biases in the soil  
336 moisture profile.  $K_{sat}$  was optimised by minimising errors between modelled and observed soil moistures over total column  
337 and in the top 0.25 m, transpiration and soil evaporation.

#### 338 **2.4.6 Soil water limitation on transpiration ( $\beta$ -*hvr*d and $\beta$ -*exp*)**

339 LSMs use different, empirical functional forms to represent the effect of water stress on vegetation function (see Introduction).  
340 To explore the influence of different functional formulations, we compare CABLE's default function (Equation 13) to two  
341 alternative parameterisations: 1) an alternative hypothesis that plants optimise their root water uptake to exploit resources, with  
342 the wettest soil layer determining soil water stress on plants ( $\beta$ -*hvr*d; Haverd et al., 2016) and 2) a site calibrated function to  
343 observations at EucFACE over the top 1.5 m ( $\beta$ -*exp*; Yang et al., 2020). We note that a number of studies have tested different  
344 water stress formulations (e.g. Egea et al. (2011)) but this process evaluation is often decoupled from analysis of other  
345 contributing errors (e.g. LAI and/or soil hydrology).

346  
347 The  $\beta$ -*hvr*d method tends to predict less water stress than the default function (Equation 13) in CABLE when the moisture is  
348 unevenly distributed within the soil column. This function takes the form:

$$349 \beta = \max (\alpha_i \cdot \delta_i, i = 1, n) \quad (16)$$

350  
351 where:

352  
353

$$\alpha = \begin{cases} \left(\frac{\theta - \theta_w}{\theta_s}\right)^{\gamma / (\theta - \theta_w)} & , (\theta - \theta_w) > 0 \\ 0 & , (\theta - \theta_w) \leq 0 \end{cases} \quad (17)$$

where  $\alpha_i$  is proportional to the root “shut-down” function (Lai and Katul, 2000) in the  $i$ th soil layer, and  $\delta_i = 1$  if there are roots at the  $i$ th soil layer, otherwise  $\delta_i = 0$ .  $n$  is the total number of soil layers.

In  $\beta$ -exp,  $\beta$  is an exponential function calibrated to the site observations. Yang et al. (2020) fitted a non-linear relationship between  $\beta$  and  $\theta$ , based on a fitted exponent term  $q$  (0.425, Table S1) using measured soil moisture over the top 1.5 m from EucFACE:

$$\beta = \sum_{i=1}^n f_{root,i} \left( \frac{\theta_i - \theta_{w,i}}{\theta_{fc,i} - \theta_{w,i}} \right)^q \quad (18)$$

#### 2.4.7. Evaluation metrics

We used five metrics to evaluate CABLE’s performance compared to observations. Root Mean Squared Error (RMSE) and Mean Bias Error (MBE) were used to evaluate overall performance and Pearson’s correlation coefficient ( $r$ ) the temporal variability. The absolute differences in modelled and observed 5<sup>th</sup> (P5) and 95<sup>th</sup> (P95) percentile values were used to evaluate the lower and upper tails, respectively. As the observed data have gaps, the metrics were only calculated for days for which observations were available.

### 3. Results

#### 3.1 Control experiment (*Ctl*)

We first evaluate the *Ctl* simulation by comparing to the observed  $E_{tr}$ ,  $E_s$  and soil moisture (Figure 2). Overall, CABLE simulates  $E_{tr}$  similarly to the observed ( $r = 0.85$ , RMSE = 0.34 mm d<sup>-1</sup>, Table 2) but overestimates peak  $E_{tr}$ , which is particularly evident in the austral summer of 2014, by 0.54 mm d<sup>-1</sup> on average (P95 in Table 2). However, it is worth noting that during the summer of 2014 there was an outbreak of psyllids leading to canopy defoliation (Gherlenda et al., 2016), which may explain part of the model-data mismatch (CABLE only accounts for [this canopy defoliation](#) via a decline in LAI [but not other damage e.g. to the phloem](#)). Compared to  $E_{tr}$ , CABLE simulates  $E_s$  less well ( $r = 0.65$ , RMSE = 0.70 mm d<sup>-1</sup>; Table 2, Figure 2a). Whilst the observations exclude rainy days when CABLE reaches its highest  $E_s$ , CABLE systematically overestimates mean and peak  $E_s$  during observed days by 0.12 and 1.22 mm d<sup>-1</sup>, respectively (MBE and P95 in Table 2). Figure 2b shows that CABLE has a significant wet bias in the top 0.25 m soil moisture and never falls to the observed values below 0.08 m<sup>3</sup> m<sup>-3</sup> during drier periods. Given the excessive  $E_s$  (Figure 2a), the failure of the top 25 cm to dry out is surprising and suggests either a parameterisation error and/or the impact of not accounting for understory transpiration (see methods). Figure 2c shows that the wet bias in soil moisture is systematic, extending throughout the soil column (particularly between 2.5 and 4.5 m).

Taken together, the evaluation of the *Ctl* simulation implies that a good simulation in one evaporative flux (Figure 2a) can be achieved for the wrong physical reasons and is associated with major systematic biases in the simulation of near surface and root zone soil moisture (Figures 2b-d).

#### 3.2 Increasing the resistance to soil evaporation experiment (*Sres*)

Implementing a litter layer (a proxy for additional surface resistance to  $E_s$ ) in CABLE significantly reduces  $E_s$  from 305 mm y<sup>-1</sup> in *Ctl* to 204 mm y<sup>-1</sup> in *Sres* (Figure 3a, Table 3). The simulation of peak  $E_s$  is significantly improved compared to *Ctl* but

CABLE still overestimated  $E_s$  (MBE and P95 in Table 2); this is particularly evident during an observed dry period in late 2013. As a consequence of lower  $E_s$  compared to *Ctl*,  $E_{tr}$  is markedly increased (from 341 mm y<sup>-1</sup> in *Ctl* to 402 mm y<sup>-1</sup> in *Sres*, Table 3) which implies a reduction in soil moisture stress in the profile (lower  $\beta$ ). This degrades the simulated  $E_{tr}$  relative to the observations for all metrics, particularly from around October 2013 to March 2014 (Figure 3b). With an overall reduction in evapotranspiration, CABLE displays a considerably worse soil moisture profile (cf. Figure 3c and 2d) and a larger wet bias through most of the soil profile (cf. Figure 3d and 2e). Thus, resolving the  $E_s$  bias alone, relocated the bias to other model components, where it less easily identified using commonly available measurements.

### 3.3 Water table (*Watr*) and vertical soil structure (*Hi-Res*) experiments

Figure 4 shows that reconciling the parameterisation of the aquifer  $\theta_{sat}$  with the bottom layer  $\theta_{sat}$  based on observed soil properties (*Watr*) leads to a marked improvement in the simulated soil moisture profile. By increasing the point of saturation and initialising the aquifer to be drier [relative to saturation](#), CABLE simulates a more negative water potential in the aquifer, which promotes vertical drainage and results in a realistic water table depth in line with observations (simulated and observed ~ 12 m over 2013-2014). The wet bias in the top 3 m is markedly reduced (cf. Figure 4d and 2e); however, the model now has a clear dry bias between 3 and 4.6 m. The simulated moisture in the top 0.25 m (Figure 4b) is now also in better agreement with the observations (0.06 m<sup>3</sup> m<sup>-3</sup> in *Watr* vs 0.11 m<sup>3</sup> m<sup>-3</sup> in *Sres*, MBE in Table S2). Finally, both the bias in the simulated  $E_s$  and  $E_{tr}$  is reduced by > 0.2 mm d<sup>-1</sup> (MBE in Table 2), particularly evident during the summer of 2014.

Increasing the number of soil layers from 6 to 31 (*Hi-Res-1*; Figure S2), leads to a small improvement in the simulated temporal correlation (0.78 in *Watr* vs 0.83 in *Hi-Res-1*; Table 2) of soil moisture, without notably changing the fluxes. The higher vertical resolution in the soil enables the transition of the dry-down to be better captured, in contrast to the alternating wet and dry patterns associated with the coarse vertical resolution at depths between 0.5-3.0 m depth in *Watr* (cf. Figure S2c and 4c).

Allowing the soil parameters to vary vertically based on observed soil texture (*Hi-Res-2*; Figure 5) reduces the dry bias in the lower layers in *Watr* (Figure 4) but leads to a greater wet bias throughout the upper soil profile (< 3 m). The error in soil moisture has reduced in the mean, low and high extremes compared to *Ctl* and *Sres* (MBE, P5 and P95 in Table 2). Overall, Figure 5 highlights a simulation with CABLE where the fluxes of  $E_{tr}$ ,  $E_s$  and soil moisture are all in reasonable agreement with the observations (Table 3), albeit with an overestimation of peak  $E_{tr}$ .

### 3.4 Soil parameter optimisation experiment (*Opt*)

To address the simulated wet bias in the soil moisture profile (Figure 5), we used observations to prescribe the critical soil hydraulic parameters  $\theta_w$  and  $\theta_{sat}$  (Figure S3) and to optimise  $K_{sat}$  (Figure S4 and S5). Prescribing  $\theta_w$  and  $\theta_{sat}$  led to a much improved “operating range” of soil moisture in the top 0.25 cm (Figure S3b) but did not reduce the wet bias in the soil profile or solve the slow drainage after rainfall events (cf. Figure 5c and Figure 2c). Overall, these changes had a limited effect on simulated  $E_{tr}$  (344 mm y<sup>-1</sup> vs 327 mm y<sup>-1</sup> in *Hi-Res-2* in Table 3) as might be expected because the profile was sufficiently wet as not to limit evapotranspiration, especially in the root zone of top 1.5 m (Figure S5d). A reduction of the simulated  $E_s$  (138 mm y<sup>-1</sup> vs 165 mm y<sup>-1</sup> in *Hi-Res-2*; Table 3) was mainly associated with the drier shallow soil (Figure S5b). The optimised  $K_{sat}$  increased drainage speed (cf. Figure 5c and Figure 3c) and [lowered/reduced](#) the overall wet biases (0.04 m<sup>3</sup> m<sup>-3</sup> in *Opt* vs 0.07 m<sup>3</sup> m<sup>-3</sup> in *Hi-Res-2*, MBE in Table 2).

### 3.5 Soil water limitation on transpiration ( $\beta$ -*hvr*d and $\beta$ -*exp*)

Replacing CABLE’s default soil moisture stress function with an alternative hypothesis that plants maximise their root water uptake to exploit resources ( $\beta$ -*hvr*d) led to a substantial increase in  $E_{tr}$  ([Figure 6a](#)) relative to experiment *Opt* (from 344 mm y



431 <sup>1</sup> to 403 mm y<sup>-1</sup>, Table 3) because the function assumes that the soil water stress on plants is determined by the availability of  
432 water in the wettest soil layer. This overestimation of  $E_{tr}$  led to a small reduction in the wet soil moisture bias (cf. Figure S5d  
433 and Figure 6d).

434  
435 Figure 7 shows the impact of using a site-calibrated  $\beta$  function ( $\beta$ -exp) (Yang et al., 2020). Using this function also increased  
436  $E_{tr}$  relative to experiment  $Opt$  (from 344 mm y<sup>-1</sup> to 373 mm y<sup>-1</sup>, Table 3), degrading the simulation relative to the standard  $\beta$   
437 ( $Opt$ ). In both experiments, owing to the overall simulated wet bias in the soil profile, a decreased sensitivity to soil moisture  
438 availability (either using  $\beta$ -hvr<sub>d</sub> or  $\beta$ -exp) did not improve simulated evapotranspiration.

### 439 3.6 Implications for Drought

440 Improving the simulation of  $E_{tr}$ ,  $E_s$  and soil moisture in LSMs is important on the seasonal timescale, but the increasing use of  
441 models to simulate future drought highlights the value of examining how these improvements impact the expression of drought  
442 in LSMs. We focus on a period of extensive drought across southeastern Australia that begins in October 2017 and extends to  
443 the end of 2019. Due to rainfall data availability, we focus on the dry-down period between October 2017 and September 2018.  
444

445 Figure 8 shows selected fluxes during the drought period over which the soil slowly dries in the observations and in the models  
446 (Figure 8a) and the shallow soil moisture was close to wilting point (e.g. Figure 6b). The  $Sres$  experiment maintains the highest  
447 soil moisture throughout the drought period and  $\beta$ -hvr<sub>d</sub> the lowest, with the range across all experiments exceeding 0.1 m<sup>3</sup> m<sup>-3</sup>.  
448 These soil moisture variations lead to inconsistent behaviour in  $E_{tr}$  (Figure 8b) due to resulting differences in  $\beta$  (Figure 8c).  
449  $\beta$ -hvr<sub>d</sub>  $E_{tr}$  is very high despite having the driest soil moisture (Figure 8a) ~~because it is derived from~~. Because the calculation  
450 uses the wettest soil layer where there is, this leads to notably muted temporal variation (Figure 8c) relative to the other methods  
451 for  $\beta$ . The differences in soil moisture, and as a result  $\beta$ , lead to differences in  $E_{tr}$  (Figure 8b) of 20 ~ 50 mm month<sup>-1</sup> until  
452 autumn/winter (~April-July) when lower evaporative demand leads to more similar simulations. Through summer  
453 (~November-February),  $E_s$  varies markedly from around 10 mm month<sup>-1</sup> ( $\beta$ -hvr<sub>d</sub>) to 35 mm month<sup>-1</sup> ( $Ctl$ ) (Figure 8d). The  
454 differences in  $E_{tr}$  and  $E_s$  are mirrored by differences in  $Q_H$  (Figure 8e) which varies by > 30 W m<sup>-2</sup> between the experiments  
455 between October 2017 and March 2018.

456  
457 Integrating the simulations over the drought period highlights the differences in simulating water stress (expressed as  $\beta$ )  
458 between experiments. Figure 9a shows that  $Sres$  and  $\beta$ -hvr<sub>d</sub> maintain a relatively high  $\beta$  during drought periods (median > 0.7)  
459 while the remaining experiments are notably lower. The  $\beta$ -exp simulates median values of 0.63, which is notably higher than  
460 the  $Hi-Res-2$  of 0.33 and  $Opt$  of 0.46. This difference originates from the calibrated functional form shown in Figure 9b, where  
461 the exponent in the  $\beta$ -exp function leads to a delay in the onset (point of inflection) of moisture stress relative to the default  
462 linear function used in CABLE. Overall, in a single model, parameterisations led to a difference of 98 % ~~between~~ relative to  
463 the averaged median of all the simulations for  $\beta$  simulated  $\beta$  during drought.

### 464 3.7 Implications for Heatwaves

465 The link between soil moisture and heatwaves is well known (Teuling et al., 2010) and is usually examined in the context of  
466 a drying soil leading to higher  $Q_H$  relative to  $Q_E$  (as our simulations are uncoupled, we cannot examine the consequences of  
467 these changes on the boundary layer).  
468

469 Figure 10 shows a heatwave that occurred on 19-22 January 2018, where the air temperatures exceeded 35°C for four  
470 consecutive days and exceeded 40°C on the last day (Figure 10a). The evaporative fraction during the daytime (9am - 4pm) is  
471 shown in Figure 10b and highlights a remarkable range from ~0.2 in  $Ctl$  to ~0.7 in  $\beta$ -hvr<sub>d</sub>, suggesting much stronger

472 evaporative cooling in  $\beta$ -*hvr*d. An obvious diurnal variation in evaporative fraction is characterised by a progressive decline  
473 from a peak at 9 am.  $Q_E$  gradually declines through the four heatwave days (Figure 10c) in all experiments. At the beginning  
474 of the heatwave (19 January) daytime  $Q_E$  ranges from  $> 200 \text{ W m}^{-2}$  in  $\beta$ -*hvr*d and *Sres* to around  $100 \text{ W m}^{-2}$  in *Ctrl*, *Watr*, *Hi-*  
475 *Res-1*, *Hi-Res-2* and *Opt*. The differences in  $Q_E$  are mirrored by differences in  $Q_H$  (Figure 10d) with daytime fluxes varying  
476 on the heatwave days by more than  $150 \text{ W m}^{-2}$ .

477  
478 Figures 10c and 10d also highlight a key divergence in energy partitioning due to parameterisations and the emergent  
479 interactions with soil water availability. Models that show a pronounced midday depression in  $Q_E$  (e.g. *Ctrl*, *Watr* and *Hi-Res-*  
480 *2*) due to increasing diurnal vapour pressure deficit ( $D$ ) and soil moisture stress, show earlier diurnal peaks in  $Q_H$  (Figure 10d).  
481 By contrast, parameterisations that are less limited by  $\beta$  (e.g.  $\beta$ -*hvr*d despite the lowest soil moisture, Figure 10a), see an  
482 emergent shift in peak in  $Q_H$  to later in the afternoon. When coupled, these emergent differences due to the role of soil water  
483 availability – and importantly, how this is translated in canopy gas exchange via  $\beta$  – may have implications for surface  
484 interactions with the boundary layer.

485  
486 Given the importance of the role of  $D$  during heat extremes, to further explore the role of high  $D$  on simulated  $E_{tr}$ , we plotted  
487 modelled and measured transpiration as a function of binned  $D$  (Figure 11). At high  $D$  ( $> 2 \text{ kPa}$ ), simulated  $E_{tr}$  is overestimated.  
488 As the mismatch between simulated  $E_{tr}$  and observed occurs at both low and high  $D$  (Figure 11), ~~it implies that~~ the model  
489 improvements are unlikely to simply ~~be~~ relate to an alternative parameterisation of the stomatal sensitivity to  $D$ , but instead  
490 ~~suggests~~ suggests a missing mechanism to limit canopy gas exchange with increasing  $D$ . The impact of this overestimation  
491 would likely have greater significance for summers with concurrent heatwaves and droughts (compound events that are  
492 common in Australia), as during heatwaves ~~when  $D$  is higher~~ the model would overestimate  $E_{tr}$ , using up available soil  
493 moisture.

#### 494 4. Discussion and conclusions

495 Land surface schemes used in climate models range in complexity and different approaches translate into contrasting  
496 predictions of the exchange of carbon, energy and water (Fisher and Koven, 2020). Perhaps critically, how strongly the land  
497 is coupled to the atmosphere also varies widely and is typically attributed to soil moisture variability (Brantley et al., 2017;  
498 Dirmeyer, 2011; Guo et al., 2006). A key component of LSMs is how soil moisture availability impacts processes internal to  
499 the land model and, in turn, how these impact fluxes of carbon and water.

500  
501 In this paper we used a rich observational dataset from a water-limited site that experiences both high temperatures and  
502 pronounced periods of low rainfall, to explore a range of alternative model-based assumptions ~~at multiple time scales (daily to~~  
503 ~~annual)~~ within a single model framework. We focussed on the capacity of the model to simulate both the state (soil moisture)  
504 and the fluxes (evapotranspiration and its components) ~~at a water-limited site. Whilst our analysis is site specific, the issues~~  
505 ~~indicated here have been reported to lead to systematic biases in LSMs across multiple sites (Ukkola et al., 2016a; Trugman~~  
506 ~~et al., 2018).~~ We demonstrated that the default simulation (*Ctrl*, Figure 2) was able to simulate good transpiration fluxes but for  
507 the wrong reasons: erroneously high soil evaporation with a marked wet soil moisture bias. Errors of this kind may not have  
508 been identified in previous LSM evaluations against eddy covariance data which mostly focus on  $Q_E$  (Best et al., 2015). Our  
509 results highlight a potential bias in model evaluations due to a limited capacity to assess soil moisture or the partitioning of  
510 evapotranspiration. We demonstrated that poor model behaviour could be overcome via four key steps: (i) reducing soil  
511 evaporation biases; (ii) correctly initialising the aquifer moisture content, (iii) adjusting soil parameters to match site conditions  
512 and (iv) replacing the function used to constrain transpiration as soil moisture becomes limiting. ~~Since our study attempts to~~

articulate the common issues in the simulated dry conditions in LSMs, we anticipate our findings would be applicable in many water-limited conditions, but equally, more mesic systems too.

Given the critical role of drought-prone ecosystems in contributing to interannual variability in the land CO<sub>2</sub> sink size (Ahlström et al., 2015), our approach has the potential to improve the representation of these systems in models. We note that despite these improvements we still simulated a persistent wet soil moisture bias (e.g. Figure 5d). We think on balance this is unlikely to originate from not simulating a seasonal understorey transpiration as *β-hvrd*, which grossly overestimated overstorey transpiration and did not sufficiently dry out the profile (cf. Figure S5d and Figure 6d). Instead the soil moisture bias must relate to CABLE's representation of sub-surface processes.

### *Soil evaporation*

Biases in soil evaporation are commonplace in model intercomparisons (De Kauwe et al., 2017). LSMs commonly overestimate soil evaporation especially under a sparse canopy or over bare land (De Kauwe et al., 2017; Swenson and Lawrence, 2014), suggesting this is a key model weakness. Errors in soil evaporation are rarely isolated in models and often contribute to errors in transpiration by limiting soil moisture availability later in the growing season (Ukkola et al., 2016b) as well as affecting the distribution of shallow versus deep soil moisture draw-down during drought. A number of approaches have been suggested to improve simulations (Haghighi and Or, 2015; Haverd and Cuntz, 2010; Lehmann et al., 2018; Or and Lehmann, 2019). Errors in soil evaporation are rarely isolated in models and often contribute to errors in transpiration by limiting soil moisture availability later in the growing season (Ukkola et al., 2016b) as well as affecting the distribution of shallow versus deep soil moisture draw-down during drought. Here we used a simple approach that increased resistance to surface evaporation, approximating the role of surface litter (Decker et al., 2017). At this site, this increased resistance to surface evaporation improved agreement with observations (*Sres*; Figure 3a) but did not resolve all biases. Notably, soil evaporation was not directly measured at the site, but instead derived from the change in observed soil moisture over the top 5 cm, while ignoring days following rain (when the soil evaporative flux would likely be largest-) (Gimeno et al., 2018a). As these fluxes also containsuch, it contains soil moisture changes due to the-transpiration offrom a seasonal grass understorey, but ignores evaporation below the top 5 cm, complicating model evaluation-is complicated. As many, Nevertheless, the magnitude of CABLE biases points to systematic errors in soil evaporation that do not merely arise from observational uncertainty. Many soil evaporation schemes used in LSMs lack a physical basis-(e.g., estimating soil evaporation from aerodynamic resistance and an empirical soil water stress and ignoring the role of soil pores);. However, a number of studies using alternative process-based schemes have been shown to improve individual model simulations (Haverd and Cuntz, 2010; Lehmann et al., 2018; Or and Lehmann, 2019). For example, Swenson and Lawrence (2014) introduced a dry surface layer-based soil evaporation resistance into CLM to depict water diffusion from dry soil, reducing biases in evapotranspiration and total water storage relative to FLUXNET-MTE and GRACE datasets. Based on a pore-scale model (Haghighi and Or, 2015), Decker et al. (2017) added the resistances of capillary-viscous and boundary layer to CABLE soil evaporation scheme and lowered the positive  $E_s$  bias in springtime and improved seasonality of evapotranspiration. Hence, a focussed intercomparison of competing approaches against data originating from different ecosystems would be a valuable area of future direction-work.

### *Aquifer initialisation*

Our results showed that the initialisation of the aquifer moisture store was critical to an improved simulation of the soil moisture profile. By default, CABLE equilibrates the aquifer state by assuming almost complete saturation at the start. If, as happened with the *Ctl*, the aquifer is initialised too wet, the simulated water table is too high and the water potential in the aquifer is unlikely to be below the lowest soil moisture layer, impeding vertical aquifer recharge. When we initialised from a drier starting position (*Wat*), the simulated soil moisture profile matched the observed better. There are a number of implications of this

554 result. First, it obviously implies that LSMs that incorporate groundwater schemes need to be careful about aquifer initialisation  
555 because it strongly affects soil moisture dynamics. Second, there is no obvious solution to this initialisation and spin-up  
556 problem because drainage into the aquifer is a slow process, and it may take hundreds of years to reach a realistic equilibrium  
557 state. For global simulations, this suggests the need to *a priori* initialise the starting aquifer state and to assess against satellite-  
558 based products like GRACE (Döll et al., 2014; Niu et al., 2007) or implement off-line spin-up using meteorological forcing  
559 consistent with the subsequent simulations. However, while spin-up with observations is attractive, when the resulting states  
560 are taken into a coupled global model, inconsistencies are inevitable. Third, CABLE currently assumes an identical spin-up  
561 approach for the aquifer as the soil moisture, iterating until state changes between sequences of years are smaller than some  
562 threshold. LSMs that employ similar iteration approaches (Gilbert et al., 2017) are likely to encounter similar problems as  
563 CABLE because the rate of drainage into the aquifer is very slow, leading to negligible changes between iterations and thus,  
564 satisfying the criteria for equilibrium.

### 565 Aquifer initialisation

566 Our results showed that the initialisation of the aquifer moisture store was critical to an improved simulation of the soil moisture  
567 profile. By default, CABLE equilibrates the aquifer state by assuming almost complete saturation at the start. If, as happened  
568 with the *Ctl*, the aquifer is initialised too wet, the simulated water table is too high and the water potential in the aquifer is  
569 unlikely to be below the lowest soil moisture layer, impeding vertical aquifer recharge. When we initialised from a drier starting  
570 position (*Watr*), the simulated soil moisture profile matched the observed better, with implications for other models using  
571 similar groundwater schemes (e.g. CLM4.5, Noah-MP, JULES and LEAFHYDRO). First, our results imply that LSMs that  
572 incorporate groundwater schemes need to be careful about aquifer initialisation because this strongly affects soil moisture  
573 dynamics. Second, there is no obvious solution to this initialisation and spin-up problem because drainage into the aquifer is a  
574 slow process, and it may take hundreds of years to reach a realistic equilibrium state. For global simulations, this suggests the  
575 need to *a priori* initialise the starting aquifer state and to assess against satellite-based products like GRACE (Döll et al., 2014;  
576 Niu et al., 2007) or implement off-line spin-up using meteorological forcing consistent with the subsequent simulations.  
577 However, while spin-up with observations is attractive, when the resulting states are incorporated into a coupled global model,  
578 inconsistencies are inevitable. Third, CABLE currently assumes an identical spin-up approach for the aquifer as the soil  
579 moisture, iterating until state changes between sequences of years are smaller than some threshold. LSMs that employ similar  
580 iteration approaches (Gilbert et al., 2017) are likely to encounter similar problems as CABLE because the rate of drainage into  
581 the aquifer is very slow, leading to negligible changes between iterations and thus satisfying the criteria for equilibrium.

### 582 *Soil layers and pedotransfer functions*

583 LSMs typically define a fixed number of soil layers globally, anywhere up to 20 layers. Most LSMs assume constant  
584 parameters across the entire soil profile, either using an experimental look-up table based on limited measurements and  
585 uncertain soil classification or estimating parameters from empirical pedotransfer functions. We explored the implications of  
586 these assumptions by first increasing the number of soil layers to match the number of observed layers (*Hi-Res-1*; Figure S2)  
587 and then implementing soil parameters that varied vertically based on site texture (*Hi-Res-2*; Figure 5). Increasing the vertical  
588 resolution had a small impact on the soil moisture and fluxes but did improve the temporal variability in soil moisture compared  
589 to observations. The use of site soil texture better depicts the moisture distribution in the soil profile but led to a slightly  
590 degraded soil moisture simulation. These results again highlight uncertainties in the translation of soil texture information to  
591 soil hydraulic parameters for water retention and hydraulic conductivity via the empirical functions, which are derived from  
592 limited observations (Van Looy et al., 2017). The development in pedotransfer functions (Van Looy et al., 2017) and the value  
593 of parameter calibration as an alternative in site-level studies. The availability of site soil information at via machine learning  
594 or multi-model ensemble provides new avenues to reduce errors from parameters (Zhang and Schaap, 2017; Dai et al., 2019).

595 [High-resolution global soil datasets \(e.g. SoilGrids, Hengl et al., 2017\) covering multiple soil layers up to 2m depth offer](#)  
596 [opportunities to improve LSM simulations of soil moisture by incorporating depth-varying soil parameters. It is noteworthy](#)  
597 [that these global datasets of soil hydraulic parameters \(Montzka et al, 2017; Zhang et al., 2019\) have existed for several years](#)  
598 [but have not been widely used. Furthermore, at the EucFACE ~~furthersite~~, the observed soil texture information](#) enabled the  
599 separation of parameter uncertainties from biases in process representations and model structural errors, a [highly](#)-valuable step  
600 in better constraining LSM simulations.

#### 601 *Calibration of soil hydraulic parameters*

602 A number of studies have used satellite-derived (passive and active microwave) estimates of soil moisture to optimise soil  
603 hydraulic parameters in the top few soil layers (Harrison et al., 2012). Clearly these approaches are a potential way to constrain  
604 LSMs globally given the plethora of satellite observations extending back to the 1970s. However, these approaches implicitly  
605 assume that improving near-surface soil moisture translates to improvements over the entire soil column, an assumption not  
606 supported by our results. Whilst the use of observation-constrained  $\theta_w$  and  $\theta_{sat}$  over top 0.3 m improved the simulated dynamics  
607 of shallow soil, it did not result in a large reduction in the bias simulated in deeper soil moisture layers (Figure S3). At this  
608 site, the inability to significantly improve soil moisture dynamics through calibration of soil hydraulic conductivity against  
609 observed soil moisture data likely relates to the complexity of the soil profile, which contains two clay layers at depth (30-80  
610 cm and 300-450 cm). This vertical texture complexity meant that it was difficult to obtain unique parameter solutions that  
611 would sufficiently improve vertical drainage, whilst simultaneously simulating moisture dynamics well (Figure S5). ~~However,~~  
612 ~~the neutron probe measurement of soil moisture also involves the calibration of instruments and assumptions of soil~~  
613 ~~characteristics. It is possible that some of the differences between our simulation and the observations are therefore associated~~  
614 ~~with measurement errors. Overall, our sensitivity experiments demonstrated that there is likely to be an upper bound to model~~  
615 ~~improvement achievable from adjusting empirical pedotransfer functions, the water retention curve and hydraulic conductivity~~  
616 ~~functions despite the utilisation of the high-quality soil texture data at the site. As such, our study~~On the other hand, the neutron  
617 probe measurements of soil moisture used for calibration also involve uncertainties (Gimeno et al. 2018a). The soil moisture  
618 estimates were derived by fitting two distinctive linear relationships between soil volumetric water content and raw neutron  
619 probe counts (see Figure S6) for clay (below 3m) and non-clay soil (above 3m). As a result, the observation error would be  
620 greatest in layers where the soil type differs from the assumed soil type at that depth. However, the fitted relationships were  
621 robust, since clay soils largely dominated the deeper profile (below 3 m depth) and sand soils mostly dominated shallow profile  
622 (above 3m depth). Overall, our sensitivity experiments suggests that optimising soil properties alone is not sufficient and  
623 calibration exercises should also account for vegetation information to reduce biases in sub-surface processes.

#### 624 *Water stress functions*

625 Studies commonly highlight the functions used to limit photosynthesis and stomatal conductance with water stress as a key  
626 weakness among models. The lack of theory in this space (Medlyn et al., 2016) has led to models employing a range of  
627 functions encompassing different shapes and sensitivities that are not constrained by data. [Trugman et al. \(2018\) explored the](#)  
628 [role of soil moisture stress in simulated “potential” gross primary productivity \(GPP\) among CMIP5 models and argued that](#)  
629 [the functional form used to represent the effect of soil moisture stress was the major driver of carbon cycle uncertainty. Here](#)  
630 [we deliberately attempted to first resolve model biases through other avenues \(e.g. soil evaporation, soil parameterisation\),](#)  
631 [because it is likely that model biases originate from multiple sources \(e.g. leaf area, soil moisture dynamics, etc.\). We were](#)  
632 [subsequently able to assess the capacity to then further improve model behaviour via the functional forms used to represent](#)  
633 [water stress.](#)



635 ~~More recently, We examined three alternative water stress functions: the linear  $\theta$ -based function used in *Ctl* (common among~~  
636 ~~models, e.g. SDGVM, Orchidee-CN and JULES), a non-linear  $\theta$ -based  $\beta$  ( $\beta$ -*exp*) calibrated for this site from Yang et al. (2020)~~  
637 ~~and plant hydraulic (Christoffersen et al., 2016; Xu et al., 2016) and stomatal optimality approaches have emerged to fill the~~  
638 ~~theoretical gap (Sperry et al., 2017) but are yet to be widely adopted in LSMs (but see (Eller et al., 2020; De Kauwe et al.,~~  
639 ~~2020; Kennedy et al., 2019; Sabot et al., 2020)). Trugman et al. (2018) explored the role of soil moisture stress in simulated~~  
640 ~~“potential” gross primary productivity (GPP) among CMIP5 models and argued that the functional form used to represent the~~  
641 ~~effect of soil moisture stress was the major driver of carbon cycle uncertainty. Here we deliberately attempted to first resolve~~  
642 ~~model biases through other avenues (e.g. soil evaporation, soil parameterisation), because it is likely that model biases originate~~  
643 ~~from multiple sources (e.g. leaf area, soil moisture dynamics, etc.). We were subsequently able to assess the capacity to then~~  
644 ~~further improve model behaviour via the functional forms used to represent water stress.~~

645  
646 ~~We examined three alternative water stress functions: the function used in *Ctl* (common among models), a function based on~~  
647 ~~Haverd et al. (2016) ( $\beta$ -*hvr*) and a calibrated  $\beta$  ( $\beta$ -*exp*) for this site based on Yang et al. (2020).~~ Haverd et al. (2016)  
648 hypothesised that plants optimise their root water uptake, only limiting function when water in the deepest accessible soil layer  
649 becomes limiting. They further argued that this behaviour did not vary among sites (and so species). De Kauwe et al. (2015)  
650 previously tested this hypothesis and demonstrated that it led to an underestimation of the effect of moisture stress, inconsistent  
651 with observations. Our results again show that this hypothesis is not supported by data and led to an overestimation of  
652 transpiration (Figure 6) and little evidence of moisture stress (Figure 9b). Integrated over the drought periods, we found that  
653 after reducing other model biases, the use of the calibrated  $\beta$ -*exp* function did reduce the simulated soil moisture stress (median  
654  $\beta = 0.63$  vs  $0.33$  in *Hi-Res-2* and  $0.46$  in *Opt*; Fig 9). Overall, the various experiments show markedly different median  $\beta$   
655 (ranging from  $0.67$  to  $0.99$ , considering all simulated years), consistent with previous evaluations that have highlighted  
656 differences in simulated  $\beta$  across models (De Kauwe et al., 2017; Medlyn et al., 2016; Powell et al., 2013; Trugman et al.,  
657 2018). However, our results highlight that differences originate as much from alternative model assumptions and biases (e.g.  
658 soil evaporation, soil parameters) as the functional forms themselves. Alternatives to the  $\beta$  functions have emerged to fill the  
659 theoretical gap, including plant hydraulic (Christoffersen et al., 2016; Xu et al., 2016) and stomatal optimality approaches  
660 (Sperry et al., 2017) but are yet to be widely adopted in LSMs (but see Eller et al., 2020; De Kauwe et al., 2020; Kennedy et  
661 al., 2019; Sabot et al., 2020). Replacing the empirical soil water stress factor by these plant physiology schemes reduces model  
662 arbitrariness associated with the representation of soil water stress and reduces the simulated biases in transpiration either over  
663 water deficit regions or areas with obvious dry seasons (Bonan et al., 2014; De Kauwe et al., 2020; Sabot et al., 2020). We can  
664 envison a wider application of these processes-based models will offer a chance to improve water stress representation in  
665 more LSMs.

## 666 *Heatwaves*

667 Differences between the versions of CABLE lead to a different initial soil moisture state at the beginning of a heatwave ranging  
668 from  $\sim 0.15 \text{ m}^3 \text{ m}^{-3}$  ( $\beta$ -*hvr*) to  $\sim 0.23 \text{ m}^3 \text{ m}^{-3}$  (*Sres*) (Figure 10). In addition to the impact of the initial state, differences  
669 between parameterisation also affect estimates of  $\beta$ , leading to large divergences in evaporative cooling during a heatwave.  
670 Consequently, some versions of CABLE respond to the heatwave with a depression/reduction of  $Q_E$  and a peak of higher  $Q_H$   
671 during the early to mid-afternoon 12 – 4 pm while other simulations maintain a high  $Q_E$  during the earlier parts of the day this  
672 period and shift the peak of high  $Q_H$  shifts to later in the afternoon (4-6 pm) (Figure 10c-d). The magnitudes of  $Q_E$  and  $Q_H$   
673 between simulations are also substantially different: *Ctl* would amplify a heatwave, warming and drying the boundary layer  
674 while  $\beta$ -*hvr* would tend to moisten and (relatively) cool the boundary layer. Many studies have shown that the land surface  
675 can play a key role in amplifying heatwaves (Hirsch et al., 2019a; Miralles et al., 2014; Teuling et al., 2010) and LSMs exhibit  
676 systematic biases in representing this feedback (Sippel et al., 2017; Ukkola et al., 2018b). For a mega-heatwave like the 2010



677 European [Heatwave](#), the contribution of local surface to sensible heat anomaly was  $\sim 20 \text{ W m}^{-2}$  (Schumacher et al.,  
678 2019). However, our results show the differences between parameterisations within a single LSM can result in a greater  
679 divergence than this value. Therefore, these feedbacks can be substantially changed through different parameterisations and,  
680 if coupled to an atmospheric model, may be large enough to change the frequency and magnitude of heatwaves within a model.  
681

682 We also showed that at high  $D$ , our model overestimated transpiration, which would have consequences for subsequent soil  
683 moisture availability. Renchon et al. (2018) recently highlighted this point at the Cumberland Plains eddy covariance site  
684 which neighbours the EucFACE site. Yang et al. (2019) showed that the MAESPA canopy gas exchange model similarly  
685 overpredicted ~~transpiration~~ [transpiration](#) at high  $D$ , leading to an overprediction of annual transpiration by 19%. By examining  
686 leaf gas exchange data, they demonstrated that the reduction of transpiration could be attributed to non-stomatal limitation of  
687 photosynthesis at high  $D$ . Although non-stomatal limitation is commonly observed under low soil moisture content (e.g. Zhou  
688 et al. 2013) and implemented in a number of LSMs (De Kauwe et al., 2015), non-stomatal limitation at high  $D$  has been much  
689 less commonly reported and is not, to our knowledge, implemented in any LSMs. To echo Yang et al. (2019), further data on  
690 non-stomatal limitation at high  $D$  should be a priority, to determine whether this mechanism is sufficiently widespread to  
691 warrant inclusion in LSMs.

### 692 *Future directions*

693 We have shown that improving a LSM for one water flux is achievable, but improving a model to capture individual  
694 components of evapotranspiration and the associated soil moisture state is more challenging. No single step is sufficient in  
695 isolation and if observations only constrain one element of a model, biases can be transferred within a model. This can lead to  
696 a tendency to hide biases in seldom observed states because soil moisture profiles are rarely measured along with aboveground  
697 fluxes. International observational networks (e.g. FLUXNET; Baldocchi et al., 2001) rarely report  $Q_E$ ,  $Q_H$  and soil moisture  
698 through and below the root zone simultaneously, although soil moisture profiles do sometimes exist. Expanding observational  
699 networks to include soil moisture profiles could accelerate model development. The EucFACE dataset holds exceptional  
700 promise as a means of evaluating model simulations and refining new theory. It is freely available, contains observations of  
701 the complete water balance and captures responses to both droughts and heatwaves. More broadly, our results also speak for  
702 the importance of multi-variable model evaluation methods for LSMs (e.g. iLAMB; Hoffman et al., 2017, and [HTESSEL](#),  
703 [Orth et al., 2017](#)).

704  
705 [While the focus of our study has been primarily on the parameterisations of hydrology and sub-surface processes, we did aim](#)  
706 [to minimise the uncertainties from the non-hydrological factors by using site characteristics, such as the aerodynamic](#)  
707 [conductance \(determined by setting the canopy height\) and photosynthesis parameters \(e.g. maximum carboxylation rate and](#)  
708 [maximum rate of electron transport\). However, due to the significance of these non-hydrological factors on evapotranspiration](#)  
709 [\(e.g. Breil et al., 2020\), further evaluation should be considered in future studies.](#)  
710

711 Finally, our results imply that caution is needed in the interpretation of simulated heatwaves and droughts in coupled climate  
712 models. The feedback via the land surface is a key component and as our model experiments show, a range of alternative  
713 approaches can produce very different coupling between the land and the atmosphere if embedded in a coupled model. Despite  
714 the difficulties in acquiring datasets of the complete water balance, as a community we need to find an avenue to better assess  
715 (coupled) model predictions. Critical Zone Observatory Networks (Brantley et al., 2017) may be one means to better constrain  
716 models, but in all likelihood, targeted field campaigns that collect observations of soil moisture, eddy-covariance and the  
717 boundary layer are also needed.  
718

719 *Code and data availability.* CABLE code is available at <https://trac.nci.org.au/trac/cable/wiki> after registration. Here, we use  
720 CABLE revision r7278. Scripts for plotting and processing model outputs are available at  
721 [https://github.com/bibivking/Evaluate\\_CABLE\\_EucFACE.git](https://github.com/bibivking/Evaluate_CABLE_EucFACE.git). EucFACE observations are publicly available in Western  
722 Sydney University's archive <http://doi.org/10.4225/35/5ab9bd1e2f4fb> (Gimeno et al., 2018b), and in  
723 <https://doi.org/10.5281/zenodo.3610698> (Yang, 2019).

724

725 *Author contributions.* MGDK, MM, AJP and AMU put forward the general scientific questions, designed the model  
726 experiments, investigated the simulations and drafted the manuscript. TEG, BEM, JY and DSE endeavoured to collect, to  
727 process and to correct the EucFACE observations. All authors participated in the discussion and revision of the manuscript.

728

729 *Competing interest.* The authors declare that they have no conflict of interest.

730

731 *Acknowledgements.* MM, MGDK, AJP and AMU acknowledge support from the Australian Research Council (ARC) Centre  
732 of Excellence for Climate Extremes (CE170100023). MM acknowledges support from the UNSW University International  
733 Postgraduate Award (UIPA) Scheme. MGDK and AJP acknowledge support from the ARC Discovery Grant (DP190101823).  
734 MGDK, TEG, BEM, JY and DSE, acknowledge support from the NSW Research Attraction and Acceleration Program  
735 (RAAP). EucFACE is supported by the Australian Commonwealth government in collaboration with the Western Sydney  
736 University. The facility was constructed as part of the nation-building initiative of the Australian government. We thank the  
737 National Computational Infrastructure at the Australian National University, an initiative of the Australian Government, for  
738 access to supercomputer resources. We sincerely appreciate Burhan Amiji and Vinod Kumar for the collection of the neutron  
739 probe measurements. We also thank Craig Barton and Craig McNamara for their excellent technical support and Mingkai Jiang  
740 for the suggestion on the EucFACE understorey.

## 741 **References**

742 Ahlström, A., Raupach, M. R., Schurgers, G., Smith, B., Arneth, A., Jung, M., Reichstein, M., Canadell, J. G., Friedlingstein,  
743 P., Jain, A. K., Kato, E., Poulter, B., Sitch, S., Stocker, B. D., Viovy, N., Wang, Y. P., Wiltshire, A., Zaehle, S. and Zeng,  
744 N.: The dominant role of semi-arid ecosystems in the trend and variability of the land CO<sub>2</sub> sink, *J. Geophys. Res. Sp.*  
745 *Phys.*, 120(6), 4503–4518, doi:10.1002/2015JA021022, 2015.

746 Allen, C. D., Breshears, D. D. and McDowell, N. G.: On underestimation of global vulnerability to tree mortality and forest  
747 die-off from hotter drought in the Anthropocene, *Ecosphere*, 6(8), 1–55, doi:10.1890/ES15-00203.1, 2015.

748 Ault, T. R.: On the essentials of drought in a changing climate, *Science*, 368(6488), 256–260, doi:10.1126/science.aaz5492,  
749 2020.

750 Baldocchi, D., Falge, E., Gu, L., Olson, R., Hollinger, D., Running, S., Anthoni, P., Bernhofer, C., Davis, K., Evans, R.,  
751 Fuentes, J., Goldstein, A., Katul, G., Law, B., Lee, X., Malhi, Y., Meyers, T., Munger, W., Oechel, W., Paw, K. T.,  
752 Pilegaard, K., Schmid, H. P., Valentini, R., Verma, S., Vesala, T., Wilson, K. and Wofsy, S.: FLUXNET: A new tool to  
753 study the temporal and spatial variability of ecosystem–scale carbon dioxide, water vapor, and energy flux densities, *Bull.*  
754 *Am. Meteorol. Soc.*, 82(11), 2415–2434, doi:10.1175/1520-0477(2001)082<2415:FANTTS>2.3.CO;2, 2001.

755 Best, M. J., Pryor, M., Clark, D. B., Rooney, G. G., Essery, R. . L. H., Ménard, C. B., Edwards, J. M., Hendry, M. A., Porson,  
756 A., Gedney, N., Mercado, L. M., Sitch, S., Blyth, E., Boucher, O., Cox, P. M., Grimmond, C. S. B. and Harding, R. J.:

- 757 The Joint UK Land Environment Simulator (JULES), model description – Part 1: Energy and water fluxes, *Geosci. Model*  
758 *Dev.*, 4(3), 677–699, doi:10.5194/gmd-4-677-2011, 2011.
- 759 Best, M. J., Abramowitz, G., Johnson, H. R., Pitman, A. J., Balsamo, G., Boone, A., Cuntz, M., Decharme, B., Dirmeyer, P.  
760 A., Dong, J., Ek, M., Guo, Z., Haverd, V., van den Hurk, B. J. J., Nearing, G. S., Pak, B., Peters-Lidard, C., Santanello,  
761 J. A., Stevens, L. and Vuichard, N.: The plumbing of land surface models: benchmarking model performance, *J.*  
762 *Hydrometeorol.*, 16(3), 1425–1442, doi:10.1175/JHM-D-14-0158.1, 2015.
- 763 Bi, D., Dix, M., Marsland, S., O’Farrell, S., Rashid, H., Uotila, P., Hirst, A., Kowalczyk, E., Golebiewski, M., Sullivan, A.,  
764 Yan, H., Hannah, N., Franklin, C., Sun, Z., Vohralik, P., Watterson, I., Zhou, X., Fiedler, R., Collier, M., Ma, Y., Noonan,  
765 J., Stevens, L., Uhe, P., Zhu, H., Griffies, S., Hill, R., Harris, C. and Puri, K.: The ACCESS coupled model: description,  
766 control climate and evaluation, *Aust. Meteorol. Oceanogr. J.*, 63(1), 41–64, doi:10.22499/2.6301.004, 2013.
- 767 [Bonan, G. B., Williams, M., Fisher, R. A. and Oleson, K. W.: Modeling stomatal conductance in the earth system: linking leaf](#)  
768 [water-use efficiency and water transport along the soil–plant–atmosphere continuum, \*Geosci. Model Dev.\*, 7\(5\), 2193–](#)  
769 [2222, doi:10.5194/gmd-7-2193-2014, 2014.](#)
- 770 Brantley, S. L., McDowell, W. H., Dietrich, W. E., White, T. S., Kumar, P., Anderson, S. P., Chorover, J., Lohse, K. A., Bales,  
771 R. C., Richter, D. D., Grant, G. and Gaillardet, J.: Designing a network of critical zone observatories to explore the living  
772 skin of the terrestrial Earth, *Earth Surf. Dyn.*, 5(4), 841–860, doi:10.5194/esurf-5-841-2017, 2017.
- 773 [Breil, M., Davin, E., and Rechid, D.: What determines the sign of the evapotranspiration response to afforestation in the](#)  
774 [European summer? \*Biogeosciences Discuss.\*, <https://doi.org/10.5194/bg-2020-275>, 2020.](#)
- 775 Christoffersen, B. O., Gloor, M., Fauset, S., Fyllas, N. M., Galbraith, D. R., Baker, T. R., Kruijt, B., Rowland, L., Fisher, R.  
776 A., Binks, O. J., Sevanto, S., Xu, C., Jansen, S., Choat, B., Mencuccini, M., McDowell, N. G. and Meir, P.: Linking  
777 hydraulic traits to tropical forest function in a size-structured and trait-driven model (TFS v.1-Hydro), *Geosci. Model*  
778 *Dev.*, 9(11), 4227–4255, doi:10.5194/gmd-9-4227-2016, 2016.
- 779 Ciais, P., Reichstein, M., Viovy, N., Granier, A., Ogée, J., Allard, V., Aubinet, M., Buchmann, N., Bernhofer, C., Carrara, A.,  
780 Chevallier, F., De Noblet, N., Friend, A. D., Friedlingstein, P., Grünwald, T., Heinesch, B., Keronen, P., Knohl, A.,  
781 Krinner, G., Loustau, D., Manca, G., Matteucci, G., Miglietta, F., Ourcival, J. M., Papale, D., Pilegaard, K., Rambal, S.,  
782 Seufert, G., Soussana, J. F., Sanz, M. J., Schulze, E. D., Vesala, T. and Valentini, R.: Europe-wide reduction in primary  
783 productivity caused by the heat and drought in 2003, *Nature*, 437(7058), 529–533, doi:10.1038/nature03972, 2005.
- 784 Clark, M. P., Fan, Y., Lawrence, D. M., Adam, J. C., Bolster, D., Gochis, D. J., Hooper, R. P., Kumar, M., Leung, L. R.,  
785 Mackay, D. S., Maxwell, R. M., Shen, C., Swenson, S. C. and Zeng, X.: Improving the representation of hydrologic  
786 processes in Earth System Models, *Water Resour. Res.*, 51(8), 5929–5956, doi:10.1002/2015WR017096, 2015.
- 787 Collins, L., Bradstock, R. A., Resco de Dios, V., Duursma, R. A., Velasco, S. and Boer, M. M.: Understorey productivity in  
788 temperate grassy woodland responds to soil water availability but not to elevated [CO<sub>2</sub>], *Glob. Chang. Biol.*, 24(6), 2366–  
789 2376, doi:10.1111/gcb.14038, 2018.
- 790 Collins, M., Knutti, R., Arblaster, J., Dufresne, J.-L., Fichefet, T., Friedlingstein, P., Gao, X., Gutowski, W. J., Johns, T.,  
791 Krinner, G., Shongwe, M., Tebaldi, C., Weaver, A. J. and Wehner, M.: Long-term climate change: projections,  
792 commitments and irreversibility, in *Climate Change 2013: The Physical Science Basis. Contribution of Working Group*  
793 *I to the Fifth Assessment Report of the Intergovernmental Panel on Climate Change*, edited by T. F. Stocker, D. Qin, G.-

- 794 K. Plattner, M. Tignor, S. K. Allen, J. Boschung, A. Nauels, Y. Xia, V. Bex, and P. M. Midgley, pp. 1029–1136,  
795 Cambridge University Press, Cambridge, United Kingdom and New York, NY, USA., 2013.
- 796 Cosby, B. J., Hornberger, G. M., Clapp, R. B. and Ginn, T. R.: A statistical exploration of the relationships of soil moisture  
797 characteristics to the physical properties of soils, *Water Resour. Res.*, 20(6), 682–690, doi:10.1029/WR020i006p00682,  
798 1984.
- 799 Crous, K. Y., Ósvaldsson, A. and Ellsworth, D. S.: Is phosphorus limiting in a mature Eucalyptus woodland? Phosphorus  
800 fertilisation stimulates stem growth, *Plant Soil*, 391(1–2), 293–305, doi:10.1007/s11104-015-2426-4, 2015.
- 801 Dai, Y., Shangguan, W., Duan, Q., Liu, B., Fu, S. and Niu, G.: Development of a China dataset of soil hydraulic parameters  
802 using pedotransfer functions for land surface modeling, *J. Hydrometeorol.*, 14(3), 869–887, doi:10.1175/JHM-D-12-  
803 0149.1, 2013.
- 804 [Dai, Y., Xin, Q., Wei, N., Zhang, Y., Shangguan, W., Yuan, H., Zhang, S., Liu, S. and Lu, X.: A Global High-Resolution Data](#)  
805 [Set of Soil Hydraulic and Thermal Properties for Land Surface Modeling, \*J. Adv. Model. Earth Syst.\*, 11\(9\), 2996–3023,](#)  
806 [doi:10.1029/2019MS001784, 2019.](#)
- 807 Decker, M.: Development and evaluation of a new soil moisture and runoff parameterization for the CABLE LSM including  
808 subgrid-scale processes, *J. Adv. Model. Earth Syst.*, 7(4), 1788–1809, doi:10.1002/2015MS000507, 2015.
- 809 Decker, M. and Zeng, X.: Impact of modified Richards equation on global soil moisture simulation in the Community Land  
810 Model (CLM3.5), *J. Adv. Model. Earth Syst.*, 1(3), 1–22, doi:10.3894/JAMES.2009.1.5, 2009.
- 811 Decker, M., Or, D., Pitman, A. and Ukkola, A.: New turbulent resistance parameterization for soil evaporation based on a  
812 pore-scale model: Impact on surface fluxes in CABLE, *J. Adv. Model. Earth Syst.*, 9(1), 220–238,  
813 doi:10.1002/2016MS000832, 2017.
- 814 Dewar, R., Mauranen, A., Mäkelä, A., Hölttä, T., Medlyn, B. and Vesala, T.: New insights into the covariation of stomatal,  
815 mesophyll and hydraulic conductances from optimization models incorporating nonstomatal limitations to  
816 photosynthesis, *New Phytol.*, 217(2), 571–585, doi:10.1111/nph.14848, 2018.
- 817 Dirmeyer, P. A.: A history and review of the Global Soil Wetness Project (GSWP), *J. Hydrometeorol.*, 12(5), 729–749,  
818 doi:10.1175/JHM-D-10-05010.1, 2011.
- 819 ~~DeHöll~~ Döll, P., Muller, H. S., Schuh, C., Portmann, F. T., Eicker, A., Schmied, H. M., Schuh, C., Portmann, F. T. and Eicker,  
820 A.: Global-scale assessment of groundwater depletion and related groundwater abstractions: Combining hydrological  
821 modeling with information from well observations and GRACE satellites, *J. Am. Water Resour. Assoc.*, 5(3), 2–2,  
822 doi:10.1111/j.1752-1688.1969.tb04897.x, 2014.
- 823 Dosio, A., Mentaschi, L., Fischer, E. M. and Wyser, K.: Extreme heat waves under 1.5 °C and 2 °C global warming, *Environ.*  
824 *Res. Lett.*, 13(5), 054006, doi:10.1088/1748-9326/aab827, 2018.
- 825 Duursma, R. A., Gimeno, T. E., Boer, M. M., Crous, K. Y., Tjoelker, M. G. and Ellsworth, D. S.: Canopy leaf area of a mature  
826 evergreen Eucalyptus woodland does not respond to elevated atmospheric [CO<sub>2</sub>] but tracks water availability, *Glob.*  
827 *Chang. Biol.*, 22(4), 1666–1676, doi:10.1111/gcb.13151, 2016.

- 828 Egea, G., Verhoef, A. and Vidale, P. L.: Towards an improved and more flexible representation of water stress in coupled  
829 photosynthesis–stomatal conductance models, *Agric. For. Meteorol.*, 151(10), 1370–1384,  
830 doi:10.1016/j.agrformet.2011.05.019, 2011.
- 831 Eller, C. B., Rowland, L., Mencuccini, M., Rosas, T., Williams, K., Harper, A., Medlyn, B. E., Wagner, Y., Klein, T., Teodoro,  
832 G. S., Oliveira, R. S., Matos, I. S., Rosado, B. H. P., Fuchs, K., Wohlfahrt, G., Montagnani, L., Meir, P., Sitch, S. and  
833 Cox, P. M.: Stomatal optimization based on xylem hydraulics (SOX) improves land surface model simulation of  
834 vegetation responses to climate, *New Phytol.*, 226(6), 1622–1637, doi:10.1111/nph.16419, 2020.
- 835 Ellsworth, D. S., Anderson, I. C., Crous, K. Y., Cooke, J., Drake, J. E., Gherlenda, A. N., Gimeno, T. E., Macdonald, C. A.,  
836 Medlyn, B. E., Powell, J. R., Tjoelker, M. G. and Reich, P. B.: Elevated CO<sub>2</sub> does not increase eucalypt forest productivity  
837 on a low-phosphorus soil, *Nat. Clim. Chang.*, 7(4), 279–282, doi:10.1038/nclimate3235, 2017.
- 838 Fischer, G., Nachtergaele, F., Prieler, S., van Velthuisen, H.T., Verelst, L. and Wiberg, D.: *Global Agro-ecological Zones*  
839 *Assessment for Agriculture (GAEZ 2008)*. IIASA, Laxenburg, Austria and FAO, Rome, Italy. 2008.
- 840 Fisher, R. A. and Koven, C. D.: Perspectives on the future of land surface models and the challenges of representing complex  
841 terrestrial systems, *J. Adv. Model. Earth Syst.*, 12(4), doi:10.1029/2018MS001453, 2020.
- 842 van Genuchten, M. T.: A closed-form equation for predicting the hydraulic conductivity of unsaturated soils, *Soil Sci. Soc.*  
843 *Am. J.*, 44(5), 892–898, doi:10.2136/sssaj1980.03615995004400050002x, 1980.
- 844 Gherlenda, A. N., Esveld, J. L., Hall, A. A. G., Duursma, R. A. and Riegler, M.: Boom and bust: rapid feedback responses  
845 between insect outbreak dynamics and canopy leaf area impacted by rainfall and CO<sub>2</sub>, *Glob. Chang. Biol.*, 22(11), 3632–  
846 3641, doi:10.1111/gcb.13334, 2016.
- 847 Gilbert, J. M., Maxwell, R. M. and Gochis, D. J.: Effects of water-table configuration on the planetary boundary layer over the  
848 San Joaquin River Watershed, California, *J. Hydrometeorol.*, 18(5), 1471–1488, doi:10.1175/JHM-D-16-0134.1, 2017.
- 849 Gimeno, T. E., Crous, K. Y., Cooke, J., O’Grady, A. P., Ósvaldsson, A., Medlyn, B. E. and Ellsworth, D. S.: Conserved  
850 stomatal behaviour under elevated CO<sub>2</sub> and varying water availability in a mature woodland, edited by D. Whitehead,  
851 *Funct. Ecol.*, 30(5), 700–709, doi:10.1111/1365-2435.12532, 2016.
- 852 Gimeno, T. E., McVicar, T. R., O’Grady, A. P., Tissue, D. T. and Ellsworth, D. S.: Elevated CO<sub>2</sub> did not affect the hydrological  
853 balance of a mature native Eucalyptus woodland, *Glob. Chang. Biol.*, 24(7), 3010–3024, doi:10.1111/gcb.14139, 2018a.
- 854 Gimeno, T. E., McVicar, T. R., O’Grady, A. P., Tissue, D. T. and Ellsworth, D. S.: EucFACE Hydrological and meteorological  
855 measurements from 2012-04-30 to 2014-11-15. Western Sydney University, <http://doi.org/10.4225/35/5ab9bd1e2f4fb>,  
856 2018b.
- 857 Guo, Z., Dirmeyer, P. A., Koster, R. D., Sud, Y. C., Bonan, G., Oleson, K. W., Chan, E., Verseghy, D., Cox, P., Gordon, C.  
858 T., McGregor, J. L., Kanae, S., Kowalczyk, E., Lawrence, D., Liu, P., Mocko, D., Lu, C.-H., Mitchell, K., Malyshev, S.,  
859 McAvaney, B., Oki, T., Yamada, T., Pitman, A., Taylor, C. M., Vasic, R. and Xue, Y.: GLACE: the Global Land–  
860 Atmosphere Coupling Experiment. part II: analysis, *J. Hydrometeorol.*, 7(4), 611–625, doi:10.1175/JHM511.1, 2006.
- 861 Haghghi, E. and Or, D.: Linking evaporative fluxes from bare soil across surface viscous sublayer with the Monin–Obukhov  
862 atmospheric flux-profile estimates, *J. Hydrol.*, 525, 684–693, doi:10.1016/j.jhydrol.2015.04.019, 2015.

- 863 Harrison, K. W., Kumar, S. V., Peters-Lidard, C. D. and Santanello, J. A.: Quantifying the change in soil moisture modeling  
864 uncertainty from remote sensing observations using Bayesian inference techniques, *Water Resour. Res.*, 48(11),  
865 doi:10.1029/2012WR012337, 2012.
- 866 Haverd, V. and Cuntz, M.: Soil–Litter–Iso: A one-dimensional model for coupled transport of heat, water and stable isotopes  
867 in soil with a litter layer and root extraction, *J. Hydrol.*, 388(3–4), 438–455, doi:10.1016/j.jhydrol.2010.05.029, 2010.
- 868 Haverd, V., Raupach, M. R., Briggs, P. R., Canadell, J. G., Isaac, P., Pickett-Heaps, C., Roxburgh, S. H., van Gorsel, E.,  
869 Viscarra Rossel, R. A. and Wang, Z.: Multiple observation types reduce uncertainty in Australia’s terrestrial carbon and  
870 water cycles, *Biogeosciences*, 10(3), 2011–2040, doi:10.5194/bg-10-2011-2013, 2013.
- 871 Haverd, V., Cuntz, M., Nieradzick, L. P. and Harman, I. N.: Improved representations of coupled soil–canopy processes in the  
872 CABLE land surface model (Subversion revision 3432), *Geosci. Model Dev.*, 9(9), 3111–3122, doi:10.5194/gmd-9-3111-  
873 2016, 2016.
- 874 Hengl, T., Mendes de Jesus, J., Heuvelink, G. B. M., Ruiperez Gonzalez, M., Kilibarda, M., Blagotić, A., Shangguan, W.,  
875 Wright, M. N., Geng, X., Bauer-Marschallinger, B., Guevara, M. A., Vargas, R., MacMillan, R. A., Batjes, N. H.,  
876 Leenaars, J. G. B., Ribeiro, E., Wheeler, I., Mantel, S. and Kempen, B.: SoilGrids250m: Global gridded soil information  
877 based on machine learning, edited by B. Bond-Lamberty, *PLoS One*, 12(2), e0169748,  
878 doi:10.1371/journal.pone.0169748, 2017.
- 879 Hirsch, A. L., Evans, J. P., Di Virgilio, G., Perkins-Kirkpatrick, S. E., Argüeso, D., Pitman, A. J., Carouge, C. C., Kala, J.,  
880 Andrys, J., Petrelli, P. and Rockel, B.: Amplification of Australian heatwaves via local land-atmosphere coupling, *J.*  
881 *Geophys. Res. Atmos.*, 124(24), 13625–13647, doi:10.1029/2019JD030665, 2019a.
- 882 Hirsch, A. L., Kala, J., Carouge, C. C., De Kauwe, M. G., Di Virgilio, G., Ukkola, A. M., Evans, J. P. and Abramowitz, G.:  
883 Evaluation of the CABLEv2.3.4 Land Surface Model Coupled to NU-WRFv3.9.1.1 in simulating temperature and  
884 precipitation means and extremes Over CORDEX AustralAsia within a WRF physics ensemble, *J. Adv. Model. Earth*  
885 *Syst.*, 11(12), 4466–4488, doi:10.1029/2019MS001845, 2019b.
- 886 Hoffman, F. M., Koven, C. D., Keppel-Aleks, G., Lawrence, D. M., Riley, W. J., Randerson, J. T., Ahlström, A., Abramowitz,  
887 G., Baldocchi, D. D., Best, M. J., Bond-Lamberty, B., De Kauwe, M. G., Denning, A. S., Desai, A. R., Eyring, V., Fisher,  
888 J. B., Fisher, R. A., Gleckler, P. J., Huang, M., Hugelius, G., Jain, A. K., Kiang, N. Y., Kim, H., Koster, R. D., Kumar,  
889 S. V., Li, H., Luo, Y., Mao, J., McDowell, N. G., Mishra, U., Moorcroft, P. R., Pau, G. S. H., Ricciuto, D. M., Schaefer,  
890 K., Schwalm, C. R., Serbin, S. P., Shevliakova, E., Slater, A. G., Tang, J., Williams, M., Xia, J., Xu, C., Joseph, R. and  
891 Koch, D.: 2016 International Land Model Benchmarking (ILAMB) Workshop Report., 2017.
- 892 Humphrey, V., Zscheischler, J., Ciais, P., Gudmundsson, L., Sitch, S. and Seneviratne, S. I.: Sensitivity of atmospheric CO<sub>2</sub>  
893 growth rate to observed changes in terrestrial water storage, *Nature*, 560(7720), 628–631, doi:10.1038/s41586-018-0424-  
894 4, 2018.
- 895 Kala, J., De Kauwe, M. G., Pitman, A. J., Lorenz, R., Medlyn, B. E., Wang, Y. P., Lin, Y.S. and Abramowitz, G.:  
896 Implementation of an optimal stomatal conductance scheme in the Australian Community Climate Earth Systems  
897 Simulator (ACCESS1.3b), *Geosci. Model Dev.*, 8(12), 3877–3889, doi:10.5194/gmd-8-3877-2015, 2015.
- 898 De Kauwe, M. G., Medlyn, B. E., Zaehle, S., Walker, A. P., Dietze, M. C., Hickler, T., Jain, A. K., Luo, Y., Parton, W. J.,  
899 Prentice, I. C., Smith, B., Thornton, P. E., Wang, S., Wang, Y. P., Wårlind, D., Weng, E., Crous, K. Y., Ellsworth, D. S.,  
900 Hanson, P. J., Seok Kim, H., Warren, J. M., Oren, R. and Norby, R. J.: Forest water use and water use efficiency at



- 901 elevated CO<sub>2</sub>: A model-data intercomparison at two contrasting temperate forest FACE sites, *Glob. Chang. Biol.*, 19(6),  
902 1759–1779, doi:10.1111/gcb.12164, 2013.
- 903 De Kauwe, M. G., Zhou, S.-X. X., Medlyn, B. E., Pitman, A. J., Wang, Y. P. Y. P. P., Duursma, R. A. and Prentice, I. C.: Do  
904 land surface models need to include differential plant species responses to drought? Examining model predictions across  
905 a mesic-xeric gradient in Europe, *Biogeosciences*, 12(24), 7503–7518, doi:10.5194/bg-12-7503-2015, 2015.
- 906 De Kauwe, M. G., Medlyn, B. E., Walker, A. P., Zaehle, S., Asao, S., Guenet, B., Harper, A. B., Hickler, T., Jain, A. K., Luo,  
907 Y., Lu, X., Luus, K., Parton, W. J., Shu, S., Wang, Y. P., Werner, C., Xia, J., Pendall, E., Morgan, J. A., Ryan, E. M.,  
908 Carrillo, Y., Dijkstra, F. A., Zelikova, T. J. and Norby, R. J.: Challenging terrestrial biosphere models with data from the  
909 long-term multifactor Prairie Heating and CO<sub>2</sub> Enrichment experiment, *Glob. Chang. Biol.*, 23(9), 3623–3645,  
910 doi:10.1111/gcb.13643, 2017.
- 911 De Kauwe, M. G., Medlyn, B. E., Ukkola, A. M., Mu, M., Sabot, M. E. B., Pitman, A. J., Meir, P., Cernusak, L., Rifai, S. W.,  
912 Choat, B., Tissue, D. T., Blackman, C. J., Li, X., Roderick, M. and Briggs, P. R.: Identifying areas at risk of drought-  
913 induced tree mortality across South-Eastern Australia, *Glob. Chang. Biol.*, gcb.15215, doi:10.1111/gcb.15215, 2020.
- 914 Kennedy, D., Swenson, S., Oleson, K. W., Lawrence, D. M., Fisher, R., Lola da Costa, A. C. and Gentine, P.: Implementing  
915 Plant Hydraulics in the Community Land Model, Version 5, *J. Adv. Model. Earth Syst.*, 11(2), 485–513,  
916 doi:10.1029/2018MS001500, 2019.
- 917 Kishné, A. S., Yimam, Y. T., Morgan, C. L. S. and Dornblaser, B. C.: Evaluation and improvement of the default soil hydraulic  
918 parameters for the Noah Land Surface Model, *Geoderma*, 285, 247–259, doi:10.1016/j.geoderma.2016.09.022, 2017.
- 919 Klein, T.: The variability of stomatal sensitivity to leaf water potential across tree species indicates a continuum between  
920 isohydric and anisohydric behaviours, edited by S. Niu, *Funct. Ecol.*, 28(6), 1313–1320, doi:10.1111/1365-2435.12289,  
921 2014.
- 922 Kowalczyk, E. A., Wang, Y. P. and Law, R. M.: The CSIRO Atmosphere Biosphere Land Exchange (CABLE) model for use  
923 in climate models and as an offline model, *CSIRO Mar. Atmos. Res. Pap.*, 13, 1–42, doi:10.4225/08/58615c6a9a51d,  
924 2006.
- 925 Lai, C. T. and Katul, G.: The dynamic role of root-water uptake in coupling potential to actual transpiration, *Adv. Water*  
926 *Resour.*, 23(4), 427–439, doi:10.1016/S0309-1708(99)00023-8, 2000.
- 927 Law, R. M., Ziehn, T., Matear, R. J., Lenton, A., Chamberlain, M. A., Stevens, L. E., Wang, Y. P., Sribinovsky, J., Bi, D., Yan,  
928 H. and Vohralik, P. F.: The carbon cycle in the Australian Community Climate and Earth System Simulator (ACCESS-  
929 ESM1) – Part 1: Model description and pre-industrial simulation, *Geosci. Model Dev.*, 10(7), 2567–2590,  
930 doi:10.5194/gmd-10-2567-2017, 2017.
- 931 Lawrence, D. M., Fisher, R. A., Koven, C. D., Oleson, K. W., Swenson, S. C., Bonan, G., Collier, N., Ghimire, B., van  
932 Kampenhout, L., Kennedy, D., Kluzek, E., Lawrence, P. J., Li, F., Li, H., Lombardozzi, D., Riley, W. J., Sacks, W. J.,  
933 Shi, M., Vertenstein, M., Wieder, W. R., Xu, C., Ali, A. A., Badger, A. M., Bisht, G., van den Broeke, M., Brunke, M.  
934 A., Burns, S. P., Buzan, J., Clark, M., Craig, A., Dahlin, K., Drewniak, B., Fisher, J. B., Flanner, M., Fox, A. M., Gentine,  
935 P., Hoffman, F., Keppel-Aleks, G., Knox, R., Kumar, S., Lenaerts, J., Leung, L. R., Lipscomb, W. H., Lu, Y., Pandey,  
936 A., Pelletier, J. D., Perket, J., Randerson, J. T., Ricciuto, D. M., Sanderson, B. M., Slater, A., Subin, Z. M., Tang, J.,  
937 Thomas, R. Q., Val Martin, M. and Zeng, X.: The Community Land Model Version 5: description of new features,

938 benchmarking, and impact of forcing uncertainty, *J. Adv. Model. Earth Syst.*, 11(12), 4245–4287,  
939 doi:10.1029/2018MS001583, 2019.

940 Lawrence, P. J. and Chase, T. N.: Representing a new MODIS consistent land surface in the Community Land Model (CLM  
941 3.0), *J. Geophys. Res.*, 112(G1), G01023, doi:10.1029/2006JG000168, 2007.

942 Lehmann, P., Merlin, O., Gentile, P. and Or, D.: Soil texture effects on surface resistance to bare-soil evaporation, *Geophys.*  
943 *Res. Lett.*, 45(19), 10,398–10,405, doi:10.1029/2018GL078803, 2018.

944 Li, L., Wang, Y. P., Yu, Q., Pak, B., Eamus, D., Yan, J., Van Gorsel, E. and Baker, I. T.: Improving the responses of the  
945 Australian community land surface model (CABLE) to seasonal drought, *J. Geophys. Res. Biogeosciences*, 117(4), 1–  
946 16, doi:10.1029/2012JG002038, 2012.

947 Lian, X., Piao, S., Huntingford, C., Li, Y., Zeng, Z., Wang, X., Ciais, P., McVicar, T. R., Peng, S., Ottlé, C., Yang, H., Yang,  
948 Y., Zhang, Y. and Wang, T.: Partitioning global land evapotranspiration using CMIP5 models constrained by  
949 observations, *Nat. Clim. Chang.*, 8(7), 640–646, doi:10.1038/s41558-018-0207-9, 2018.

950 Lin, Y.-S., Medlyn, B. E., Duursma, R. a., Prentice, I. C., Wang, H., Baig, S., Eamus, D., de Dios, V. R., Mitchell, P., Ellsworth,  
951 D. S., de Beeck, M. O., Wallin, G., Uddling, J., Tarvainen, L., Linderson, M.-L., Cernusak, L. a., Nippert, J. B., Ocheltree,  
952 T. W., Tissue, D. T., Martin-StPaul, N. K., Rogers, A., Warren, J. M., De Angelis, P., Hikosaka, K., Han, Q., Onoda, Y.,  
953 Gimeno, T. E., Barton, C. V. M., Bennie, J., Bonal, D., Bosc, A., Löw, M., Macinins-Ng, C., Rey, A., Rowland, L.,  
954 Setterfield, S. a., Tausz-Posch, S., Zaragoza-Castells, J., Broadmeadow, M. S. J., Drake, J. E., Freeman, M., Ghannoum,  
955 O., Hutley, L. B., Kelly, J. W., Kikuzawa, K., Kolari, P., Koyama, K., Limousin, J.-M., Meir, P., Lola da Costa, A. C.,  
956 Mikkelsen, T. N., Salinas, N., Sun, W. and Wingate, L.: Optimal stomatal behaviour around the world, *Nat. Clim. Chang.*,  
957 5(5), 459–464, doi:10.1038/nclimate2550, 2015.

958 Van Looy, K., Bouma, J., Herbst, M., Koestel, J., Minasny, B., Mishra, U., Montzka, C., Nemes, A., Pachepsky, Y. A.,  
959 Padarian, J., Schaap, M. G., Tóth, B., Verhoef, A., Vanderborght, J., Ploeg, M. J., Weihermüller, L., Zacharias, S., Zhang,  
960 Y. and Vereecken, H.: Pedotransfer functions in earth system science: challenges and perspectives, *Rev. Geophys.*, 55(4),  
961 1199–1256, doi:10.1002/2017RG000581, 2017.

962 Lorenz, R., Pitman, A. J., Donat, M. G., Hirsch, A. L., Kala, J., Kowalczyk, E. A., Law, R. M. and Srbinovsky, J.:  
963 Representation of climate extreme indices in the ACCESS1.3b coupled atmosphere-land surface model, *Geosci. Model*  
964 *Dev.*, 7(2), 545–567, doi:10.5194/gmd-7-545-2014, 2014.

965 Matthews, T. K. R. R., Wilby, R. L. and Murphy, C.: Communicating the deadly consequences of global warming for human  
966 heat stress, *Proc. Natl. Acad. Sci.*, 114(15), 3861–3866, doi:10.1073/pnas.1617526114, 2017.

967 Mazdiyasi, O. and AghaKouchak, A.: Substantial increase in concurrent droughts and heatwaves in the United States, *Proc.*  
968 *Natl. Acad. Sci.*, 112(37), 11484–11489, doi:10.1073/pnas.1422945112, 2015.

969 Medlyn, B. E., Duursma, R. A., Eamus, D., Ellsworth, D. S., Prentice, I. C., Barton, C. V. M., Crous, K. Y., De Angelis, P.,  
970 Freeman, M. and Wingate, L.: Reconciling the optimal and empirical approaches to modelling stomatal conductance,  
971 *Glob. Chang. Biol.*, 17(6), 2134–2144, doi:10.1111/j.1365-2486.2010.02375.x, 2011.

972 Medlyn, B. E., De Kauwe, M. G., Zaehle, S., Walker, A. P., Duursma, R. A., Luus, K., Mishurov, M., Pak, B., Smith, B.,  
973 Wang, Y. P., Yang, X., Crous, K. Y., Drake, J. E., Gimeno, T. E., Macdonald, C. A., Norby, R. J., Power, S. A., Tjoelker,  
974 M. G. and Ellsworth, D. S.: Using models to guide field experiments: a priori predictions for the CO<sub>2</sub> response of a

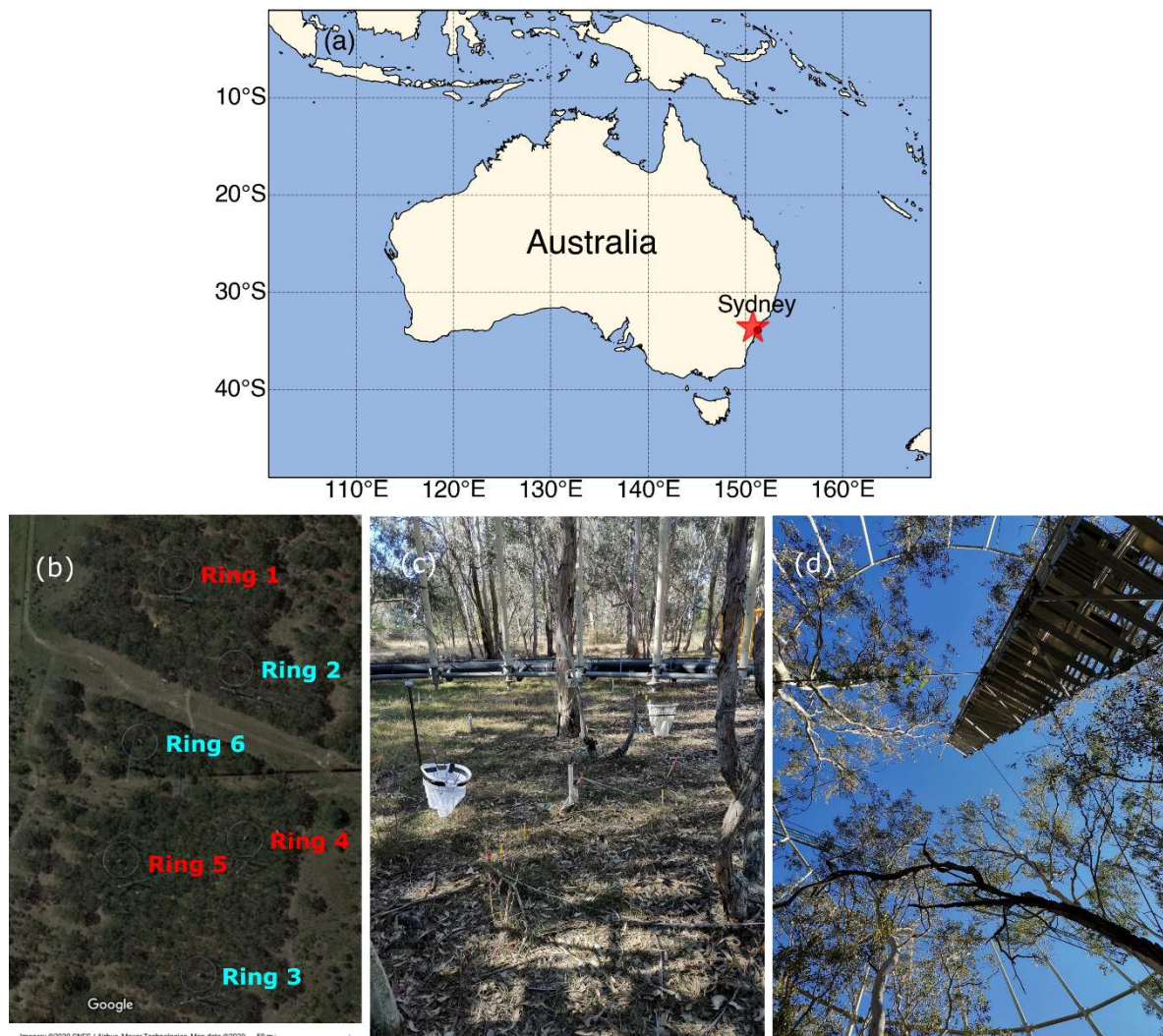
- 975 nutrient- and water-limited native Eucalypt woodland, *Glob. Chang. Biol.*, 22(8), 2834–2851, doi:10.1111/gcb.13268,  
976 2016.
- 977 Miralles, D. G., Teuling, A. J., Van Heerwaarden, C. C. and De Arellano, J. V. G.: Mega-heatwave temperatures due to  
978 combined soil desiccation and atmospheric heat accumulation, *Nat. Geosci.*, 7(5), 345–349, doi:10.1038/ngeo2141, 2014.
- 979 Miralles, D. G., Gentile, P., Seneviratne, S. I. and Teuling, A. J.: Land-atmospheric feedbacks during droughts and heatwaves:  
980 state of the science and current challenges, *Ann. N. Y. Acad. Sci.*, 1436(1), 19–35, doi:10.1111/nyas.13912, 2019.
- 981 [Montzka, C., Herbst, M., Weihermüller, L., Verhoef, A. and Vereecken, H.: A global data set of soil hydraulic properties and](#)  
982 [sub-grid variability of soil water retention and hydraulic conductivity curves, \*Earth Syst. Sci. Data\*, 9\(2\), 529–543,](#)  
983 [doi:10.5194/essd-9-529-2017, 2017.](#)
- 984 Niu, G.-Y., Yang, Z.-L., Dickinson, R. E., Gulden, L. E. and Su, H.: Development of a simple groundwater model for use in  
985 climate models and evaluation with Gravity Recovery and Climate Experiment data, *J. Geophys. Res.*, 112(D7), D07103,  
986 doi:10.1029/2006JD007522, 2007.
- 987 Oleson, K. W., Niu, G.-Y., Yang, Z.-L., Lawrence, D. M., Thornton, P. E., Lawrence, P. J., Stöckli, R., Dickinson, R. E.,  
988 Bonan, G. B., Levis, S., Dai, A. and Qian, T.: Improvements to the Community Land Model and their impact on the  
989 hydrological cycle, *J. Geophys. Res. Biogeosciences*, 113(G1), 1–26, doi:10.1029/2007JG000563, 2008.
- 990 Or, D. and Lehmann, P.: Surface evaporative capacitance: how soil type and rainfall characteristics affect global-scale surface  
991 evaporation, *Water Resour. Res.*, 55(1), 519–539, doi:10.1029/2018WR024050, 2019.
- 992 [Orth, R. and Destouni, G.: Drought reduces blue-water fluxes more strongly than green-water fluxes in Europe, \*Nat. Commun.\*,](#)  
993 [9, 1–8, doi:10.1038/s41467-018-06013-7, 2018.](#)
- 994 [Orth, R., Dutra, E., Trigo, I. F. and Balsamo, G.: Advancing land surface model development with satellite-based Earth](#)  
995 [observations, \*Hydrol. Earth Syst. Sci.\* 21, 2483–2495, doi: 10.5194/hess-21-2483-2017, 2017.](#)
- 996 Pal, J. S. and Eltahir, E. A. B.: Future temperature in southwest Asia projected to exceed a threshold for human adaptability,  
997 *Nat. Clim. Chang.*, 6(2), 197–200, doi:10.1038/nclimate2833, 2016.
- 998 Pan, S., Pan, N., Tian, H., Friedlingstein, P., Sitch, S., Shi, H., Arora, V. K., Haverd, V., Jain, A. K., Kato, E., Lienert, S.,  
999 Lombardozi, D., Nabel, J. E. M. S. M. S., Otlé, C., Poulter, B., Zaehle, S. and Running, S. W.: Evaluation of global  
1000 terrestrial evapotranspiration using state-of-the-art approaches in remote sensing, machine learning and land surface  
1001 modeling, *Hydrol. Earth Syst. Sci.*, 24(3), 1485–1509, doi:10.5194/hess-24-1485-2020, 2020.
- 1002 Pathare, V. S., Crous, K. Y., Cooke, J., Creek, D., Ghannoum, O. and Ellsworth, D. S.: Water availability affects seasonal  
1003 CO<sub>2</sub>-induced photosynthetic enhancement in herbaceous species in a periodically dry woodland, *Glob. Chang. Biol.*,  
1004 23(12), 5164–5178, doi:10.1111/gcb.13778, 2017.
- 1005 Powell, T. L., Galbraith, D. R., Christoffersen, B. O., Harper, A., Imbuzeiro, H. M. A., Rowland, L., Almeida, S., Brando, P.  
1006 M., da Costa, A. C. L., Costa, M. H., Levine, N. M., Malhi, Y., Saleska, S. R., Sotta, E., Williams, M., Meir, P. and  
1007 Moorcroft, P. R.: Confronting model predictions of carbon fluxes with measurements of Amazon forests subjected to  
1008 experimental drought, *New Phytol.*, 200(2), 350–365, doi:10.1111/nph.12390, 2013.
- 1009 Puhlmann, H. and von Wilpert, K.: Pedotransfer functions for water retention and unsaturated hydraulic conductivity of forest  
1010 soils, *J. Plant Nutr. Soil Sci.*, 175(2), 221–235, doi:10.1002/jpln.201100139, 2012.

- 1011 Reichstein, M., Bahn, M., Ciais, P., Frank, D., Mahecha, M. D., Seneviratne, S. I., Zscheischler, J., Beer, C., Buchmann, N.,  
1012 Frank, D. C., Papale, D., Rammig, A., Smith, P., Thonicke, K., van der Velde, M., Vicca, S., Walz, A. and Wattenbach,  
1013 M.: Climate extremes and the carbon cycle, *Nature*, 500(7462), 287–295, doi:10.1038/nature12350, 2013.
- 1014 Renchon, A. A., Griebel, A., Metzen, D., Williams, C. A., Medlyn, B., Duursma, R. A., Barton, C. V. M., Maier, C., Boer, M.  
1015 M., Isaac, P., Tissue, D., Resco De Dios, V. and Pendall, E.: Upside-down fluxes Down Under: CO<sub>2</sub> net sink in winter  
1016 and net source in summer in a temperate evergreen broadleaf forest, *Biogeosciences*, 15(12), 3703–3716, doi:10.5194/bg-  
1017 15-3703-2018, 2018.
- 1018 Sabot, M. E. B. B., De Kauwe, M. G., Pitman, A. J., Medlyn, B. E., Verhoef, A., Ukkola, A. M. and Abramowitz, G.: Plant  
1019 profit maximization improves predictions of European forest responses to drought, *New Phytol.*, 226(6), 1638–1655,  
1020 doi:10.1111/nph.16376, 2020.
- 1021 Sakaguchi, K. and Zeng, X.: Effects of soil wetness, plant litter, and under-canopy atmospheric stability on ground evaporation  
1022 in the Community Land Model (CLM3.5), *J. Geophys. Res. Atmos.*, 114(1), 1–14, doi:10.1029/2008JD010834, 2009.
- 1023 Schlosser, C. A., Slater, A. G., Robock, A., Pitman, A. J., Vinnikov, K. Y., Henderson-Sellers, A., Speranskaya, N. A.,  
1024 Mitchell, K.: Simulations of a boreal grassland hydrology at Valdai, Russia: PILPS Phase 2(d), *Mon. Weather Rev.*,  
1025 128(2), 301–321, doi:10.1175/1520-0493(2000)128<0301:SOABGH>2.0.CO;2, 2000.
- 1026 Schumacher, D. L., Keune, J., van Heerwaarden, C. C., Vilà-Guerau de Arellano, J., Teuling, A. J. and Miralles, D. G.:  
1027 Amplification of mega-heatwaves through heat torrents fuelled by upwind drought, *Nat. Geosci.*, 12(9), 712–717,  
1028 doi:10.1038/s41561-019-0431-6, 2019.
- 1029 Seneviratne, S. I., Corti, T., Davin, E. L., Hirschi, M., Jaeger, E. B., Lehner, I., Orlowsky, B. and Teuling, A. J.: Investigating  
1030 soil moisture-climate interactions in a changing climate: A review, *Earth-Science Rev.*, 99(3–4), 125–161,  
1031 doi:10.1016/j.earscirev.2010.02.004, 2010.
- 1032 Sippel, S., Zscheischler, J., Mahecha, M. D., Orth, R., Reichstein, M., Vogel, M. and Seneviratne, S. I.: Refining multi-model  
1033 projections of temperature extremes by evaluation against land–atmosphere coupling diagnostics, *Earth Syst. Dyn.*, 8(2),  
1034 387–403, doi:10.5194/esd-8-387-2017, 2017.
- 1035 Sperry, J. S., Venturas, M. D., Anderegg, W. R. L., Mencuccini, M., Mackay, D. S., Wang, Y. and Love, D. M.: Predicting  
1036 stomatal responses to the environment from the optimization of photosynthetic gain and hydraulic cost, *Plant. Cell*  
1037 *Environ.*, 40(6), 816–830, doi:10.1111/pce.12852, 2017.
- 1038 ~~Swann, A. L. S.: Plants and drought in a changing climate, *Curr. Clim. Chang. Reports*, 4(2), 192–201, doi:10.1007/s40641-~~  
1039 ~~018-0097-y, 2018.~~
- 1040 Swenson, S. C. and Lawrence, D. M.: Assessing a dry surface layer-based soil resistance parameterization for the Community  
1041 Land Model using GRACE and FLUXNET-MTE data, *J. Geophys. Res. Atmos.*, 119(17), 10,299–10,312,  
1042 doi:10.1002/2014JD022314, 2014.
- 1043 Tallaksen, L. M. and Stahl, K.: Spatial and temporal patterns of large-scale droughts in Europe: Model dispersion and  
1044 performance, *Geophys. Res. Lett.*, 41(2), 429–434, doi:10.1002/2013GL058573, 2014.
- 1045 Teuling, A. J., Seneviratne, S. I., Stöckli, R., Reichstein, M., Moors, E., Ciais, P., Luysaert, S., van den Hurk, B., Ammann,  
1046 C., Bernhofer, C., Dellwik, E., Gianelle, D., Gielen, B., Grünwald, T., Klumpp, K., Montagnani, L., Moureaux, C.,

- 1047 Sottocornola, M. and Wohlfahrt, G.: Contrasting response of European forest and grassland energy exchange to  
1048 heatwaves, *Nat. Geosci.*, 3(10), 722–727, doi:10.1038/ngeo950, 2010.
- 1049 Trugman, A. T., Medvigy, D., Mankin, J. S. and Anderegg, W. R. L.: Soil moisture stress as a major driver of carbon cycle  
1050 uncertainty, *Geophys. Res. Lett.*, 45(13), 6495–6503, doi:10.1029/2018GL078131, 2018.
- 1051 Ukkola, A. M., De Kauwe, M. G., Pitman, A. J., Best, M. J., Abramowitz, G., Haverd, V., Decker, M. and Houghton, N.: Land  
1052 surface models systematically overestimate the intensity, duration and magnitude of seasonal-scale evaporative droughts,  
1053 *Environ. Res. Lett.*, 11(10), 104012, doi:10.1088/1748-9326/11/10/104012, 2016a.
- 1054 Ukkola, A. M., Pitman, A. J., Decker, M., De Kauwe, M. G., Abramowitz, G., Kala, J. and Wang, Y. P.: Modelling  
1055 evapotranspiration during precipitation deficits: identifying critical processes in a land surface model, *Hydrol. Earth Syst.  
1056 Sci.*, 20(6), 2403–2419, doi:10.5194/hess-20-2403-2016, 2016b.
- 1057 Ukkola, A. M., Pitman, A. J., De Kauwe, M. G., Abramowitz, G., Herger, N., Evans, J. P. and Decker, M.: Evaluating CMIP5  
1058 model agreement for multiple drought metrics, *J. Hydrometeorol.*, 19(6), 969–988, doi:10.1175/jhm-d-17-0099.1, 2018a.
- 1059 Ukkola, A. M., Pitman, A. J., Donat, M. G., De Kauwe, M. G. and Angéilil, O.: Evaluating the contribution of land-atmosphere  
1060 coupling to heat extremes in CMIP5 models, *Geophys. Res. Lett.*, 45(17), 9003–9012, doi:10.1029/2018GL079102,  
1061 2018b.
- 1062 Vogel, M. M., Orth, R., Cheruy, F., Hagemann, S., Lorenz, R., van den Hurk, B. J. J. M. and Seneviratne, S. I.: Regional  
1063 amplification of projected changes in extreme temperatures strongly controlled by soil moisture-temperature feedbacks,  
1064 *Geophys. Res. Lett.*, 44(3), 1511–1519, doi:10.1002/2016GL071235, 2017.
- 1065 ~~Wagner, B., Tarnawski, V. R., Hennings, V., Muller, U., Wessolek, G. and Plagge, R.: Evaluation of pedo-transfer functions  
1066 for unsaturated soil hydraulic conductivity using an independent data set, *Geoderma*, 108(1–2), 145–147,  
1067 doi:10.1016/S0016-7061(02)00127-1, 2001.~~
- 1068 Wang, Y. P., Kowalczyk, E., Leuning, R., Abramowitz, G., Raupach, M. R., Pak, B., van Gorsel, E. and Luhar, A.: Diagnosing  
1069 errors in a land surface model (CABLE) in the time and frequency domains, *J. Geophys. Res.*, 116(G1), G01034,  
1070 doi:10.1029/2010JG001385, 2011.
- 1071 Williams, M., Richardson, A. D., Reichstein, M., Stoy, P. C., Peylin, P., Verbeeck, H., Carvalhais, N., Jung, M., Hollinger, D.  
1072 Y., Kattge, J., Leuning, R., Luo, Y., Tomelleri, E., Trudinger, C. M. and Wang, Y. P.: Improving land surface models  
1073 with FLUXNET data, *Biogeosciences*, 6(7), 1341–1359, doi:10.5194/bg-6-1341-2009, 2009.
- 1074 Wolf, A., Anderegg, W. R. L. and Pacala, S. W.: Optimal stomatal behavior with competition for water and risk of hydraulic  
1075 impairment, *Proc. Natl. Acad. Sci.*, 113(46), E7222–E7230, doi:10.1073/pnas.1615144113, 2016.
- 1076 Xu, X., Medvigy, D., Powers, J. S., Becknell, J. M. and Guan, K.: Diversity in plant hydraulic traits explains seasonal and  
1077 inter-annual variations of vegetation dynamics in seasonally dry tropical forests, *New Phytol.*, 212(1), 80–95,  
1078 doi:10.1111/nph.14009, 2016.
- 1079 Yang, J.: MAESPA\_EUCFACE\_PARAM: Low sensitivity of gross primary production to elevated CO<sub>2</sub> in a mature eucalypt  
1080 woodland, <https://doi.org/10.5281/zenodo.3610698>, 2019.
- 1081 Yang, J., Duursma, R. A., De Kauwe, M. G., Kumarathunge, D., Jiang, M., Mahmud, K., Gimeno, T. E., Crous, K. Y.,  
1082 Ellsworth, D. S., Peters, J., Choat, B., Eamus, D. and Medlyn, B. E.: Incorporating non-stomatal limitation improves the

- 1083 performance of leaf and canopy models at high vapour pressure deficit, *Tree Physiol.*, 39(12), 1961–1974,  
1084 doi:10.1093/treephys/tpz103, 2019.
- 1085 Yang, J., Medlyn, B. E., De Kauwe, M. G., Duursma, R. A., Jiang, M., Kumarathunge, D., Crous, K. Y., Gimeno, T. E.,  
1086 Wujeska-Klaue, A. and Ellsworth, D. S.: Low sensitivity of gross primary production to elevated CO<sub>2</sub> in a mature  
1087 eucalypt woodland, *Biogeosciences*, 17(2), 265–279, doi:10.5194/bg-17-265-2020, 2020.
- 1088 Zhang, Y. and Schaap, M. G.: Estimation of saturated hydraulic conductivity with pedotransfer functions: A review, *J. Hydrol.*,  
1089 575, 1011–1030, doi:10.1016/j.jhydrol.2019.05.058, 2019.
- 1090 [Zhang, Y. and Schaap, M. G.: Weighted recalibration of the Rosetta pedotransfer model with improved estimates of hydraulic  
1091 parameter distributions and summary statistics \(Rosetta3\), \*J. Hydrol.\*, 547, 39–53, doi:10.1016/j.jhydrol.2017.01.004,  
1092 2017.](#)
- 1093 Zhao, T. and Dai, A.: Uncertainties in historical changes and future projections of drought. Part II: model-simulated historical  
1094 and future drought changes, *Clim. Change*, 144(3), 535–548, doi:10.1007/s10584-016-1742-x, 2017.
- 1095 Zhou, S., Duursma, R. A., Medlyn, B. E., Kelly, J. W. G. and Prentice, I. C.: How should we model plant responses to drought?  
1096 An analysis of stomatal and non-stomatal responses to water stress, *Agric. For. Meteorol.*, 182–183, 204–214,  
1097 doi:10.1016/j.agrformet.2013.05.009, 2013.
- 1098 Zhou, S., Medlyn, B., Sabaté, S., Sperlich, D., Prentice, I. C. and Whitehead, D.: Short-term water stress impacts on stomatal,  
1099 mesophyll and biochemical limitations to photosynthesis differ consistently among tree species from contrasting climates,  
1100 *Tree Physiol.*, 34(10), 1035–1046, doi:10.1093/treephys/tpu072, 2014.





1104  
 1105 **Figure 1.** (a) Location of the experimental site in western Sydney, Australia ( $33^{\circ}36'59''\text{S}$ ,  $150^{\circ}44'17''\text{E}$ ) shown by the red star. (b)  
 1106 Distribution of six rings (© Google Maps, 2020. EucFACE experiment site, 1:50. Google Maps [[https://www.google.com/maps/@-](https://www.google.com/maps/@-33.6177915,150.7379194,356m/data=!3m1!1e3)  
 1107 [33.6177915,150.7379194,356m/data=!3m1!1e3](https://www.google.com/maps/@-33.6177915,150.7379194,356m/data=!3m1!1e3)]). (c) Understorey vegetation and infrastructure inside a ring (photograph taken by M. M.).  
 1108 (d) Canopy structure and central tower (photograph taken by M. M.).  
 1109  
 1110

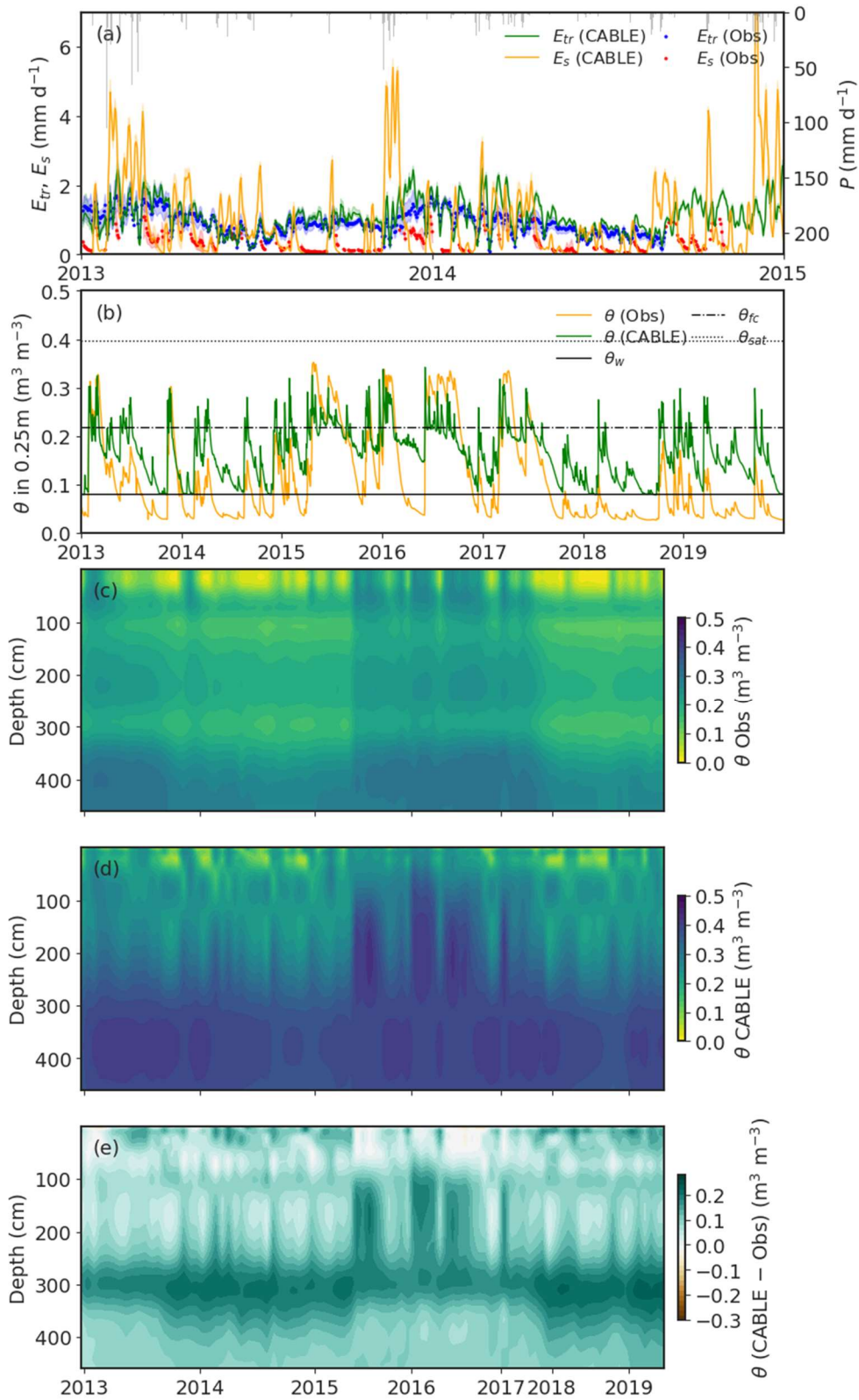


**Figure 2.** Control simulation (*Ctl*). (a)  $E_{tr}$ ,  $E_s$  and precipitation ( $P$ ) between 2013 and 2015. The shaded areas represent uncertainty between three ambient rings. Both simulations and observations are smoothed with a 3-day window to aid visualisation. (b)  $\theta$  in the top 0.25m from 2013 to 2019. (c) The vertical distribution of  $\theta$  measured at observed dates from 2013 to 2019. (d) The vertical distribution of  $\theta$  in *Ctl* for observed dates from 2013 to 2019. (e)  $\theta$  differences between CABLE and observations (note: Note the different time axis for (c), (d)–(e) relative to (a–b) due to different sampling intervals for soil moisture and (e) the horizontal axis is not linear, rather it reflects periods of observations).—fluxes.

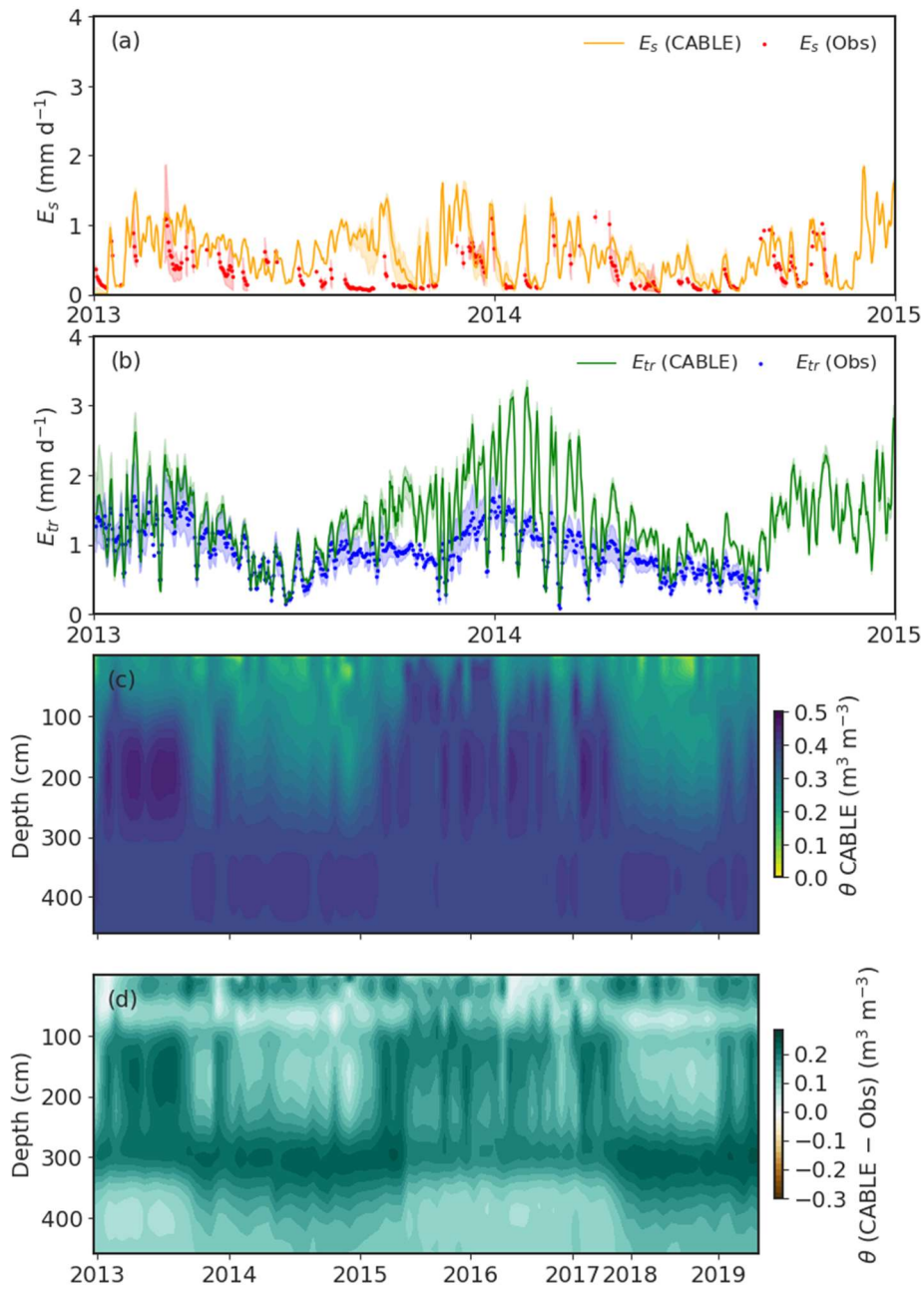


**Figure 3.** Increasing soil evaporation resistance experiment (*Sres*). (a)  $E_s$  between 2013 and 2015. (b)  $E_{tr}$  between 2013 and 2015. In panel (a) and (b) the shaded areas represent uncertainty between three ambient rings, and both simulations and observations are smoothed with a 3-day window to aid visualisation. (c) The vertical distribution of  $\theta$  in *Sres* at observed dates from 2013 to 2019. (d)  $\theta$  difference between CABLE and observations (note, for (c) and (d) the horizontal axis is not linear, rather it reflects periods of observations). Note the different time axis for (c-d) relative to (a-b) due to different sampling intervals for soil moisture and fluxes.



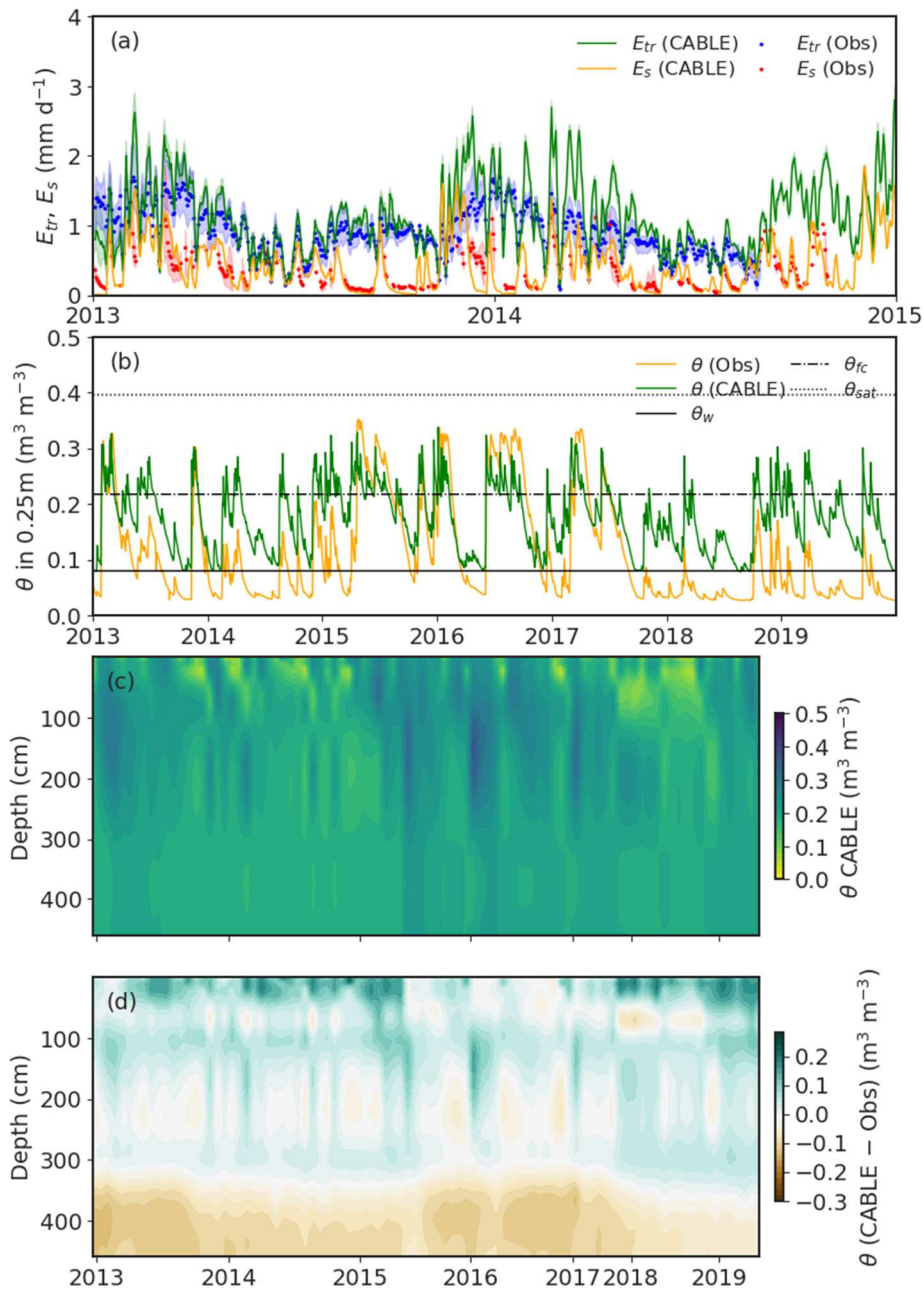


**Figure 4.** Water table initialisation experiment (*Watr*). (a)  $E_{tr}$  and  $E_s$  between 2013 and 2015. The shaded areas represent uncertainty between three ambient rings. Both simulations and observations are smoothed with a 3-day window to aid visualisation. (b)  $\theta$  in the top 0.25m from 2013 to 2019. (c) The vertical distribution of  $\theta$  in *Watr* at observed dates from 2013 to 2019. (d)  $\theta$  difference between CABLE and observations (note, for (c) and (d) the horizontal axis is not linear, rather it reflects periods of observations). Note the different time axis for (c-d) relative to (a-b) due to different sampling intervals for soil moisture and fluxes.

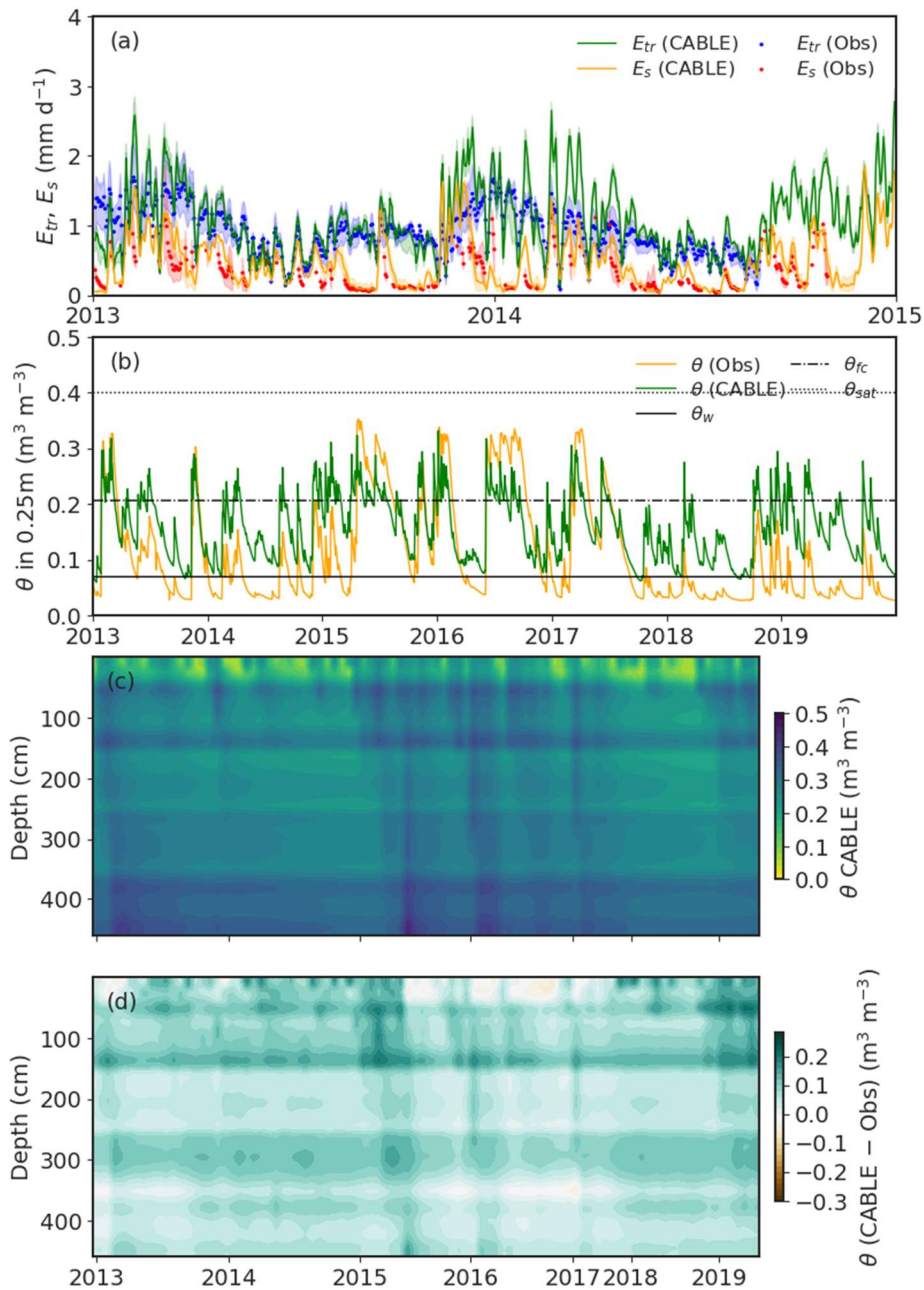
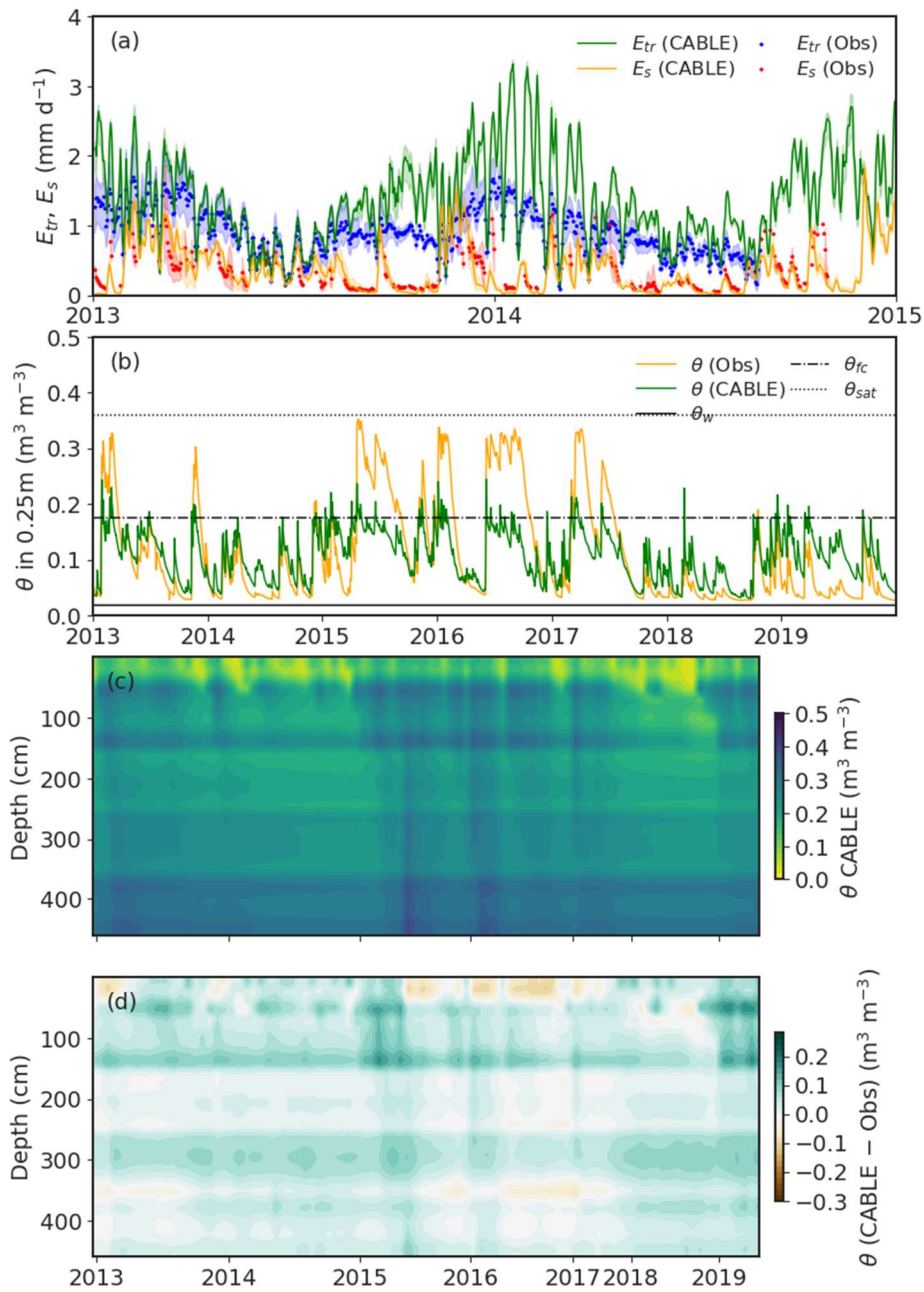
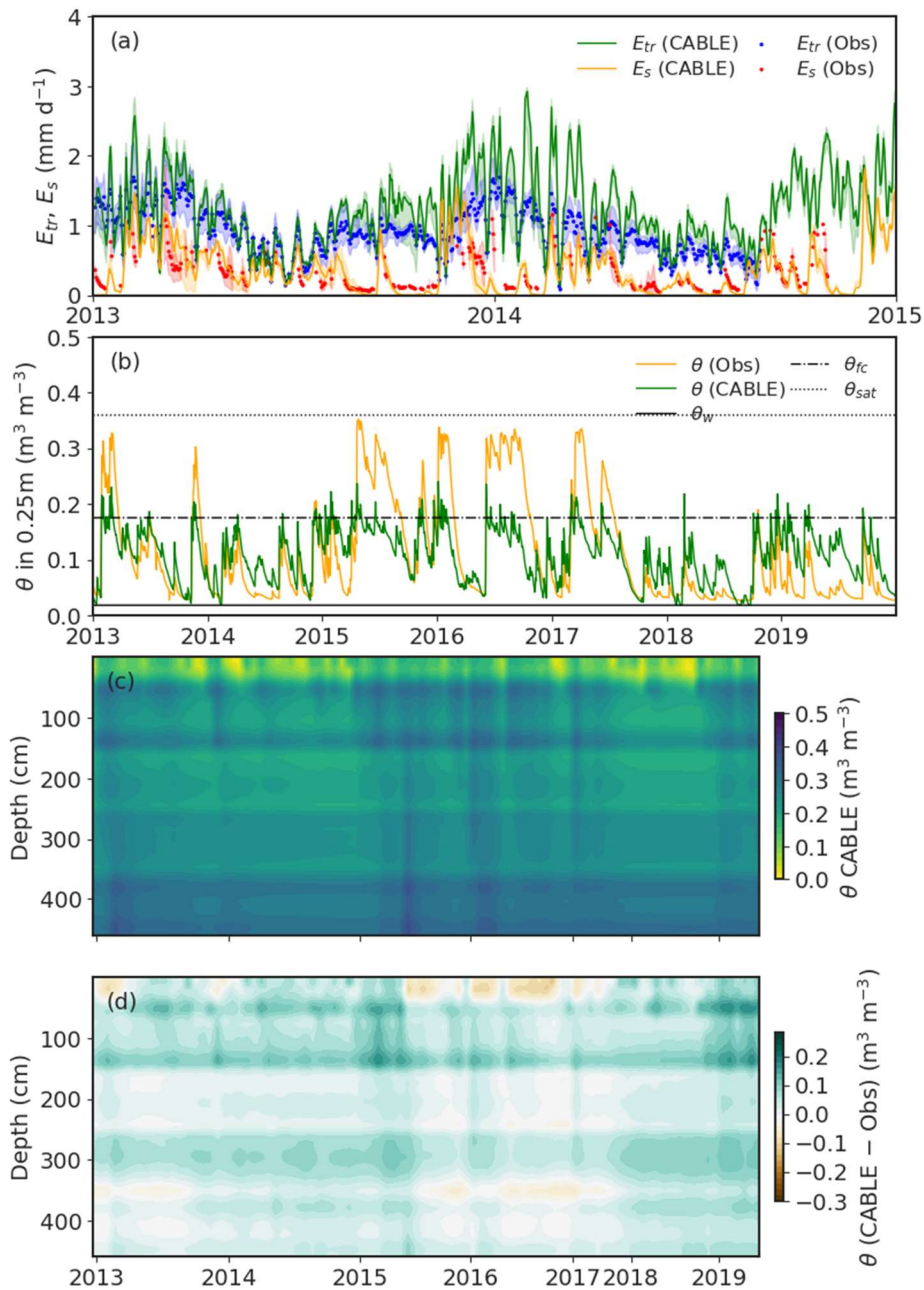


**Figure 5.** High soil resolution experiment (*Hi-Res-2*), which uses 31 soil layers with depth-varying hydraulic parameters informed by observed soil properties. (a)  $E_{tr}$  and  $E_s$  between 2013 and 2015. The shaded areas represent uncertainty between three ambient rings. Both simulations and observations are smoothed with a 3-day window to aid visualisation. (b)  $\theta$  in the top 0.25 m from 2013 to 2019. (c) The vertical distribution of  $\theta$  in *Hi-Res-2* at observed dates from 2013 to 2019. (d)  $\theta$  difference between CABLE and observations (note, Note the different time axis for (c-d) relative to (a-b) due to different sampling intervals for soil moisture and (d) the horizontal axis is not linear, rather it reflects periods of observations)-fluxes.

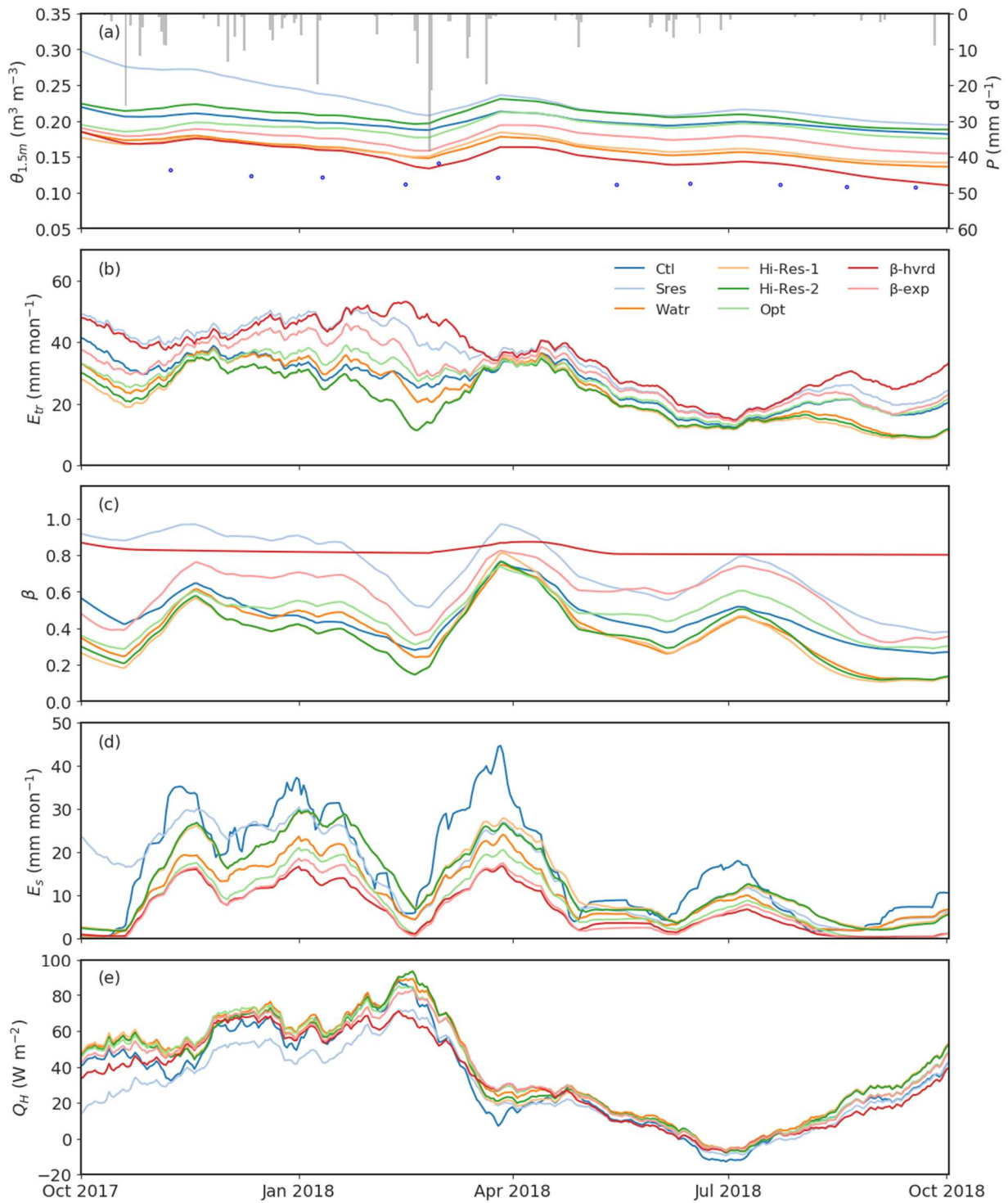


1147 **Figure 6.** Haverd water stress function experiment ( $\beta$ -hvrd). (a)  $E_{tr}$  and  $E_s$  between 2013 and 2015. The shaded areas represent uncertainty  
 1148 between three ambient rings. Both simulations and observations are smoothed with a 3-day window to aid visualisation. (b)  $\theta$  in the top  
 1149 0.25m from 2013 to 2019. (c) The vertical distribution of  $\theta$  in  $\beta$ -hvrd at observed dates from 2013 to 2019. (d)  $\theta$  difference between CABLE  
 1150 and observations (note, for (c) and (d) the horizontal axis is not linear, rather it reflects periods of observations). Note the different time axis  
 1151 for (c-d) relative to (a-b) due to different sampling intervals for soil moisture and fluxes.  
 1152  
 1153

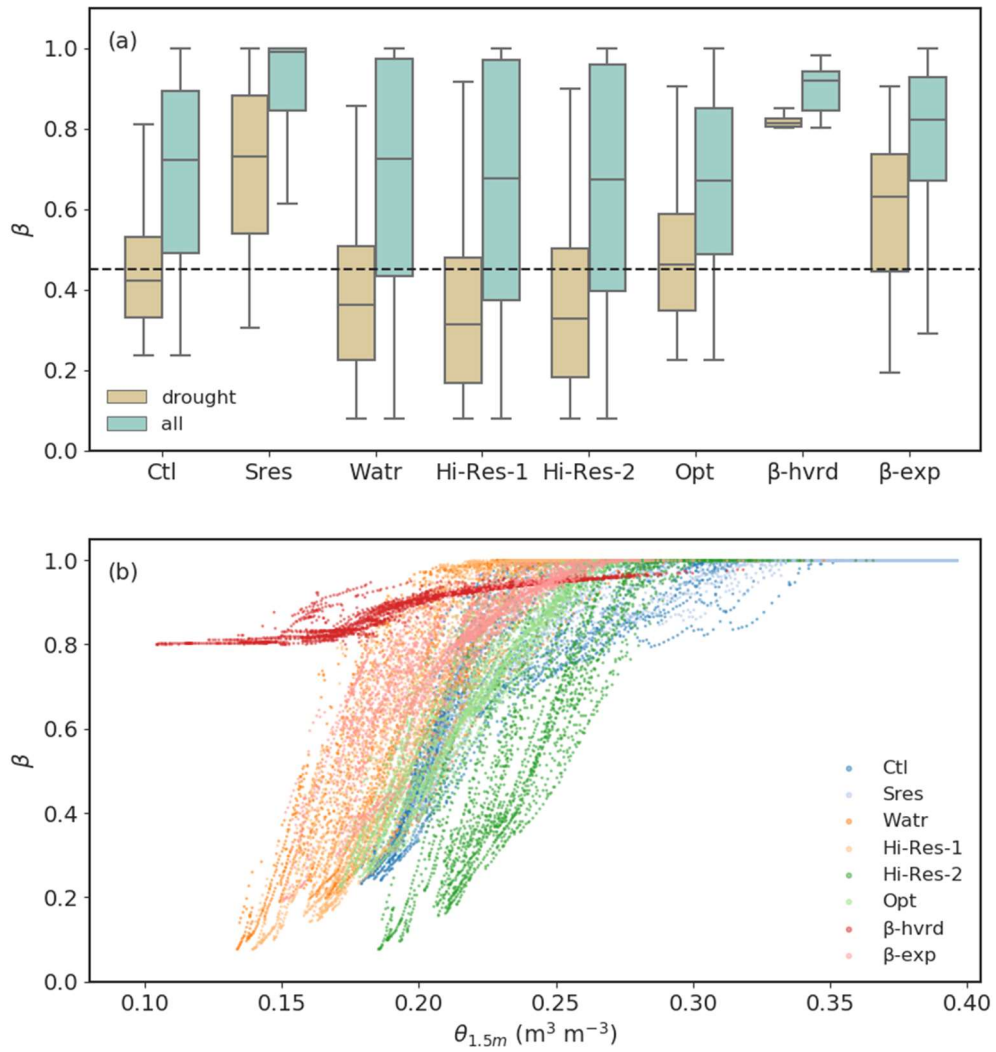




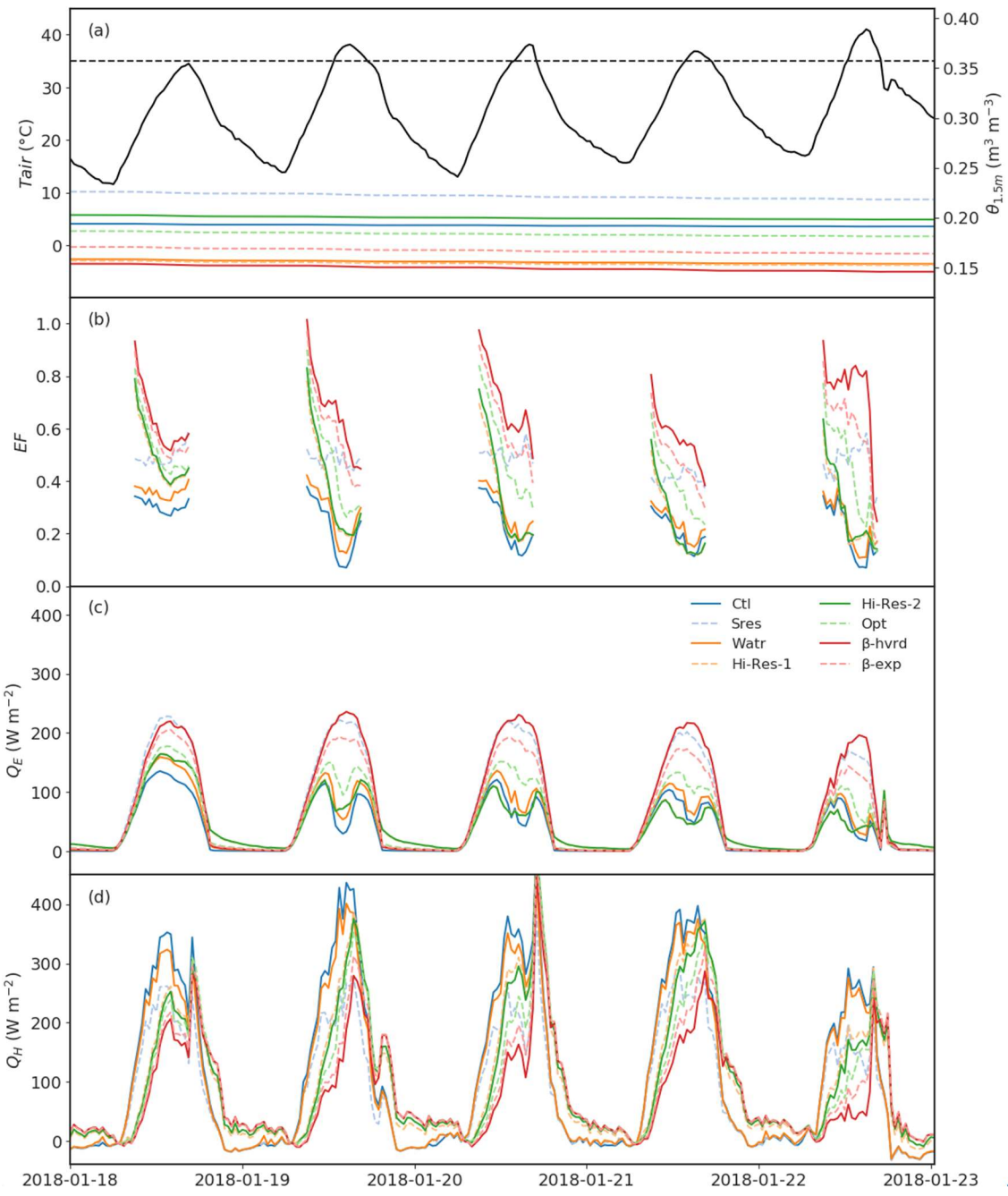
1154  
 1155 **Figure 7.** Site-based water stress function experiment ( $\beta$ -exp). (a)  $E_{tr}$  and  $E_s$  between 2013 and 2015. The shaded areas represent uncertainty  
 1156 between three ambient rings. Both simulations and observations are smoothed with a 3-day window to aid visualisation. (b)  $\theta$  in the top  
 1157 0.25m from 2013 to 2019. (c) The vertical distribution of  $\theta$  in  $\beta$ -exp at observed dates from 2013 to 2019. (d)  $\theta$  difference between CABLE  
 1158 and observations (note, for (c) and (d) the horizontal axis is not linear, rather it reflects periods of observations). Note the different time axis  
 1159 for (c-d) relative to (a-b) due to different sampling intervals for soil moisture and fluxes.  
 1160  
 1161



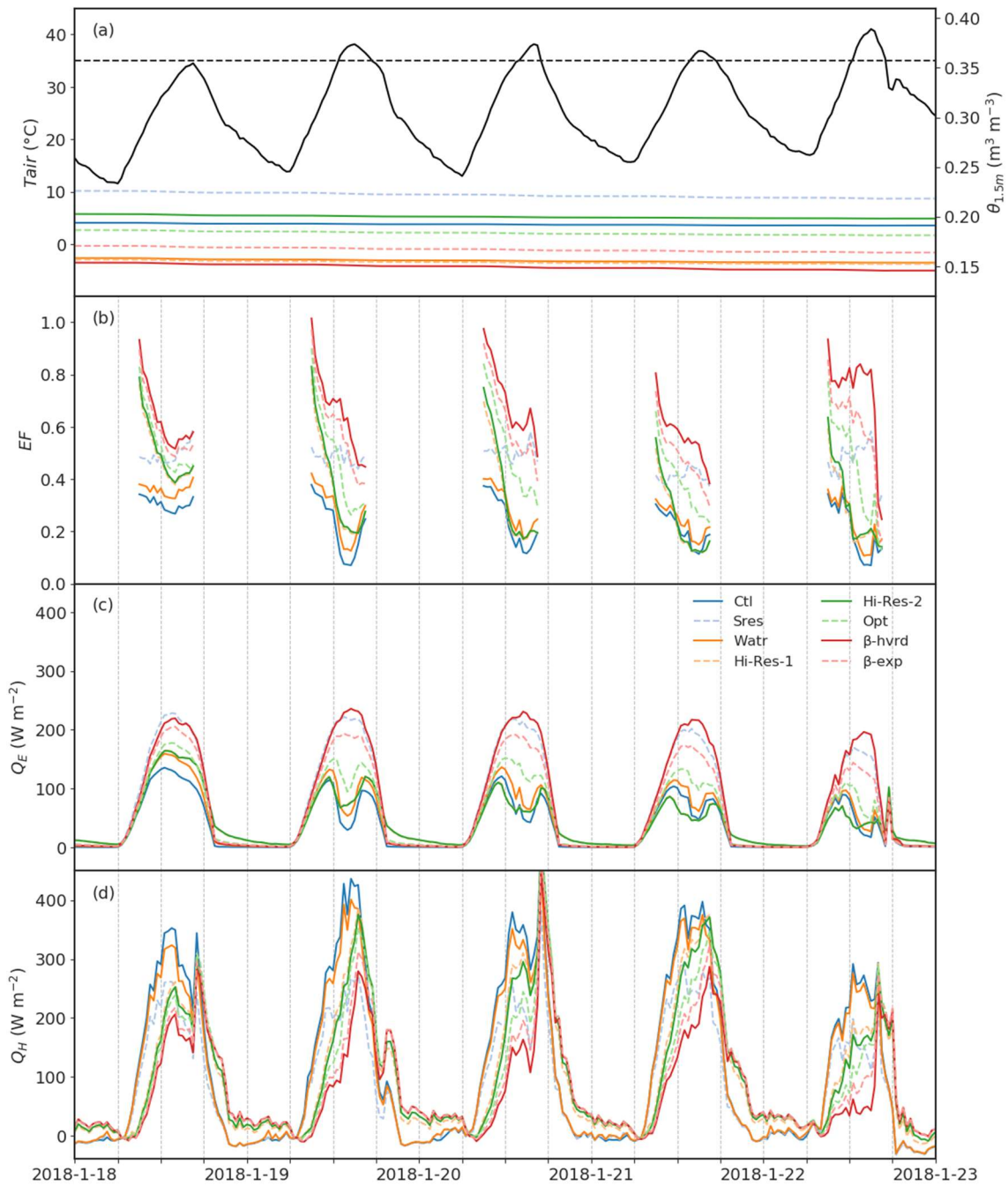
1162  
 1163 **Figure 8.** Simulations for each experiment during the drought period (October 2017 to September 2018). (a) the root zone soil moisture over  
 1164 top 1.5 m ( $\theta_{1.5m}$ ) and rainfall ( $P$ ; bars), with blue dots showing the observed soil moisture. (b)  $E_{tr}$ , (c) water stress factor ( $\beta$ ), (d)  $E_s$  and (e)  
 1165 sensible heat ( $Q_H$ ). All lines are smoothed with a 30-day window.  
 1166



1167  
 1168 **Figure 9.** (a) Box plot of simulated  $\beta$  during a drought year (October 2017 - September 2018) and all simulated years (2013-2019). The  
 1169 dashed line is the mean value of  $\beta$  in *Ctl* over the dry period. (b)  $\beta$  variance with root zone soil moisture over the top 1.5m ( $\theta_{1.5m}$ ) during all  
 1170 simulated years.  
 1171  
 1172



1173



1174  
 1175 **Figure 10.** Simulations during an observed heatwave with relatively low soil moisture (19-22 January 2018). (a) Air temperature ( $T_{air}$ ; in  
 1176 black) and soil moisture within root zone over the top 1.5m ( $\theta_{1.5m}$ ). The black dashed line shows the 35°C threshold. (b) evaporative fraction  
 1177 ( $EF$ ; calculated for day-time conditions), (c) latent heat ( $Q_E$ ) and (d) sensible heat ( $Q_H$ ). [The vertical dash lines in panel b-d are at a 6-hour](#)  
 1178 [interval to assist plot reading.](#) One day before the heatwave is also shown.  
 1179  
 1180



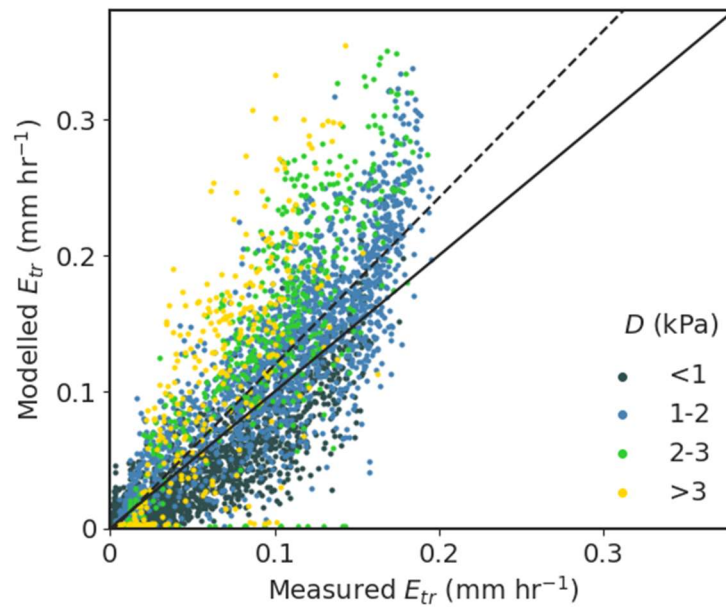


**Figure 11.** Modelled hourly  $E_{tr}$  compared with measured hourly  $E_{tr}$  over 2013. The solid line represents the 1:1 line. The dashed line is the linear fit between modelled and measured  $E_{tr}$ . Colours of dots indicate the range of vapour pressure deficit.

1181  
 1182  
 1183  
 1184  
 1185  
 1186  
 1187  
 1188  
 1189  
 1190  
 1191  
 1192  
 1193  
 1194  
 1195  
 1196  
 1197  
 1198  
 1199  
 1200  
 1201  
 1202  
 1203  
 1204  
 1205  
 1206  
 1207  
 1208  
 1209  
 1210  
 1211  
 1212  
 1213  
 1214  
 1215  
 1216  
 1217  
 1218



1219  
1220  
1221  
1222

**Table 1.** The experiments conducted. Layers refers to the number of soil layers. Increase resistance refers to whether increasing surface resistance to soil evaporation. Soil heterogeneity indicates whether soil properties and hydraulic parameters change with depth. The adjustment of  $\theta_w$ ,  $\theta_{sat}$  and  $K_{sat}$  and the method used to calculate  $\beta$  are the final two columns.

Experiment	Layers	Increase Resistance	Soil heterogeneity	Parameter adjustment	$\beta$
<i>Ctl</i>	6				default
<i>Sres</i>	6	Y			default
<i>Watr</i>	6	Y			default
<i>Hi-Res-1</i>	31	Y			default
<i>Hi-Res-2</i>	31	Y	Y		default
<i>Opt</i>	31	Y	Y	Constrain $\theta_w$ over 4.6m, $\theta_{sat}$ over top 0.3m and $K_{sat} \times 10$ over 4.6m	default
$\beta$ -hvr	31	Y	Y	As per <i>Opt</i>	Haverd
$\beta$ -exp	31	Y	Y	As per <i>Opt</i>	in situ

1223  
1224  
1225  
1226

**Table 2.** Performance metrics for the different experiments. Bold numbers are the best value among these experiments.

Simulation	Variable	r	RMSE	MBE	P5	P95
			mm or $m^3 m^{-3}$	mm or $m^3 m^{-3}$	mm or $m^3 m^{-3}$	mm or $m^3 m^{-3}$
<i>Ctl</i>	$E_{tr}$	0.85	<b>0.34</b>	0.15	0.00	<b>0.54</b>
<i>Sres</i>		0.84	0.59	0.40	0.03	1.04
<i>Watr</i>		0.83	0.40	0.19	0.01	0.64
<i>Hi-Res-1</i>		0.80	0.38	<b>0.11</b>	<b>0.00</b>	0.58
<i>Hi-Res-2</i>		0.82	0.37	0.13	0.01	0.57
<i>Opt</i>		<b>0.86</b>	0.37	0.19	0.01	0.62
$\beta$ -hvr		0.84	0.61	0.41	0.02	1.10
$\beta$ -exp		0.86	0.46	0.29	0.02	0.82
<i>Ctl</i>	$E_s$	0.65	0.70	0.12	-0.06	1.22
<i>Sres</i>		0.55	0.42	0.24	0.00	0.26
<i>Watr</i>		0.67	0.29	0.00	-0.05	0.08
<i>Hi-Res-1</i>		0.65	0.32	0.11	<b>0.00</b>	0.19
<i>Hi-Res-2</i>		0.66	0.31	0.09	-0.01	0.16
<i>Opt</i>		<b>0.68</b>	0.28	<b>0.00</b>	-0.06	0.07
$\beta$ -hvr		0.67	<b>0.27</b>	-0.04	-0.04	<b>0.05</b>
$\beta$ -exp		0.67	0.28	-0.04	-0.06	0.07
<i>Ctl</i>	$\theta$	<b>0.90</b>	0.12	0.12	0.13	0.11
<i>Sres</i>		0.89	0.15	0.15	0.15	0.14
<i>Watr</i>		0.78	<b>0.02</b>	<b>0.00</b>	<b>0.01</b>	-0.01
<i>Hi-Res-1</i>		0.83	0.02	0.01	0.02	<b>0.00</b>
<i>Hi-Res-2</i>		0.83	0.08	0.07	0.08	0.06
<i>Opt</i>		0.68	0.05	0.04	0.06	0.03
$\beta$ -hvr		0.81	0.04	0.04	0.04	0.02
$\beta$ -exp		0.73	0.05	0.04	0.05	0.03

1227  
1228  
1229  
1230  
1231  
1232

**Table 3.** Average values from each experiment. Precipitation ( $P$ ), total evapotranspiration ( $ET$ ), transpiration ( $E_{tr}$ ), soil evaporation ( $E_s$ ), canopy evaporation ( $E_c$ ), total runoff ( $R$ ) including surface and subsurface runoff, soil water drainage to aquifer ( $D_r$ ), gross primary production ( $GPP$ ), latent heat ( $Q_E$ ), sensible heat ( $Q_H$ ), and volumetric water content in the 4.6m soil column ( $\theta$ ).

	<i>Ctl</i>	<i>Sres</i>	<i>Watr</i>	<i>Hi-Res-1</i>	<i>Hi-Res-2</i>	<i>Opt</i>	$\beta$ -hvr	$\beta$ -exp
$P$ (mm $y^{-1}$ )	661							
$ET$ (mm $y^{-1}$ )	657	617	499	505	504	494	542	512
$E_{tr}$ (mm $y^{-1}$ )	341	402	344	323	327	344	403	373
$E_s$ (mm $y^{-1}$ )	305	204	143	170	165	138	126	127
$E_c$ (mm $y^{-1}$ )	11	12	12	12	12	12	12	12
$R$ (mm $y^{-1}$ )	7	49	1	2	2	0	0	0
$D_r$ (mm $y^{-1}$ )	0	0	153	152	158	163	120	147
$GPP$ (g C $m^{-2} y^{-1}$ )	1703	1770	1682	1653	1665	1704	1776	1741
$Q_E$ (W $m^{-2}$ )	52	49	40	40	40	39	43	41
$Q_H$ (W $m^{-2}$ )	15	17	25	25	26	27	24	26
$\theta$ ( $m^3 m^{-3}$ )	0.33	0.35	0.20	0.21	0.27	0.25	0.24	0.24

1233